Neural cell models for disease modeling and drug discovery

Exploiting 3D differentiation of human stem cells

Ana Paula Terrasso

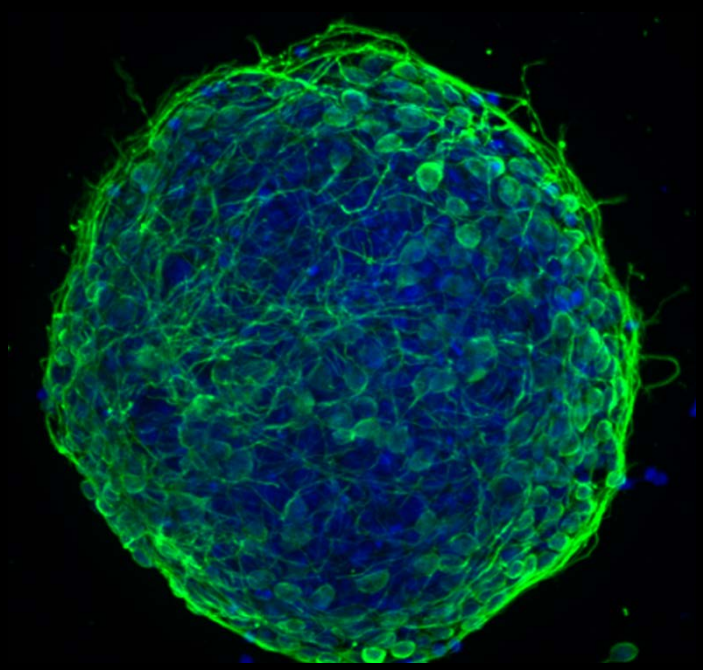

Dissertation presented to obtain the Ph.D degree in Sciences of Engineering and Technology, Biomedical Engineering

Instituto de Tecnologia Química e Biológica António Xavier | Universidade Nova de Lisboa

Oeiras
April, 2018

UNIVERSIDADE NOVA DE LISBOA

Neural cell models for disease modeling and drug discovery

Exploiting 3D differentiation of human stem cells

Ana Paula Barreto Terrasso

Dissertation presented to obtain the Ph.D degree in Sciences of Engineering and Technology, Biomedical Engineering

Instituto de Tecnologia Química e Biológica António Xavier | Universidade Nova de Lisboa

Oeiras, April, 2018

Neural cell models for disease modeling and drug discovery

Exploiting 3D differentiation of human stem cells

Ana Paula Barreto Terrasso

The work developed in this thesis was supervised by:

- Doctor Catarina Brito, Instituto de Biologia Experimental e Tecnológica (iBET) e Instituto de Tecnologia Quimica e Biológica António Xavier, Universidade Nova de Lisboa (ITQB-NOVA) (supervisor)

- Doctor Cláudia Almeida, CEDOC - Chronic Diseases Research Center, NOVA Medical School, Universidade Nova de Lisboa (co-supervisor)

Neural cell models for disease modeling and drug discovery: exploiting 3D differentiation of human stem cells

Instituto de Tecnologia Química e Biológica António Xavier
Universidade Nova de Lisboa

From left to right: Dr. Duarte Barral, Dr. Júlia Costa, Dr. Luís Pereira de Almeida, Dr. Catarina Brito, Ana Terrasso, Dr. Cláudia Almeida, Dr. Dominik Paquet and Dr. Miguel Teixeira

Supervisors

- Doctor Catarina Brito, Instituto de Biologia Experimental e Tecnológica (iBET) e Instituto de Tecnologia Quimica e Biológica António Xavier, Universidade Nova de Lisboa (ITQB-NOVA), Portugal (supervisor)
- Doctor Cláudia Almeida, CEDOC - Chronic Diseases Research Center, NOVA Medical School, Universidade Nova de Lisboa, Portugal (co-supervisor)

Jury

- Doctor Dominik Paquet, Professor, Institute for Stroke and Dementia Research (ISD), University Hospital, Ludwig-Maximilians Universität Munich, Germany
- Doctor Luís Pereira de Almeida, Auxiliar Professor, Faculty of Pharmacy, University of Coimbra, Portugal
- Doctor Júlia Carvalho Costa, Principal Investigator, Instituto de Tecnologia Química e Biológica António Xavier, Universidade Nova de Lisboa (ITQB-NOVA), Portugal
- Doctor Duarte C. Barral, Principal Investigator, CEDOC - Chronic Diseases Research Center, Nova Medical School, Universidade Nova de Lisboa
- Doctor Miguel Teixeira, Cathedratic Professor, Instituto de Tecnologia Química e Biológica António Xavier, Universidade Nova de Lisboa (ITQB-NOVA), Portugal

Finantial support from :

Fundação para a Ciência e Tecnologia (FCT)

Ph.D grant PD/BD/52473/2014

iNOVA4Health (UID/Multi/04462/2013) financially supported by FCT/MEC, through national funds and co-funded by FEDER under PT2020

Tecnimede – Sociedade Técnico Medicinal S.A., the European Regional Development Fund (FEDER) and the System of Incentives for the Research and Technological Development (QREN) of the Portuguese Government (project n.º 33913 – acronym PROiNEURO)

À minha família

Acknowledgements

I would like to express my gratitude to all the people who have contributed directly or indirectly to this thesis.

To my supervisor, Dr. Catarina Brito, for sharing this journey with me and for the constant support, guidance and motivation throughout these years. Thank you for the confidence, for the hours of scientific discussions and for the friendly conversation, and for always pushing me towards my goals and making me to potentiate my skills and grow as scientist. Also for stimulating such a challenging environment and the team spirit within the Advanced Cell Models Laboratory.

To my co-supervisor, Dr. Claudia Almeida, for introducing me to the field of neuronal intracellular trafficking, for all the fruitful scientific discussions and for inspiring me with your enthusiasm for research.

To Prof. Paula Alves, for the strong example of leadership and for transmitting us that excellence, rigor and hard work are fundamental for success. Thank you for giving me the opportunity to work in such an inspiring and excellent scientific environment at the Animal Cell Technology Unit.

To Dr. Augusto Filipe from Tecnimede - Sociedade Técnico-Medicinal, for the collaboration. For making available the compounds tested on the NT2 model and for always keeping the enthusiasm about our research.

To Dr. Eric Kremer, for all the support provided during our collaboration, for the fruitful discussions, for the knowledge shared about MPS VII and for receiving me in your lab.

To my colleagues in Advanced cell Models Lab, for being a truly team, for the discussion and critical suggestions and for the excitement shared. A special thanks to Catarina Pinto, Daniel Simão, Sofia Rebelo, Marta Estrada and Francisca Arez for the strong team spirit and for sharing this journey with me, for always being there, in good and not so good moments. Especially to Daniel, thank you for all the support, exchange of ideas and fruitful discussions. A thank to Marcos Sousa for the help with bioprocess operations. Also a thank to the rest of the people that

contributed to the great atmosphere inside and outside the lab, especially to Marta Silva, João Sá, Mafalda, João Vidigal and Ana Oliveira. To all my colleagues, present and former members of the Animal Cell Technology Unit, for all the help provided and for creating such a great working environment, where we can continuously learn so much from all the different fields.

To Neuronal Trafficking in Aging Lab former and present members, especially to Tatiana Burrinha, for receiving me so well, for discussions and for the friendship.

Pessoalmente gostaria de agradecer,

A todos os meus amigos, por todo o apoio, por todos os momentos de descontração que passamos juntos e que me ajudam a seguir em frente.

Ao Paulo, pelo carinho, apoio e incentivo constantes, por toda a paciência e por estares sempre ao meu lado. Obrigado por acreditares sempre em mim e por me estimulares a querer sempre ir mais longe e melhor, por todos os momentos de descontracção e por toda a força que me deste.

À minha familia, que são a base de tudo. Ao meu irmão Zé Luis e aos meus pais, Ana Maria e António, sem vocês nada seria possível, obrigado por todo o amor, confiança e incentivo para seguir em frente, por estarem presentes e por todo o apoio incondicional. Obrigado por tudo o que me ensinaram, por serem um exemplo a seguir e por fazerem de mim aquilo que sou hoje.

Abstract

Neurological disorders are a major public health problem and are expected to rise dramatically together with the higher life expectancy and the shift towards an ageing society. Current therapeutic options can only ameliorate some of the symptoms and there are no effective treatments to target pathological mechanisms and stop disease progression. The human brain complexity hampers the understanding of the brain functioning at the molecular, cellular, and pathophysiological levels for many neurological disorders. This highlights the need for new brain models, which can contribute to unveil molecular mechanisms of neurological disorders, identify therapeutic targets and evaluate preclinically new therapies in a more adequate and predictive basis, withstanding its successful translation to the clinics. Despite their undeniable value, traditional animal models diverge from humans at biochemical and genetic levels. Moreover, 2D *in vitro* cell-based models do not mimic important aspects of brain cellular heterogeneity, architecture and microenvironment.

The main goal of this thesis was the development, validation and interrogation of 3D *in vitro* brain models for disease modeling and drug discovery. These models should include the presence of differentiated and functional human neurons and astrocytes, able to recapitulate the neuron-astrocyte interactions present in human brain, and mimic the endogenous microenvironment without the confounding effects of an exogenous matrix. To accomplish this, we took advantage of agitation-based culture systems to promote cellular aggregation and neural differentiation into neurospheroids. This strategy allows neural cells to establish cell-cell and cell-extracellular matrix (ECM) interactions and generate complex 3D networks within the neurospheroids.

For drug screening applications, the human NTera2 (NT2) cell line was chosen to develop neurospheroids, since it provides an unlimited number of cells, with less expensive and time-consuming differentiation protocols. The development of a scalable and reliable bioprocess able to sustain the production of differentiated

neurospheroids enriched in mature and functional human neurons and astrocytes is described in chapter 2. Toxicity assessment of prototypical neurotoxicants, combining endpoints based on neuronal- and astrocytic-specific gene expression and functionality in 3D, validated this brain cell model as a powerful tool to evaluate human neuronal and astrocytic toxicity. The potential of the NT2-derived neurospheroids for neuroprotection assessment was further validated. Implementation of an *in vitro* neuroprotection assay combining the human neuron-astrocyte co-culture neurospheroids with a cell viability endpoint is described in chapter 3. The neuroprotection assay setup was applied to several chemical and naturally-synthesized compounds and revealed several candidates with neuroprotective effect against an oxidant lesion. The robustness and simplicity of these assays enabled the use of complex 3D brain cell models as a platform to identify neurotoxic agents and to identify and validate drug candidates. This highlights the potential of 3D human brain cell models for drug testing, including both neurotoxicity and neuroprotection assessment.

For disease modelling, patient-specific induced pluripotent stem cells (iPSC) were used, as these can be differentiated *in vitro* into relevant somatic lineages with the genetic background of the patients. In chapter 4, the development of a Mucopolysaccharidosis type VII (MPS VII) human disease model, able to recapitulate the neuronopathic form of the disease is described. MPS VII is an orphan, ultra-rare, lysosomal storage disease (LSD) caused by a deficiency in β-glucuronidase enzymatic activity, which leads to an abnormal accumulation of glycosaminoglycans (GAGs) in the lysosomes of many tissues, including in the brain. For healthy and MPS VII iPSC-derived neural progenitor cells (NPC) 3D neural differentiation we took advantage of a strategy previously implemented in our laboratory using software-controlled perfusion stirred-tank bioreactors. The results demonstrated that neural differentiation of human MPS VII iPSC-NPC recapitulate major disease features, specifically GAGs accumulation. MPS VII neurospheroids interrogation revealed an upregulation in astrocytic GFAP gene expression and a

disturbance in MPS VII neuronal network activity and network functional connectivity, when compared with neurospheroids derived from iPSC of a healthy donor. This MPS VII human brain cell model can potentially contribute to elucidate the cellular processes responsible for disease progression and brain dysfunction and be applied for *in vitro* assessment of appropriate pharmacological treatments. The tools developed, namely the 3D neurospheroid culture system combined with the neuronal connectivity assay, have potential to assess neurological defects in other LSD and neurological disorders with variable phenotypes.

The work developed in this thesis provides simple and versatile *in vitro* approaches to generate human brain cell models for disease modeling and drug discovery that recapitulate human neuron-astrocyte interactions. Furthermore, the strategies described herein can be applied to other sources of neural cells or to iPSC from other neurological disorders and to evaluate different therapies in preclinical research.

Resumo

As doenças neurológicas consituem um problema de saúde pública grave e prevê-se que a sua incidência aumente em paralelo com o aumento da esperança média de vida e o consequente envelhecimento da população. Os tratamentos disponiveis atualmente apenas aliviam alguns dos sintomas, não existem tratamentos efetivos, direccionados aos mecanismos patológicos e que impeçam a progressão das doenças. A elevada complexidade do cérebro humano dificulta a compreensão do seu funcionamento a nivel molecular, celular e patofisiológico. Isto demonstra a necessidade de desenvolver novos modelos celulares que contribuam para desvendar os mecanismos moleculares envolvidos no desenvolvimento e progressão das doenças neurológicas, identificar alvos terapêuticos e avaliar novas terapias de forma mais adequada e preditiva, garantindo o sucesso na sua translação para a clinica. Apesar da sua importância, os modelos animais usados tradicionalmente divergem dos humanos a nivel bioquimico e genético. Além disso, os modelos celulares bidimensionais (2D) não mimetizam aspectos importantes do cérebro humano, tais como a sua heterogeneidade celular, arquitectura e microambiente.

O objectivo principal desta tese é o desenvolvimento, validação e interrogação de modelos celulares de cérebro, com aplicação na descoberta de fármacos e em modelos de doenças neurológicas. Estes devem incluir neurónios e astrócitos humanos, diferenciados e funcionais, capazes de recapitular as interacções neurónio-astrócito existentes no cérebro humano e mimetizar o microambiente endógeno, sem a perturbação de uma matriz exógena. Foram usados sistemas de cultura agitados para promover a agregação celular e a diferenciação neural. Esta estratégia permite às células nos neuroesferóides estabelecer interacções célula-célula e célula-matriz e gerar redes neuronais tridimensionais complexas.

Para aplicações em testes de fármacos, foi escolhida a linha celular Ntera2 (NT2), uma vez que permite obter um número ilimitado de células, com protocolos de diferenciação menos dispendiosos e demorados. O desenvolvimento de um

bioprocesso robusto e escalonavél, que permitiu a produção de neuroesferóides enriquecidos em neurónios e astrócitos humanos, maturos e funcionais, é descrito no capitulo 2. A avaliação da toxicidade de compostos neurotóxicos prototípicos, combinando *endpoints* baseados na expressão génica e na funcionalidade neuronal e astrocitica, permitiu validar este modelo como uma metodologia eficaz para avaliar toxicidade em neurónios e astrócitos humanos. A possibilidade dos neuroesferóides serem utilizados para avaliação de neuroprotecção foi também avaliada. A implementação de um ensaio *in vitro* para avaliar neuroprotecção, combinando a co-cultura de neurónios e astrócitos humanos em neuroesferóides e um *endpoint* de viabilidade celular, é descrita no capitulo 3. Este ensaio foi aplicado a diversos compostos, quimicos e sintetizados naturalmente e revelou vários candidatos com efeito neuroprotector contra uma lesão oxidativa. A robustez e a simplicadade destes ensaios potencia o uso de modelos celulares 3D mais complexos como plataforma para identificar compostos neurotóxicos e novos fármacos. Isto demonstra o potencial da aplicação de modelos celulares neurais para teste de fármacos, incluindo avaliação de neurotoxicidade e de neuroprotecção.

Para desenvolvimento de um modelo de doença, foram usadas células estaminais pluripotentes induzidas (iPSC), uma vez que estas podem ser diferenciadas *in vitro* em linhagens somáticas relevantes para o fenótipo da doença com os antecedentes genéticos dos pacientes. No capitulo 4 é descrito o desenvolvimento de um modelo celular humano que recapitula a forma neuronopática da doença Mucopolissacaridose tipo VII (MPS VII). A MPS VII é uma doença lisossomal de sobrecarga (DLS), orfã e ultra-rara, causada por uma deficiência na actividade do enzima β-glucuronidase, que leva à acumulação de glicosaminoglicanos (GAGs) nos lisosomas de diversos tecidos, incluindo no cérebro. Para diferenciação de células progenitoras neurais (NPC) derivadas de iPSC de um dador saudável e de outro com MPS VII, foi aplicada uma estratégia já implementada no laboratório, usando biorreatores de tanque agitado em perfusão.

Os resultados demonstraram que o modelo neural de MPS VII, derivado de iPSC-NPC humanas, recapitula as principais caracteristicas da doença, nomeadamente a acumulação de GAGs. Os neuroesferóides da doença revelaram uma sobreexpressão do gene astrocitico GFAP e distúrbios na funcionalidade da rede neuronal e na sua conectividade, quando comparados com os neuroesferóides derivados do dador saudável. Este modelo celular humano de MPS VII pode contribuir para elucidar os mecanismos celulares responsáveis pela progressão da doença e pela disfunção cerebral e ser aplicado na avaliação de tratamentos farmacológicos adequados para a doença. As metodologias desenvolvidas, nomeadamente o sistema de cultura de neuroesferóides, combinado com o ensaio de avaliação da funcionalidade e conectividade neuronal, podem ser aplicados na avaliação de defeitos neurológicos em outras DLS e doenças neurológicas com fenótipos variáveis.

O trabalho desenvolvido nesta tese fornece abordagens simples e versáteis para gerar modelos *in vitro* de células neurais humanas, com aplicação em ensaios pré-clínicos, que recapitulam as interações neurónio-astrócito presentes no cérebro humano. Para além disso, esta estratégia pode ser aplicada a outras fontes de células neurais ou a células de outras doenças neurológicas, para avaliar possiveis terapias em ensaios pré-clinicos.

Thesis publications

Terrasso AP, Pinto C, Serra M, Filipe A, Almeida S, Ferreira AL, Predroso P, Brito C, Alves PM. 2015. Novel scalable 3D cell based-model for *in vitro* neurotoxicity testing: combining human differentiated neurospheres with gene expression and functional endpoints. Journal of Biotechnology, 205, 82–92, doi: 10.1016/j.jbiotec.2014.12.011.

Terrasso AP, Silva AC, Filipe A, Pedroso P, Ferreira AL, Alves PM, Brito C. 2017. Human neuron-astrocyte 3D co-culture-based assay for evaluation of neuroprotective compounds. Journal of pharmacological and toxicological methods, 83, 72–79, doi: 10.1016/j.vascn.2016.10.001.

Bayó-Puxan N*, **Terrasso AP***, Creyssels S, Simão D, Begon-Pescia C, Lavigne M, Salinas S, Bernex F, Bosch A, Kalatzis V, Levade T, Cuervo AM, Lory P, Consiglio A[#], Brito C[#], Kremer EJ[#] (*equal contribution; [#]co-senior authors). 2018. Lysosomal and network alterations in human mucopolysaccharidosis type VII iPSC-derived neurons. Journal of Cell Science. *Under Revision*.

Additional publications

Simão D, Silva MM, **Terrasso AP**,Arez F, Sousa MF, Mehrjardi NZ, Šarić T, Gomes-Alves P, Raimundo N, Alves PM, Brito C. 2018. 3D differentiation of iPSC-derived NPC recapitulates human brain microenvironment. Stem Cell Reports. *Under final revision.*

Figueira I, Tavares L, Jardim C, Costa I, **Terrasso AP**, ..., Santos CN. 2017. Blood–brain barrier transport and neuroprotective potential of blackberry-digested polyphenols: an *in vitro* study. European Journal of Nutrition, 1-18, doi: 10.1007/s00394-017-1576-y.

Figueira I, Garcia G, Pimpao RC, **Terrasso AP**, ..., Brito C, Santos CN. 2017. Polyphenols journey through blood-brain barrier towards neuronal protection. Scientific Reports 7(1), doi: 10.1038/s41598-017-11512-6.

Simão D, **Terrasso AP**, Teixeira AP, Brito C, Sonnewald U, Alves PM. 2016. Functional metabolic interactions of human neuron-astrocyte 3D *in vitro* networks. Scientific Reports, 6:33285, doi: 10.1038/srep33285.

Simão D, Arez F, **Terrasso AP**, Pinto C, Sousa MF, Brito C, Alves PM. 2016. Perfusion Stirred-Tank Bioreactors for 3D Differentiation of Human Neural Stem Cells. Methods in Molecular Biology, doi: 10.1007/7651_2016_333.

Materne EM, Ramme AP, **Terrasso AP**, Serra M, Alves PM, Brito C, Sakharov DA, Tonevitsky AG, Lauster R, Marx U. 2015. A multi-organ chip co-culture of neurospheres and liver equivalents for long-term substance testing. Journal of Biotechnology, 205, doi: 10.1016/j.jbiotec.2015.02.002.

Table of contents

List of figures

List of tables

Abbreviations

2D	Two-dimensional
3D	Three-dimensional
Acr	Acrylamide
AD	Alzheimer disease
ASD	Autism spectrum disorder
BDNF	Brain-derived neurotrophic factor
BMP	Bone morphogenic protein
cAMP	Cyclic adenosine monophosphate
CNS	Central Nervous System
CSPGs	Chondroitin sulfate proteoglycans
DIV	Days *in vitro*
DMEM	Dulbecco's Modified Eagle's Medium
EB	Embryoid bodies
ECM	Extracellular matrix
EGF	Embryonic growth factor
ERT	Enzyme replacement therapy
ESC	Embryonic stem cells
FBS	Fetal bovine serum
FDA	Fluorescein diacetate
FGF	Fibroblast growth factor
FSG	Fish skin gelatin
GABA	γ-aminobutyric acid
GAD65/67	Glutamate decarboxylase 65/67
GAGs	Glycosaminoglycans
GDNF	Glia-derived neurotrophic factor
GFAP	Glial fibrillary acidic protein
GLAST	Glutamate aspartate transporter

Gln	Glutamine
GLT-1	Glutamate transporter 1
Glu	Glutamate
GS	Glutamine synthase
HTS	High-throughput screening
iN	Induced neurons
iNSC	Induced neural stem cells
iOPC	Induced oligodendrocyte progenitor cells
iPSC	Induced pluripotent stem cells
LPS	Lipopolysaccharides
LSD	Lysosomal storage diseases
MPS	Mucopolysaccharidosis
MPS VII	Mucopolysaccharidosis type VII
NE	Neuroepithelial
NGF	Nerve growth factor
NPC	Neural progenitor cells
NSC	Neural stem cells
NT2	NTera2 clone D1
P/S	Penicillin and Streptomycin
PBS	Phosphate buffered saline
PCNA	Proliferating cell nuclear antigen
PD	Parkinson disease
PFA	Paraformaldehyde
PGs	Proteoglycans
PI	Propidium iodide
PNNs	Perineuronal nets
PSC	Pluripotent stem cells
qRT-PCR	Quantitative real-time polymerase chain reaction
RA	Retinoic acid

RG	Radial glia
RPL22	Ribosomal protein L22
RT	Room temperature
SD	Standard deviation
SDS-PAGE	Sodium dodecyl sulphate - polyacrylamide gel electrophoresis
SFEBq	Serum-free, floating embryoid body-like, quick aggregates
SHH	Sonic hedgehog
tBHP	Tert-butyl hydroperoxide
TGF- β	Transforming growth factor β
TH	Tyrosine hydroxylase
TLR4	Toll-like receptor 4
Tx-100	Triton X-100
vGluT1	Vesicular glutamate transporter
β-gluc	β-glucuronidase
r β-gluc	Recombinant β-glucuronidase
βIII-tub	βIII-tubulin
β-tub	β-tubulin
ChaT	Choline acetyltransferase
DAPI	4’-6-diamino-2-phenylindole
Syn	Synaptophysin
PSD-95	Postsynaptic density protein 95
PVDF	Polyvinylidene difluoride
VGluT1	Vesicular glutamate transporter 1
β-hex	β-hexosaminidase
Ca^{++}	Calcium

CHAPTER 1

Introduction

Table of contents

1. Neuroscience research: need for CNS modeling

Neurological disorders are a major public health problem and are expected to rise dramatically together with the increase in life expectancy and the shift towards an ageing society. Around 450 million people currently suffer from mental disorders and the forecasts indicate that by 2050 the number will triple (WHO Mental Disorders Fact Sheet, 2017). Neurological disorders represent significant economic and social burdens and high costs for healthcare systems, accounting for as much as 45% of the annual health budget in Europe (DiLuca et al., 2014; Harper, 2014; Rosemann, 2015). Current treatments for most neurological disorders only ameliorate some of the symptoms, alleviating patient's mental impairment. Despite major and continuously growing investment, there are no effective disease-modifying treatments available to target pathological mechanisms and stop disease progression (Calcoen et al., 2015; Payne et al., 2015). Drug development pipeline have proven lengthy, costly and relatively unproductive process (Fig. 1.1) with a high number of late-stage failures and attrition rates around 90% (Calcoen et al., 2015; Hay et al., 2014). This is even worst for central nervous system (CNS) drugs, which are more likely to fail in Phase III drug development than non-CNS drugs, mainly due to lack of efficacy (Kesselheim et al., 2015). On average, the overall success rate is of 4.1%, but for example, in Alzheimer's disease (AD) drug development, from 2002 to 2012, 413 clinical trials have been performed, mainly with drugs to improve cognition and disease-modifying small molecules or immunotherapies, with an overall success rate of only 0.4% (Calcoen et al., 2015; Cummings et al., 2014).

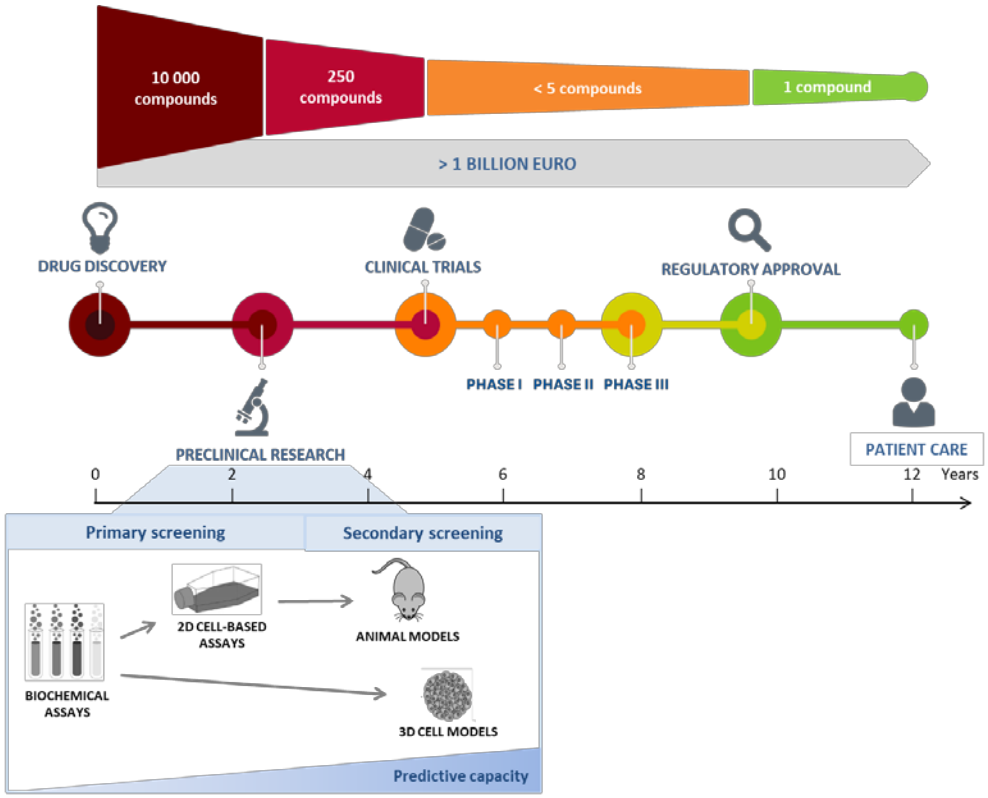

Figure 1.1: Drug discovery pipeline in the pharmaceutical industry. The different stages of drug development process (drug discovery, preclinical research, clinical trials and regulatory approval); typically only 1 in 10 000 compounds are approved and the process costs more than 1 billion euro overall. 3D cell models can represent a complementary tool in preclinical research, offering increased predictive capacity, when compared to 2D cell-based assays. The use of these models can be parallel to animal models, reducing the dependency on animal models, costs and time. Adapted from Kunz-Schughart et al., (2004) and from http:// www.researchamerica.org/ advocacy-action/ issues-researchamerica-advocates/bench-bedside-drug-development-pipeline.

This highlights the need for novel preclinical models that enable new therapies to be developed and tested in a more adequate and predictive context, reducing the number of drugs that will fail in late-stages clinical trials (Fig. 1.1). To do so, the understanding of the pathophysiological bases for many neurological disorders is essential. However, the high degree of complexity of the human brain and its poor accessibility *in vivo* makes it difficult to investigate specific biochemical and cellular mechanisms. While of undeniable value, animal models and several *in vitro* cell-based models fail to precisely recapitulate the clinical pathophysiological state, hampering the relevance of preclinical studies using these models. This can be

accounted for the fact that animal and *in vitro* models do not mimic important aspects of the *in vivo* brain cellular composition, architecture and microenvironment. Animal models have been widely used to study genetic and pathological mechanisms of neurodegenerative diseases and to test new therapeutic drugs (Breslin and O'Driscoll, 2013; Fitzgerald et al., 2015). While mimicking brain tissue complexity, at biochemical and genetic levels there are differences between species and many human diseases resulting from complex interactions between genes and environmental factors can not be recapitulated in animals (Payne et al., 2015). Indeed, concordance between rodents and human toxicity can be very low with rodents being predictive of human toxicity in less than half of the cases (Olson et al., 2000). The transcriptional profile of AD mouse models is not similar to human AD (Hargis and Blalock, 2018) and these models do not reflect the extensive neuronal loss seen in the human condition (LaFerla and Green, 2012). Consequently, numerous drugs that demonstrated efficacy in the animal models have not shown efficacy when translated to the clinic. In fact, around 500 neuroprotective therapies that were successfully developed in rodent models of stroke, failed at some stage when translated to humans, with only one treatment being approved (O'Collins et al., 2006; Sena et al., 2010). Furthermore, human *in vitro* models for neurological disorders are commonly based on neuronal-like cell lines, mainly tumor-derived, but these do not recapitulate the cell heterogeneity of human brain and its microenvironmental features and are not genetically matched to the patient (Choi and Tanzi, 2012; Ross and Akimov, 2014). The recent advances in cell reprogramming technologies and pluripotent stem cell (PSC) neural differentiation strategies, allowing obtaining neural cells with the genetic background of the patient, provided unique opportunities to investigate important aspects of brain function, development and disease pathogenesis at cellular level. Therefore, given our poor understanding of the pathogenesis of complex diseases and the low predictive capacity of currently available animal and

in vitro models, it is clear that there is a high demand to develop brain cell models that can withstand a successful translation of drugs to the clinics.

2. Human cell sources for CNS modeling

Human cell sources available for the derivation of neural cells for CNS modeling can be divided into two main categories: (1) primary cultures of human brain cells and (2) immortalized cell lines and *in vitro* differentiation of neural cells (Fig. 1.2).

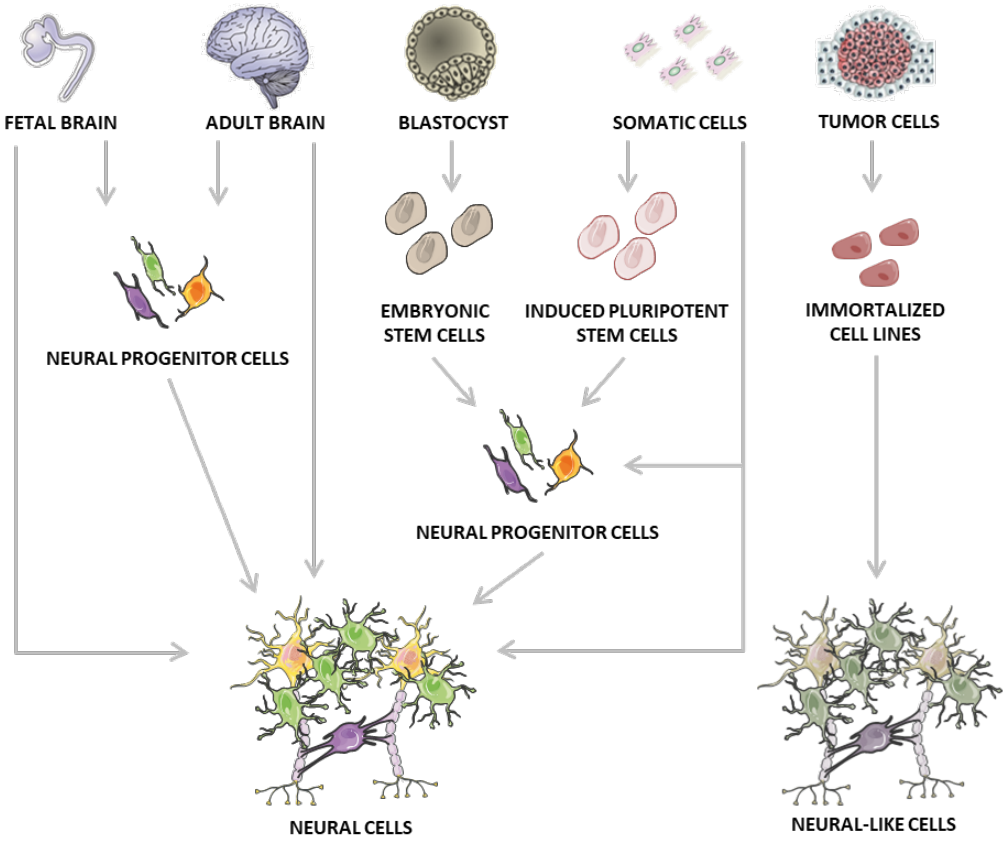

Figure 1.2: Different cell sources available for the derivation of human neural cells. Neural progenitor cells (NPC) or neural cells can be isolated directly from human fetal or adult brains. NPC are able to keep to some extent their self-renewal and multipotent capacities and can be differentiated into neural cells. Embryonic stem cells, isolated from blastocyst inner cell mass, and induced pluripotent stem cells, can be committed towards the neural lineage through neural induction protocols, generating neural progenitor cells, which can be further differentiated into neural cells. Somatic cells can be reprogrammed into induced pluripotent stem cells or directly reprogrammed into neural progenitor cells or terminally-differentiated neural cells. Immortalized cell lines are usually derived from tumor cells and some of these present ability to differentiate towards neural lineage into neural-like cells by addition of neurotrophic factors. Adapted from Conti and Cattaneo, (2010) and Jakel et al., (2004).

2.1. Primary cultures

Human brain cells isolated from *fetus*, can be maintained *in vitro* as primary cultures, including one or several brain cell types (Darbinyan et al., 2013; Mattson and Rychlik, 1990; Ray et al., 2014), or *ex vivo* as organotypic slice cultures, keeping the *in situ* cellular organization and three-dimensional (3D) tissue architecture within the slice (Humpel, 2015). The first cell culture of human neurons isolated from live adult brain was recently reported (Spaethling et al., 2017), with identification of 5 distinct cell types in culture: oligodendrocytes, microglia, neurons, endothelial cells and astrocytes and cell-type- and individual-specific transcriptional hierarchies were identified. Although it is a very valuable resource, the use of human brain tissue is limited due to the lack of availability and ethical concerns. Additionally, human brain tissue to study development and early defects in neurological disorders is not readily available, as brain biopsies from living patients are limited, and autopsy material is normally representative of later disease stages and limits sample quality (Darmanis et al., 2015). The use of terminally-differentiated cell types isolated from the CNS, as neurons, is also limited due to the impossibility of expansion *in vitro*. To overcome these issues, self-renewing multipotent neural stem cells (NSC) can be isolated from specific niches in fetal or adult brain tissue and expanded and terminally differentiated *in vitro* into neurons and glia cells (Conti and Cattaneo, 2010; Simão et al., 2014). Primary NSC have a limited self-renewal capacity *in vitro* due to the low level of expression of telomerase, which is required for continuous cell proliferation (Ostenfeld et al., 2000). Moreover, NSC differentiation potential, temporal development and phenotype varies with the tissue age, *in vitro* expansion and culturing method (Conti and Cattaneo, 2010; Zhang, 2006). Altogether, these aspects highlight the great limitations in the use of primary cell sources from CNS origin for *in vitro* modeling.

2.2. Immortalized cell lines and *in vitro* differentiation of neural cells

Historically, the first hypothesis to overcome the difficulties associated with the use of primary cultures of brain cells was to establish immortalized cell lines. These can be from tumoral origin or immortalized *in vitro* by transfection of oncogenes. The advantages include being easy to obtain and allowing expansion of large numbers of cells. However, most of immortalized cell lines, as the widely used neuroblastoma cell lines, have the disadvantage of continuous proliferation, as they not generate post-mitotic cell-types and therefore do not allow the recapitulation of the neuronal development occurring in the CNS, as well as the organ-specific structural and functional features (Conti and Cattaneo, 2010; Gupta et al., 2012). The majority of the cell lines can be induced *in vitro* to differentiate in a more neuronal-like phenotype, usually by removal of specific growth factors or addition of neurotrophic factors. The human neuroblastoma cell line SH-SY5Y, which grows continuously as an undifferentiated cell population with neuroblast-like morphology, can be differentiated towards neuronal-like cells, with retinoic acid (RA) or specific neurotrophic factors, such as brain-derived neurotrophic factor (BDNF) (Shipley et al., 2016). SH-SY5Y cells have been used for neurotoxicity and neuroprotection testing *in vitro* and to understand the mechanisms of action of neurotoxic chemicals, such as okadaic acid and antidepressant drugs (Choi et al., 2011; Del Barrio et al., 2011). Also, Parkinson's disease (PD) and AD-associated neuronal defects have also been modeled using neuroblastoma cell lines (Dodel et al., 2011; Fang et al., 2006; Presgraves et al., 2004). However, these models comprise immature neuronal-like cells and do not take into account the multiple cell types involved in the brain pathology and their interactions, which contribute to the disease.

Neural progenitor cells (NPC) can be immortalized *in vitro*, usually by transfection of oncogenes, to overcome its limited self-renewal capacity due to growth arrest and senescence. These immortal NSC lines can be expanded *in vitro*

and differentiated in neural cells. The human fetal NPC Lund mesencephalic cell line (LUHMES), immortalized by a tetracycline-controlled v-myc gene, can be differentiated into morphologically and biochemically mature dopamine-like neurons, following exposure to tetracycline, glial cell line-derived neurotrophic factor (GDNF) and dibutyryl cyclic adenosine monophosphate (cAMP). LUHMES were used for neurotoxicity testing and for PD modeling (Scholz et al., 2011; Zhang et al., 2014), either in co-culture with astrocytic cells (Efremova et al., 2015) or in a 3D culture setup (Smirnova et al., 2016), in an attempt to increase the level of mimicry of the human brain of the model. NPC immortalized *in vitro* by overexpression of the myc family transcription factors (ReNcell cells) were differentiated into the three neuronal lineages by removal of growth factors and addition of neurotrophic factors (Donato et al., 2007). A high-throughput screening assay for evaluation of chemical compounds effects was implemented using this ReNcell line (Breier et al., 2008) and differentiated neuronal cells were applied in AD modeling, based on overexpression of human b-amyloid precursor protein (APP) or APP and presenilin 1 (PSEN1), containing familial AD mutations (Choi et al., 2014). This 3D culture of differentiated neurons in Matrigel has been reported to recapitulate amyloid and tau pathologies with robust extracellular deposition of β-amyloid, and detection of aggregates of phosphorylated tau in neuronal cell soma and neurites (Choi et al., 2014). Notably, this was the first cell-based model able to recapitulate key features of AD pathophysiology *in vitro*, which have not been previously observed in mouse models and in *in vitro* 2D culture systems. The largely studied NTera-2 (NT2) cell line, a pluripotent cell line derived from a malignant embryonic carcinoma (Pal and Ravindran, 2006; Pleasure and Lee, 1993), upon exposure to RA, can be differentiated into neural cells, including neurons and astrocytes (Bani-Yaghoub et al., 1999; Goodfellow et al., 2011; Pleasure and Lee, 1993; Terrasso et al., 2015). NT2-derived neurons maintain a post-mitotic neuronal phenotype, with axons and dendrites elaborating processes and synaptic contacts and present different neurotransmitter subtypes, mainly glutamatergic and

GABAergic neurons (Coyle et al., 2011; Podrygajlo et al., 2009). NT2-derived astrocytic cells show phenotypic and functional markers, such as glial fibrillary acid protein (GFAP), the glutamate transporters GLAST and GLT-1 and the glutamine synthase (GS) enzyme (Goodfellow et al., 2011; Hill et al., 2012). NT2 cell line has been widely used to model specific neural functions (Goodfellow et al., 2011; Hill et al., 2012) and for neurotoxicity studies (Hill et al., 2008; Stern et al., 2013) due to its easy expansion *in vitro* and the simple neural differentiation protocol. In comparison with other cell lines, NT2-derived neural cells can attain a high degree of maturation, making them an useful human brain cell source. We promoted neural differentiation of NT2 cells as aggregates, generating neurospheroids that were mainly composed of functional neurons and astrocytes and were further applied for drug testing (Simão et al., 2016; Terrasso et al., 2017, 2015).

Several technological advances are nowadays allowing the derivation of human neural cells from different cell sources, such as embryonic stem cell (ESC) and induced pluripotent stem cells (iPSC). First human ESC lines were derived by Thomson and colleagues in 1998, providing a new starting point to attain recapitulation of tissue development *in vitro* and to generate a wide variety of cells types. A decade ago, reprogramming human somatic cells into iPSC by the introduction of four embryonic transcription factors (Oct4, Sox2, Klf4 and c-Myc) was firstly published by Yamanaka and colleagues (Takahashi et al., 2007). This technology opened the possibility of generating PSC with the genetic background of patients, which could then be induced to differentiate towards relevant somatic lineages, including the neural lineage (Chambers et al., 2009; Fernandes et al., 2015; Shi et al., 2012).

Initially ESC were differentiated towards the neural lineage via embryoid bodies (EB) formation (Dhara and Stice, 2008; Zhang et al., 2001), but more recently directed differentiation factors have been employed to differentiate ESC and iPSC into neural cells (Chambers et al., 2009; Shi et al., 2012). NPC can be efficiently generated from ESC and iPSC, in adherent culture, through inhibition of

bone morphogenetic protein (BMP) signaling by its antagonist noggin (Gerrard et al., 2005). RA and nerve growth factor (NGF) were found to be potent enhancers of neuronal differentiation, eliciting extensive outgrowth of processes and the expression of neuron-specific molecules (Schuldiner et al., 2001). Directed ESC or iPSC differentiation to enriched populations of specific neuronal subtypes can also be achieved. Derivation of midbrain dopaminergic neurons was induced by sequential application of the patterning molecules Sonic hedgehog (SHH), Fibroblast growth factor 8 (FGF8), BDNF, GDNF, transforming growth factor type β (TGF-β), dibutyryl cAMP and ascorbic acid (Perrier et al., 2004; Zhang and Zhang, 2010). Human iPSC-derived dopaminergic progenitor cells, differentiated by floor plate induction protocol, using BDNF, GDNF, cAMP and ascorbic acid, were grafted into the brain of a primate model of PD (Kikuchi et al., 2017). The authors reported that cells survived and functioned as mature midbrain dopaminergic neurons, extended dense neurites into the host striatum, indicating that human iPSC-derived dopaminergic progenitors are clinically applicable for the treatment of patients with PD (Kikuchi et al., 2017). Enriched populations of forebrain GABAergic neurons were obtained using purmorphamine and SHH interchangeably for neuroepithelia patterning (Ma et al., 2012). Human iPSC generated from Huntington's disease patient were differentiated into striatal GABAergic neurons by combining morphogens and neurotrophins SHH, BDNF, dibutyryl cAMP and valpromide that contain the same CAG repeat expansion as the mutation in the HD patient (Zhang et al., 2010). The generation of a culture enriched in ESC-derived astrocytes was first reported by Gupta and colleagues (2012) by combining BMP-mediated Smad and LIF-mediated JAK-STAT signaling. These astrocytes promoted the protection of ESC-derived neurons against oxidative insults (Gupta et al., 2012). One year later, a chemically defined xeno-free medium was developed for fast generation of astrocytes from NSC derived from PSC (Shaltouki et al., 2013). Astrocytes differentiated by this culture method have been reported to display similar gene expression patterns, morphological characteristics and functional properties to

primary astrocytes (Shaltouki et al., 2013). Human iPSC from healthy individuals and patients with early-onset familial AD or late-onset sporadic form of AD were differentiated into astrocytes by addition of FGF2, ciliary neurotrophic factor and BMP2 (Jones et al., 2017). These astrocytes expressed functional markers, including GFAP, GLT-1 and GS, comparable to that of adult astrocytes *in vivo*, and AD astrocytes exhibited a pronounced pathological phenotype, with a significantly less complex morphological appearance than healthy astrocytes and aberrant expression and localization of GLT-1 and GS (Jones et al., 2017).

To shortcut the differentiation process from PSC, somatic cells can be directly reprogrammed into a terminally differentiated neural cell types, skipping all developmental precursor cell stages, or into an intermediate progenitor stage, such as multipotent NSC (Mertens et al., 2016; Pang et al., 2011). Payne and colleagues reported that a combination of four transcription factors (Brn2, Ascl1, Myt1l and NeuroD1) was enough to convert human fibroblasts into induced neurons (iN) that expressed multiple neuronal markers and matured to form synapses and generate action potentials. A minimal set of three transcription factors (Mash1, also known as Ascl1, Nurr1 and Lmx1a) was described to directly generate functional dopaminergic neurons from mouse and human fibroblasts (Caiazzo et al., 2011). Direct neuronal conversion, contrary to iPSC reprogramming, does not revert putative cellular aging markers. Therefore, these iN could be important tools to develop models of sporadic, late-onset neurodegenerative diseases, as aging is one of the most important risk factor for these disorders. Contrary, differentiation of neural cells from PSC recapitulates human neural development, potentially allowing studying neurodevelopmental diseases, impossible to address with iN (Mertens et al., 2016). For the generation of induced NSC (iNSC), human fibroblasts were directly reprogrammed with a single factor, Sox2 (Ring et al., 2012). Induced oligodendrocyte progenitor cells (iOPC) were generated by direct lineage conversion of mouse fibroblasts using different sets of three transcription factors, Sox10, Olig2 and Nkx6.2 (Najm et al., 2013) or Sox10, Olig2 and Zfp536 (Yang et al.,

2013). Embryonic and postnatal mouse fibroblasts were recently convert into astrocytes (iastrocytes) by three transcription factors involved in defining the astroglial cell fate, NFIA, NFIB, and SOX9 (Caiazzo et al., 2015). Small molecules can also be used to directly convert mouse and human fibroblasts into functional astrocytes without genetic manipulation (Tian et al., 2016). Direct neural reprogramming could be a more efficient strategy, in terms of time and costs than neural differentiation of iPSC. Still, iN are post-mitotic cells that cannot be expanded *in vitro*, which is a major disadvantage (Mertens et al., 2016). Thus, applications that require large numbers of neural cells may favor iNSC or iPSC-based strategies.

The widespread implementation of iPSC was accelerated by the knowledge accumulated with the ESC field and the fact that iPSC bypass the ethical concerns underlying the use of tissue from embryonic origin. With the recent advances in gene editing tools, such as CRISPR-Cas9, new strategies to precise genetic manipulations to introduce or to correct disease-associated mutations in iPSC are available, allowing accurate functional analysis (Doudna and Charpentier, 2014; Hockemeyer and Jaenisch, 2016). Recently, a set of isogenic stem cell lines containing PD-associated mutations in α-synuclein was generated by CRISPR-Cas9 gene editing (Arias-Fuenzalida et al., 2017). iPSC rapidly became a valuable tool for modelling human neurological disorders and for drug testing. For example, neurotoxicity of the chemotherapeutic drugs paclitaxel, vincristine and cisplatin was evaluated in iPSC-derived neurons that showed morphological disruption, decreased neurite outgrowth, decreased cellular viability and apoptosis (Wheeler et al., 2015). iPSC technology has also been widely applied for disease modeling, potentially contributing to elucidate early disease mechanisms and progression of neurological disorders. Indeed, disorders such as AD (Israel et al., 2012; Kondo et al., 2013), Down syndrome (Briggs et al., 2013), autism spectrum disorder (ASD) (DeRosa et al., 2010) and schizophrenia (Brennand et al., 2011) have been modeled using iPSC. Familial and sporadic AD iPSC-derived neurons showed phenotypes

relevant to the disease, such as accumulation of β-amyloid and phosphorylated tau protein (Israel et al., 2012; Kondo et al., 2013). Down syndrome iPSC-derived neural cultures showed a two-fold bias towards glial lineages and were up to two times more sensitive to oxidative stress-induced apoptosis than healthy neural cultures (Briggs et al., 2013). Schizophrenia iPSC-derived neurons showed reduced neuronal connectivity together with decreased neurite number, postsynaptic density protein 95 (PSD-95) levels and glutamate receptor expression (Brennand et al., 2011). Also, the neuronopathic forms of lysosomal storage diseases (LSD), such as mucopolysaccharidosis (MPS) IIIB (Lemonnier et al., 2011), MPS IIIC (Canals et al., 2015) and Pompe disease (Higuchi et al., 2014) were modeled employing human iPSC lines. The knowledge generated contributed to understanding disease mechanisms and to the treatment of these rare diseases (Borger et al., 2017). Further, this demonstrates that patient-specific iPSC can be used to model features of neurological disorders *in vitro*, for analyzing disease pathogenesis and evaluating drugs. Still, some limitations of iPSC-based disease modeling must be circumvent. These limitations include the time, costs and labor required for iPSC reprogramming and neural differentiation. Further, improve the maturity of neural cells differentiated from PSC is another of the challenges the field is facing. It is required to develop PSC neural differentiation strategies that allow obtaining fully mature and functional neural cells, which age in culture in order to mimic late-onset neurodegenerative diseases phenotypes.

3. Cell fate determinants: patterning and differentiation towards neural lineage

In vivo, following implantation of the blastocyst and gastrulation, 3 distinct germ-layers are generated: endoderm (that gives rise to internal organs), mesoderm (that gives rise to bone, muscle, heart and vasculature) and ectoderm (that gives rise to the nervous system and the skin). Neurodevelopment is spatiotemporally regulated and requires sequential and progressive restrictions in

cell fate from embryonic ectoderm. Three main events characterize early neurodevelopment: (1) neural induction through specification of the embryonic ectoderm to form the neural plate, mainly composed of neuroepithelial (NE) cells; (2) neurulation through serial morphogenetic transformations, including cell division, morphological changes and migration, to generate the neural tube along the developing embryo; and (3) neural patterning through expansion and division of the neural tube into functionally and spatially distinct neuraxial regions; NE cells originate radial glia (RG) cells, which maintain their epithelial characteristic (Price et al., 2011; Zirra et al., 2016). Further differentiated cell types, such as intermediate progenitors and terminally differentiated distinct neural subtypes, are generated from self-renewing asymmetric divisions of RG cells, through concerted molecular programs in specific regions of the nervous system. Once neurons are produced, they migrate outwards to their final locations, extend axons to target other neurons and begin forming the neural network (Kelava and Lancaster, 2017; Zirra et al., 2016).

Neurogenesis precedes gliogenesis, with radial glial serving as NSC substrate for both cell types and as scaffold for migration. Neurons and oligodendrocytes develop following a step-wise process: (a) stem cells are specified towards the neural lineage; (b) NSC migrate away from the germinal centers; (c) NSC exit cell cycle and (d) undergo terminal differentiation during which a given cell type initiates its physiological function (Molofsky and Deneen, 2015). Whether astrocytes follow the same pattern of development as neurons and oligodendrocytes has not yet been established (Molofsky and Deneen, 2015). However, it has become increasingly clear that the same patterning factors that control neuronal subtype generation also play an instructive role in astrocyte differentiation and regulate astrocyte subtype generation (Molofsky and Deneen, 2015).

During embryogenesis, germ-layer specification is highly dependent on TGF-β superfamily, which comprises Activin, Nodal, TGF-β and BMP families and signals

through a number of SMAD proteins downstream effectors (Pauklin and Vallier, 2015). Non-neural identities are promoted by BMP and Activin/Nodal signaling. Combined gradients of Nodal and BMP within the primitive steak control endoderm and mesoderm germ layer specification, whilst blocking neuroectoderm formation (Pauklin and Vallier, 2015; Zirra et al., 2016). BMP4 and its downstream effectors Smad1/5/8 interact with mesoderm regulators to repress endoderm markers, induced by Nodal and the downstream Smad2/3 that directly controls the transcriptional activity of a broad number of endoderm genes (Pauklin and Vallier, 2015). Furthermore, Smad1/5/8 and Smad2/3 bind to the same region of Nanog promoter, suggesting that these might compete to modulate the expression of key pluripotency markers.

Differentiation of PSC into neural cells requires the combination of mitogens and morphogens that mimic the *in vivo* developmental cues to specify cell identity. Insights from developmental neurobiology provided a conceptual framework to rationalize media composition for the directed differentiation of human PSC towards the neural lineage: the ectoderm produces BMPs to promote epidermal differentiation, while neural inducing regions antagonize BMPs to permit neural induction. Based on these mechanisms, Chambers and colleagues (2009) developed the most widely adopted approach for neural conversion of PSC, termed the dual-Smad inhibition protocol. The need for an intermediate EB stage is bypassed and the efficiency of generation of neural rosettes increased greatly by applying both Nodal and BMP4 antagonists in combination, for inhibition of downstream SMAD proteins. This protocol was further modified by addition of retinoids, improving the efficiency of specification towards a forebrain identity (Shi et al., 2012). Still, current approaches for directed differentiation of human PSC often fail to capture the dynamic and overlapping nature of the neurodevelopmental processes (Zirra et al., 2016). *In vivo*, the stem cell niche is regulated by multiple factors, such as the differentiating cell types and secreted signaling molecules, extracellular matrix (ECM) components, the 3D structural architecture of cells within the niche and

mechanical forces such as tension, rigidity and even fluid flow (Murrow et al., 2017). Nevertheless, the precise mechanisms by which individual components regulate the niche are still largely unknown.

The role of extracellular cues, including ECM and other microenvironmental factors, in cell growth and differentiation is now beginning to be understood. The mechanical properties of the ECM, such as the stiffness or the elasticity, affect the adhesion and the interactions between the cells and the matrix, thus affecting cell morphology and resulting in the transduction of signals that can regulate cell differentiation (Guilak et al., 2009). Structurally, the ECM provides binding sites to neural cells and facilitates its organization into distinct CNS regions. Chemically, it is a source of diverse molecular signals that guide cellular growth, activity and survival. During CNS development, specific ECM components are dynamically regulated in a temporal and spatial manner to facilitate neurogenesis, neural cell migration and differentiation and axonal growth and guidance (Lau et al., 2013). The neural ECM of healthy brain tissue is a complex mixture of proteins, mainly composed by hyaluronan, proteoglycans (PGs) and tenascins (Fig. 1.3).

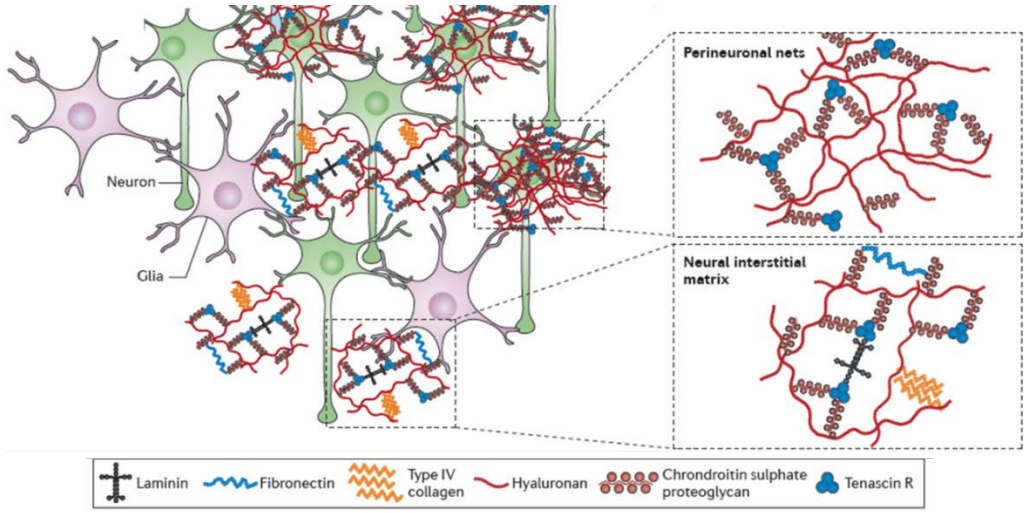

Figure 1.3: Major components of brain extracellular matrix (ECM). ECM components are mainly arranged into perineuronal nets that are condensed around cell bodies and dendrites of neurons or diffused as the neural interstitial matrix between cells of the brain parenchyma. Adapted from Lau et al. (2013).

The chondroitin sulfate PGs (CSPGs) aggrecan, versican, neurocan and brevican are the primary organizational component of the brain ECM. These PGs bind tenascin glycoproteins, which act as linkers and provide binding sites to the cells (Hopkins et al., 2015; Lau et al., 2013). Hyaluronan is a negatively charged glycosaminoglycan (GAG), thereby attracting cations and charged proteins and increasing the hydration of brain tissue (Hopkins et al., 2015). Brain ECM is distributed within the perineuronal nets (PNNs) and the neural interstitial matrix, which consists of ECM components in the brain parenchyma that are not as tightly associated as in the PNNs (Fig. 1.3) (Lau et al., 2013). PNNs compose most of the brain ECM and are a condensed layer of a mesh-like matrix consisting mainly in PGs, tenascin r and link proteins, located around neuronal cell bodies and proximal dendrites. PNNs prevent random synapse formation and are thought to be critical for synaptic plasticity (Hopkins et al., 2015; Lau et al., 2013). Enzymatic degradation of CSPGs or destabilization of PNNs was shown to enhance neuronal activity and synaptic plasticity after CNS injury (Soleman et al., 2013).

4. Culture strategies for CNS modelling and drug screening

Typical strategies for culturing neural cells for CNS modelling rely on monolayer systems (2D). These, although easy to manipulate, fail to recapitulate the *in vivo* microenvironment and lack the structural architecture of the tissue, in many cases precluding the establishment of physiologically-relevant cell-cell and cell-ECM interactions (Breslin and Driscoll, 2013; Fitzgerald et al., 2015; Picollet-D'hahan et al., 2016). Contrasting with 2D, three-dimensional (3D) culture systems allow cells to establish a network of cell-cell and cell-ECM interactions in all planes, which affects cell morphology, polarity, cell signaling and gene expression (Pampaloni et al., 2007).

As mentioned previously, precise control of stem cell differentiation and tissue architecture is essential for development, organogenesis and tissue homeostasis. 3D culture methods enable the formation of self-organizing tissue-like structures

that recapitulate key aspects of the tissue of origin, such as the presence of multiple differentiated cell types, cell migration and activation of developmental gene expression programs (Murrow et al., 2017). This 3D environment can be relevant not only for neuronal maturation, functionality and signaling, but also for the penetration and action of drugs (Kim et al., 2004), potentially improving the outcome of cell-based assays in drug screening.

A vast number of distinct 3D culture strategies have been developed and employed in the last years. Nonetheless, several limitations need to be circumvent to take advantage of the full potential of 3D cultures. The 3D culture strategies can be divided in two main categories: (1) scaffold-dependent cultures, employing scaffolds based on natural or synthetic biomaterials as cell supportive matrixes and (2) scaffold-free cultures, in which cells were allowed to self-assemble into aggregates without an exogenous matrix.

4.1. Scaffold-dependent cultures

Aiming at recreating the *in vivo* cues such as mimicking tissue structure, mechanical and biochemical properties, a wide range of synthetic and biologically-derived materials have been used as scaffolds for 3D culture (Pampaloni et al., 2007; Picollet-D'hahan et al., 2016). These are mainly hydrogels and include biologically inert polymers, such as alginate, agarose or chitosan, or biologically active polymers, such as collagen or hyaluronan (Picollet-D'hahan et al., 2016). Biological active external cues (e.g. RGD adhesion domains) can also be incorporated in the scaffold in order to further enhance cell adhesion to the matrix, cell migration, cell differentiation and cellular functions (Guilak et al., 2009). For example, by controlling the density of the ligand ephrin-B2 along a soluble biopolymer, NSC differentiation was enhanced *in vitro* and *in vivo*, and ephrin-B1 conjugates strongly enhance PSC differentiation toward a dopaminergic phenotype (Conway et al., 2013).

Two main strategies can be followed for cell incorporation in the scaffold: (1) cells are directly seeded in a pre-formed scaffold or (2) cells are encapsulated

within the scaffold material, allowing them to spontaneously organize. Both strategies have already been applied for 3D culture of neural cells and generation of neural tissue-like structures (Irons et al., 2008; Lancaster et al., 2013). More recently, the field has been extended to more sophisticated scaffolding methods that include microfabrication, microfluidics and 3D bioprinting (Picollet-D'hahan et al., 2016). The combination of cellular supporting matrices and microfluidics technology, which controls physical and chemical conditions (e.g. temperature, gas tension, medium and soluble factors composition and precise control of fluid flow and shear stress) at microscale level, allows the generation of organ-on-chip models (Sackmann et al., 2014). These can potentially enhance the differentiation, function, and long-term survival of many cell types. The 3D bioprinting approaches allow creating complex and layered scaffolds able to sustain cell survival, proliferation and neural differentiation (Devillard et al., 2014; Lozano et al., 2015). Although presenting a great potential in recreating the natural physical and structural environment of living tissues, biologically active scaffold components can profoundly affect the properties of the culture and cell phenotype, which can lead to confounding effects specially when modeling disease. Further, scaffold-dependent culture methods are difficult to control in terms of diffusion of gases and nutrients (Kelava and Lancaster, 2017; Ranga et al., 2016; Serra et al., 2012). These methods are laborious, require technical knowledge and equipment and the analysis of most biological readouts is challenging, making difficult its applicability in high-throughput screenings (Hopkins et al. 2015).

Ideal 3D scaffolds should provide native spatial arrangement, adequate biomechanical properties and biocompatibility. The mechanical properties of the scaffold should match the CNS tissue characteristics, not affect, or affect positively, cell differentiation and ensure efficient neurite outgrowth and neural connectivity. Cell culture on hydrogel surfaces with variable moduli indicated that softer gels (100–500 Pa) favour neuronal differentiation while harder gels (1–10 kPa) favour glial differentiation (Saha et al., 2008). Brain tissue stiffness *in vivo* is decreased in

neurodegenerative disorders such as AD so, when modeling disease, stiffer scaffolds should be chosen to better mimic the pathological state (Franze et al., 2013). Still, the ideal 3D scaffold cannot be defined due to the lack of knowledge on disease-induced ECM changes.

4.2. Scaffold-free cultures

Scaffold-free methods take advantage of the capability of some cell types to self-assemble into aggregates, without the support of an exogenous scaffold. This allows cells to produce their own ECM without the confounding effects of an exogenous matrix, which can overlook the biochemical and biophysical contribution of the endogenous ECM factors.

Conditions in which the adhesive forces between the cells are greater than for the substrate are required for cells to aggregate. Cell aggregation can be facilitated by buoyancy or stirring. Thus, cell spheroids can be generated in static systems by forced floating methods, such as low-adherence culture surfaces and hanging-drop methods, or in agitation-based culture systems, such as shake flasks, spinner flasks, rotary wall vessels and stirred-tank bioreactors.

In low adherence surfaces and in the hanging drop method, no adherence cue is provided to the cells, cell aggregation is forced and is strongly dependent on cell-cell contacts. Depending on the heterogeneity of the initial cell population and its aggregation capacity, some lack of reproducibility could exist and control of tissue size is difficult, while being also time-consuming and cumbersome aggregation methods (Picollet-D'hahan et al., 2016). Moreover, these systems provide low mass transfer properties and inherently it is difficult to maintain long-term cultures and the scalability of the system is very low, precluding many applications.

Agitation-based culture systems allow the generation of more homogenous cultures, presenting improved mass transfer properties over static culture systems. Cell aggregation is highly dependent not only on the cell type but also on system hydrodynamics. The geometry of the vessel, the stirring rate, and the type and size of the impeller are parameters that affect the culture hydrodynamics and,

therefore, are important to optimize when aiming at promoting cell aggregation and culturing aggregates (Kinney et al., 2011). The stirring creates shear, which may increase the number of cell-cell contacts and promote cell aggregation and aid in controlling the size of the aggregates (Kehoe et al., 2010). However, stirring can also subject the cells to shear stress, which can negatively impact cell physiology. To minimizing detrimental effects of shear stress, impellers able to suspend cells and mix the fluid gently and operating at lower stirrer speed were developed for PSC culture (Marks, 2003; Olmer et al., 2012).

Software-controlled stirred-tank bioreactors allow monitoring and controlling physical and chemical culture parameters, such as hydrodynamics, temperature, pH and dissolved oxygen. Furthermore, operation in a perfusion mode allows a stable flow of nutrients and differentiation/ neurotrophic factors, while clearing the cell debris and toxic byproducts at a controlled rate and maintaining the cells within the vessel (Simão et al., 2016). The major disadvantages of stirred tank bioreactors are the requirement for technical knowledge and specialized equipment, which is costly.

Efficient neuronal differentiation of PSC and NSC spheroids can be performed in scaffold-free 3D cultures, attaining increased neuronal differentiation efficiencies with reduced culture times, when compared to static 2D cultures (Chandrasekaran et al., 2017; Simão et al., 2014; Terrasso et al., 2015). We recently showed that iPSC-derived NSC cultured in a stirred suspension culture system self-assemble into aggregates, and differentiate into the three neural lineages, neurons, astrocytes and oligodendrocytes (Simão et al., 2016; Simão et al., 2018). Neurospheroids proteome and transcriptome dynamics revealed significant changes at cell membrane and ECM composition during neural differentiation, with an enrichment in PGs typical of brain ECM (Simão et al., 2018). These results demonstrate that iPSC-NSC 3D neural differentiation recapitulates extracellular space dynamics, with accumulation of endogenous ECM and secreted components and remodeling along differentiation.

With current advances in automation, microscopy imaging, and processing of large amount of data, cellular spheroids are being increasingly employed for *in vitro* drug testing and disease modelling. Spheroid aggregation can be easily automated in scalable agitation-based culture systems and, therefore, scaling-up cellular spheroid-based assays to feed high-throughput neurotoxicity testing platforms is feasible. Alternatively, to generate larger spheroid amounts, a scale-out approach can be followed simply multiplying the number of parallel cultures performed. This approach can be cost-, space- and labour-intensive but provides some advantages over scale-up approaches, such as the reduction of scale-up risks, better costs control and flexible process designs and validation strategies.

5. Brain i*n vitro* models for neuroscience research

Neuroscience research has relied on animal models for many years, with rodents being the most popular. However, as above mentioned, animals fail to precisely recapitulate the human pathophysiological state. There are differences between species and many human diseases result from complex interactions between genes and environmental factors that can not be recapitulated in animals, as referred in section 1. Additionally, animal models are not suitable for high-throughput screening platforms, precluding its use in early stage drug development.

The first human cell models used for neuroscience research were brain organotypic slice cultures or neuronal-like cell lines, mainly tumor-derived. Brain organotypic slices preserve cellular organization and architecture but post-mortem human tissue is scarce and the culture is technically difficult and highly variable (Walsh et al., 2005). Cell lines are a renewable source of neural-like cells and less complex models, technically easier to work with, but do not recapitulate the environmental features of native neurons, as discussed in section 2.2 above.

In recent years, there is growing evidence that combining PSC-derived neural cells combined with 3D culture strategies is a promising approach to develop new

brain cell models for disease modeling and drug discovery with higher physiological and pathophysiological relevance. While methods for neural induction of human PSC were developed, the field of the 3D cultures of human brain cells grew exponentially. Several 3D culture strategies have been explored with the ultimate goal of achieving the desired level of mimicry of specific features of the human brain. These include the generation of: brain organoids (cell aggregates embedded into Matrigel (Choi et al., 2014; Lancaster et al., 2013) or other synthetic matrices capable of support tissue morphogenesis (Ranga et al., 2016)), scaffold-free cultures of neural-like tissue in air-liquid interface (Preynat-Seauve et al., 2009), and the brain spheroids cultures (Birey et al., 2017; Paşca et al., 2015; Rigamonti et al., 2016; Simão et al., 2016).

Brain organoids are self-organized 3D structures derived from stem cells that can recapitulate multi-lineage differentiation and aspects of *in vivo* architecture, functionality and genetic signature of the original *in vivo* tissue (Dutta et al., 2017). Organoids can be derived from PSC, mimicking embryonic developmental processes, or from adult stem cells, as neural stem cells (Dutta et al., 2017; Murrow et al., 2017). Usually Matrigel is employed as extracellular supportive matrix. Several researchers have already generated brain organoids from human PSC, capable of recapitulating to some extent the composition, cell diversity and architecture of the fetal brain, to model diseases as microcephaly and infectious diseases (Lancaster et al., 2013; Qian et al., 2017). The spontaneous nature of organoids self-organization results in variability in morphology and composition between various areas of the tissue-like structure and between different batches, occasionally with formation of non-neural entities. This leads to issues with reproducibility and suitability for high-throughput screening with robust and reliable readouts (Kelava and Lancaster, 2017; Lancaster et al., 2013; Quadrato et al., 2017). To increase reproducibility and improve architecture of forebrain organoids, Lancaster and colleagues (2017) used poly(lactide-co-glycolide) copolymer (PLGA) fiber microfilaments as a floating scaffold to guide cell self-

organization and generate elongated EBs. Upon neural differentiation these modelled the radial organization of the cerebral cortex and allowed the study of neuronal migration (Lancaster et al., 2017). Individual organoids can reach up to 4 mm in diameter (Kelava and Lancaster, 2017), which is one of the major limitations of these 3D models; supply of oxygen and nutrients is insufficient to the center of the organoids, limiting the presence of healthy cells to the surface of the tissue. This is an important hurdle to overcome in the near future.

One of the disadvantages of these scaffold-dependent culture strategies is the use of Matrigel an extract of the ECM secreted by the Engelbreth-Holm-Swarm mouse sarcoma cell line, with characteristics similar to a basement membrane. This undefined matrix has low mechanical flexibility and high batch-to-batch variation and therefore can produce a source of variability in experimental results (Kleinman and Martin, 2005). Moreover, basement membrane properties are different from mature brain ECM, which contain low levels of basement membrane constituents collagen, laminin and fibronectin. Nowadays, synthetic matrices capable of support tissue morphogenesis are being developed to replace the widely used hydrogels such as Matrigel (Lemke et al., 2017; Ranga et al., 2016). Ranga and colleagues (2016) showed that defined modular synthetic 3D matrices can be used to explore the role of the ECM in the development of complex 3D neuroepithelial cysts. The authors demonstrated that key steps of early neural morphogenesis, such as the specification of cytoskeletal-mediated symmetry-breaking events that lead to neural tube-like patterning along the dorsal-ventral axis, can be precisely controlled by the extracellular microenvironment (Ranga et al., 2016).

Scaffold-free neural cultures have also been developed and improved in last years (Birey et al., 2017; Mariani et al., 2012; Paşca et al., 2015; Preynat-Seauve et al., 2009; Simão et al., 2016). An air-liquid interface-based culture for 3D PSC expansion and neural differentiation, spontaneously guided by endogenous developmental cues and in the absence of added growth factors, allowed generation of a neural-like tissue with an organization that resembles early

developing brain (Preynat-Seauve et al., 2009). Employing a method previously described for neural differentiation of ESC that involves formation of serum-free, floating EB-like, quick aggregates (SFEBq) (Eiraku et al., 2008) and a cell-replating step on Matrigel, Mariani and colleagues generated iPSC-derived 3D structures containing polarized RG, intermediate progenitors and layer-specific cortical neurons (Mariani et al., 2012). Further improvements generated a SFEBq neural 3D culture with organoid's transcriptome similar to those of the human dorsal telencephalon during early fetal development, recapitulating the second trimester of the developing forebrain (Mariani et al., 2015). These organoids were used to model ASD, employing iPSC derived from ASD patients. ASD organoids presented increased production of inhibitory neurons caused by increased FOXG1 gene expression, identifying this gene as a molecular signature of idiopathic ASD and a potential drug target (Mariani et al., 2015).

By combining the dual-Smad inhibition protocol with the SFEBq approach, eliminating the cell replating in Matrigel and maintaining the cell aggregates in floating conditions, Paşca and colleagues (2015) generated cortical and dorsal or ventral forebrain spheroids with multiple rosette-like structures and homogeneous morphology, able to differentiate into several neural and glial identities within a 3D context (Birey et al., 2017; Paşca et al., 2015). To recapitulate a more elaborated developmental process, the saltatory migration of interneurons observed in the fetal forebrain, the authors assembled the dorsal and ventral forebrain spheroids into 3D structures that they referred to as brain assembloids (Birey et al., 2017). Moreover, these brain assembloids were used to model Timothy syndrome, a neurodevelopmental disorder caused by mutations in the CaV1.2 calcium channel. The authors reported that interneurons displayed abnormal migratory saltations, which were not possible to detect in other 3D brain cell models that do not allow for the recapitulation of saltatory migration of interneurons (Birey et al., 2017).

In a different approach, our group employed agitation-based culture systems to promote cell aggregation and, upon neural differentiation, generate human

neurospheroids from fetal NPC (Simão et al., 2014) and from the NT2 cell line (Serra et al., 2009; Terrasso et al., 2015). We showed applicability of these neurospheroids for neurotoxicity testing and for modeling neural functionality and neuron-astrocyte interactions (Simão et al., 2018, 2016, 2014, Terrasso et al., 2017, 2015).

Further optimization of the available models is still required as the native microenvironment includes not only the endogenous ECM, but also other cell types, such as vascular and immune cells, which directly contribute to this microenvironment (Dutta et al., 2017). The embryonic brain begins to develop in the absence of vasculature, but later brain development requires blood vessels to provide a neural progenitor niche (McCauley and Wells, 2017). Mimicking vascular networks *in vitro* will provide not only oxygen and nutrients to the center of the *in vitro* tissue-like structures, even those with larger diameters, but also support neural differentiation by providing a basement membrane where neural cells can attach their basal processes, as occur *in vivo* (Kelava and Lancaster, 2017). Incorporation of microglia cells in the neural models will provide an opportunity to study the interactions between these cells and other neural cell types during brain development and understand the role of microglia in neurodegenerative diseases and drug action mechanisms. Recent reports point to the role of microglia in contributing both to tissue injury and repair. Several neurodegenerative disorders involve synapse loss and emerging evidence from mouse models suggest that microglia can mediate this loss (Hong and Stevens, 2016). It is becoming increasingly recognised that microglial aging and senescence is linked to functional changes that can contribute to the development of dystrophic microglia and an increase of microglia-mediated neuroinflammatory responses, which in turn can contribute to the progression of neurodegenerative diseases such as AD, PD, and ALS (Hong and Stevens, 2016; Spittau, 2017). For example, in AD context, any loss or decrease in phagocytic ability of microglial cells would result in the extracellular accumulation of AD-related β-amyloid proteins (Flanary, 2005; Michell-Robinson et

al., 2015). Recently, the generation of microglia-like cells from PSC has been described and these cells have been incorporated in a 3D organotypic neural environment, responding to cellular damage (Muffat et al., 2016) and providing new tools to study the role of microglia in disease.

The onset of most neurodegenerative diseases occurs during the later stages of life, with exception to familiar forms in which a particular mutation reduces the age of onset. The challenges to model sporadic diseases are enormous. Currently, to mimic *in vitro* late onset sporadic neurodegenerative diseases, exogenous chemicals are used to induce cellular stress and/ or aging. However, this may also induce mutational changes and lead to changes in cell phenotype that are not disease-related, affecting the recapitulative capacity of the model (Payne et al., 2015). Thus, other of the major challenges the field is facing is to improve the maturity and aging of the neural cell types differentiated *in vitro*. It is essential to develop strategies to further mature 3D brain tissue-like structures to allow the generation of endogenous cellular diversity with truly mature and functional neuronal networks that will age along culture time. This will allow the study of brain functions that rely on complex cellular interactions and mature and functional neural networks as well as late-onset diseases.

Essentially, when generating new model systems for neuroscience research, it is extremely important to take into account the balance between complexity and heterogeneity and the desired goal. Simpler and homogeneous model systems, easier to scale-up, are more suited for screening approaches while more complex systems are more suited to perform neurobiological studies, where the recapitulation of the interactions between several cell types and the microenvironment is essential for the recreation of the pathophysiology.

6. Lysosomal storage diseases – Mucopolysaccharidosis type VII

LSD are a group of over 50 rare metabolic disorders caused by lysosomal dysfunction and genetically inherited, mostly as autosomal recessive traits.

Lysosomal dysfunction is mainly due to the absence or deficiency of a lysosomal enzyme; defects in the post-translational modifications, in the metabolic trafficking or in the activity of the lysosomal enzyme can occur (Borger et al., 2017; Khan et al., 2016; Lemonnier et al., 2011). These defects can lead to numerous metabolic alterations, including storage of undigested metabolic products and impaired endocytosis, sorting, digestion of cellular and extracellular products and exocytosis (Alroy et al., 2014a; Vitner et al., 2010). Further, interruption of intracellular trafficking can result in a variety of pathogenic cascades, including alteration of calcium homeostasis, oxidative stress, inflammation and altered autophagy (Alroy et al., 2014b; Vitner et al., 2010). LSD generally occur at a frequency of 1 in 4000 live births (Borger et al., 2017) and represent the major cause of neurodegeneration in infants and children (Lemonnier et al., 2011). Near two thirds of LSD patients present some neurological defect, although the clinical manifestations are heterogeneous and defects appear at different ages and progress at different rates (Fraldi et al., 2016). LSD have been a major focus of rare disease research, with a growing interest due the recent evidence implicating lysosomal dysfunction in aging and age-related neurodegenerative diseases (Carmona-Gutierrez et al., 2016; Fraldi et al., 2016). Clinical features depend on the cell types affected and the organs involved and the level of residual enzyme activity. LSD are classified according to the major storage compound, thus disorders with accumulation of glycosaminoglycan fragments are classified as mucopolysaccharidoses, and those dominated by lipid storage as lipidoses. More than 30 % of all lysosomal diseases are MPS and there are nine subtypes of MPS described, each caused by a deficiency in one of the enzymes responsible for the stepwise degradation of GAGs (Fig. 1.4).

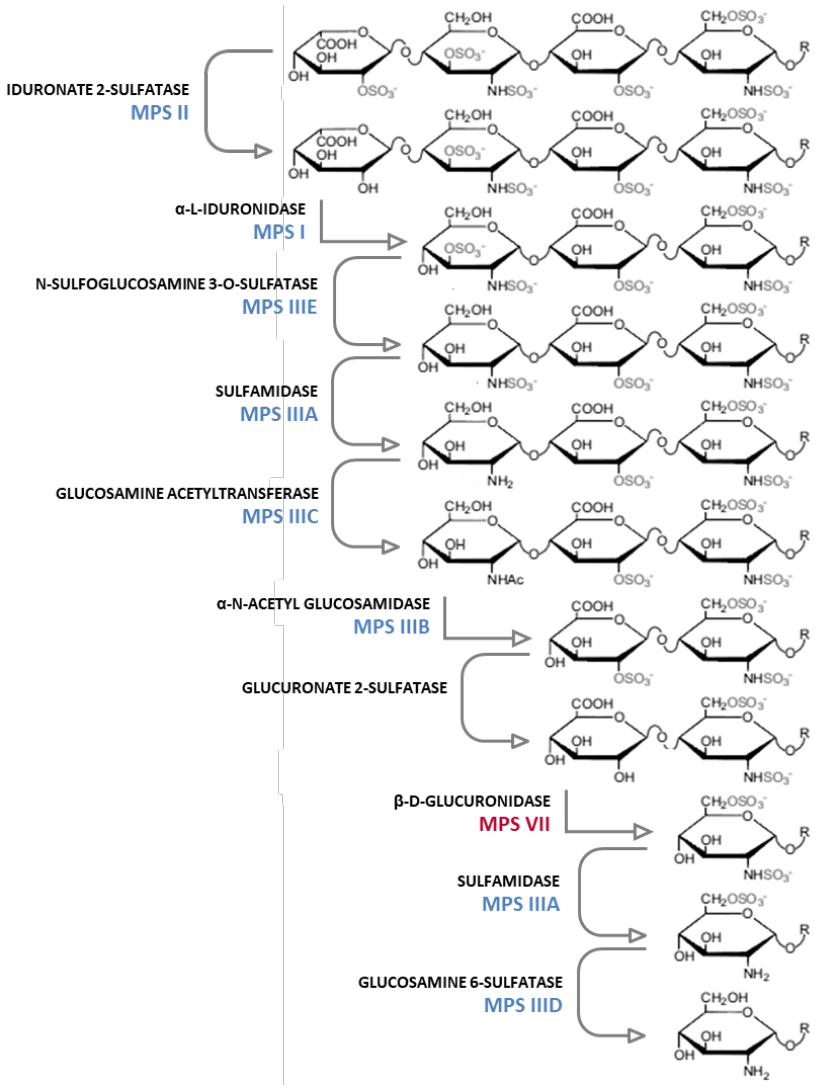

Figure 1.4: Stepwise degradation of glycosaminoglycans (GAGs). Example of heparan sulfate catabolism. The scheme illustrates the 9 enzymatic activities required for the sequential catabolism of GAGs to lead to a complete degradation of its chain. The deficiency in the activity of one of these enzymes generates a pathological condition called mucopolysaccharidosis (MPS, in blue). There are 9 different MPS, depending on the deficient enzyme. MPS VII (in red) is caused by a deficiency in β-D-glucuronidase. Adapted from Kowalewski et al.(2012).

MPS type VII (MPS VII; Sly syndrome) is an ultra-rare neuronopathic form of MPS, with an estimated frequency of ~1: 2 000 000. It has an autosomal recessive inheritance pattern and is characterized by a deficiency in the activity of β-D-glucuronidase (β-gluc; EC 3.2.1.31; Fig 1.4) (Montaño et al., 2016; Tomatsu et al., 2009). Most patients with MPS VII have cognitive impairment,

hepatosplenomegaly, cardiac abnormalities, recurrent pulmonary infections, skeletal dysplasia and early death. However, the phenotypic consequences in patients are extremely variable, ranging from late-onset milder forms with fewer manifestations, mild skeletal abnormalities and near-normal intelligence to early-onset severe forms with non-immune hydrops fetalis at birth and a few months of life expectancy (Montaño et al., 2016; Tomatsu et al., 2009). Up to now, 49 disease-causing mutations have been identified along the β-GUS gene and these include mainly missense mutations, but also nonsense mutations, deletions and splice-site mutations (Khan et al., 2016; Montaño et al., 2016). β-gluc catalyses the hydrolysis of β-D-glucuronic acid residues from the non-reducing terminal of GAGs (Khan et al., 2016) (Fig. 1.4). Deficient β-gluc activity leads to the progressive abnormal accumulation of partially degraded chondroitin sulfate, dermatan sulfate and heparan sulfate GAGs within the lysosomes of the majority of the cell types, affecting many tissues, including the brain (Montano et al., 2016). In the brain, GAGs accumulation is followed by the secondary accumulation of GM2 and GM3 gangliosides (Archer et al., 2014). While no clear connection was established between the primary lysosomal accumulation of GAGs and the secondary accumulation of GM2 and GM3 gangliosides it is possible that GAGs accumulation can lead to the overall dysfunction of the lysosomal system and to the storage of multiple substrates and several mechanisms can be hypothesized. These could include alterations in normal trafficking or fusion of vesicles, which can result in a compromised movement of a variety of materials for further degradation or the inhibition of lysosomal enzymes by the accumulating GAGs or by other changes in lysosomal environment, such as a pH alteration, leading to reduced degradation of additional substrates.

In addition to lysosomal GM2 and GM3 gangliosides accumulation, there are several other secondary pathological processes that have been identified in MPS, including disturbance of the vesicular network (e.g. blocking of autophagy and secondary storage of misfolded proteins, endosomal-lysosomal fusion, altered

vesicle trafficking), of the mitochondrial function (oxidative stress, apoptosis), and of the signalling response (TLR4, TGF-β pathway) and inflammation (cytokines, chemokines), amongst others (Plotegher and Duchen, 2017; Salazar et al., 2016). GAGs breakdown products could activate TLR4 signalling pathway due to its structural similarity with the canonical ligand of TLR4, LPS, thus inducing a pro-inflammatory response and the release of cytokines such as MIP1α and TNFα (Ballabio and Gieselmann, 2009; Xing et al., 2015).

During many years palliative therapies were the only resource for MPS VII patients. Intravenous enzyme replacement therapies (ERT) were alternatives to change the course of the mild phenotype of the disease in mouse models and in human clinical trials, while requiring infusions at regular intervals and not appropriately addressing all disease phenotypes and being ineffective in some organs, including the brain (Giugliani et al., 2016; Montaño et al., 2016). In 2017, FDA approved MEPSEVII from UltraGenix, a recombinant human β-GUS replacement therapy for MPS VII. Nevertheless, ERT has no impact on the neuronopathic phenotypes, as the infused recombinant enzyme is unable to cross the blood-brain barrier (BBB; Borger et al., 2017). Therefore, the treatment of neurological defects associated with MPS VII still representing an unmet medical need (Giugliani et al., 2016; Montaño et al., 2016). Gene therapy represents the ultimate treatment for monogenic diseases and several studies demonstrated positive effects in MPS VII. It has been shown that intracerebral injections of adeno-associated vectors (Giugliani et al., 2016) or canine adenovirus (Ariza et al., 2014; Cubizolle et al., 2013) could reverse cognitive impairment. The potential of *ex vivo* gene therapy was also recently demonstrated by the transplant of genetically corrected NSC differentiated *in vitro* from iPSC isolated from a MPS VII patient in a mouse model of MPS VII (Griffin et al., 2015).

Whereas the primary effects of MPS disorders are well described, the limitation of the current animal models hampered the study of cascades of events downstream to GAGs accumulation, which can lead to more deleterious effects.

Thus, the development of novel disease-relevant human models that better mimic human brain cells and its interactions and microenvironment has the potential to provide further insight to the mechanisms of disease onset and progression and new tools to accurately identify potential therapeutic targets and evaluate promising drug candidates.

7. Aims and Scope of the thesis

The development of 3D cell models that recapitulate features of the human brain can potentially contribute to unveil specific neurological disease mechanisms, to identify potential therapeutic targets and to accurately evaluate promising drug candidates. The main goal of this thesis was the development, characterization and interrogation of 3D neural cell models for disease modeling and drug discovery, in which phenotypic and functional features of human brain tissue would be recapitulated, namely functional neuron-astrocytes interactions (Fig 1.5). We hypothesized that (1) concomitant neuronal and astrocytic differentiation in a 3D context would allow neural cells to mature and establish functional neuron-astrocyte interactions, generating complex 3D networks; and (2) the establishment of neuron-astrocyte interactions would contribute to recapitulate disease mechanisms in which those have impact. Therefore, this thesis focused on 3D neural differentiation of human stem cells, exploring agitation-based cultured systems to promote stem cell aggregation and concomitant differentiation in to neuronal and astrocytic lineages.

In **Chapter 2**, we employed the NT2 cell line for the establishment of a differentiation strategy to obtain a co-culture of neurons and astrocytes (neurospheroids), building up on a bioprocess for 3D neuronal differentiation previously implemented at our laboratory. The process was optimized to achieve mature and functional cells, as demonstrated by the establishment of neuron-astrocyte interactions. Furthermore, gene expression and functionality endpoints

were implemented to distinguish between neuronal and astrocytic toxicity within neurospheroids.

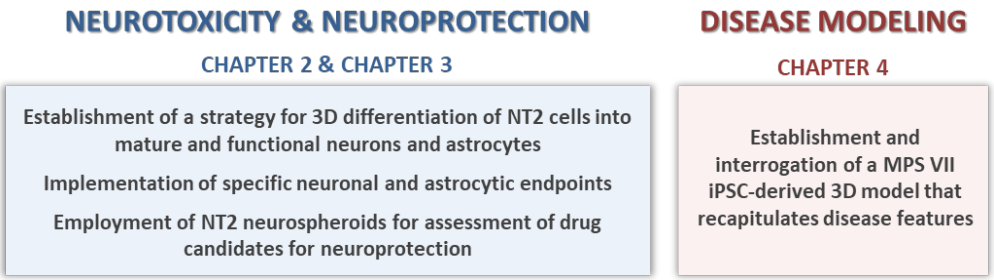

Figure 1.5: Thesis aims and its discrimination by chapter. NT2 – Ntera2/ clone D1 cell line; MPS VII – Mucopolysaccharidosis type VII; iPSC-NPC – induced pluripotent stem cells-derived neural progenitor cells.

In **Chapter 3**, the applicability of NT2 neurospheroids to assess the neuroprotective effect of drug candidates was evaluated. The implementation of an *in vitro* neuroprotection assay, which combines neurospheroid culture with a cell viability endpoint, is described and several drug candidates were tested as a proof-of-concept.

In **Chapter 4** the goal was to establish and interrogate a disease model in which establishment of neuron-astrocyte interactions would potentially contribute to the recapitulation of disease features. MPS VII patient-derived iPSC were used as cell source for neural differentiation. The recapitulation of disease features, neural gene expression and neuronal network functionality were evaluated in MPS VII neurospheroids.

Finally, in **chapter 5**, results obtained along this work were further discussed, integrating thesis outcomes with state-of-the-art literature in the fields addressed throughout the previous chapters.

8. References

Abbott, N.J., Rönnbäck, L., Hansson, E., 2006. Astrocyte–endothelial interactions at the blood–brain barrier. Nat. Rev. Neurosci. 7, 41–53. doi:10.1038/nrn1824

Allen, N.J., Barres, B.A., 2009. Glia — more than just brain glue. Neuroscience 457, 675–677.

Alroy, J., Garganta, C., Wiederschain, G., 2014a. Secondary biochemical and morphological

consequences in lysosomal storage diseases. Biochemistry 79, 619–636. doi:10.1134/S0006297914070049

Alroy, J., Garganta, C., Wiederschain, G., 2014b. Secondary biochemical and morphological consequences in lysosomal storage diseases. Biochemistry 79, 619–636. doi:10.1134/S0006297914070049

Amaral, A.I., Meisingset, T.W., Kotter, M.R., Sonnewald, U., 2013. Metabolic aspects of neuron-oligodendrocyte-astrocyte interactions. Front. Endocrinol. 4.

Archer, L.D., Langford-Smith, K.J., Bigger, B.W., Fildes, J.E., 2014. Mucopolysaccharide diseases: A complex interplay between neuroinflammation, microglial activation and adaptive immunity. J. Inherit. Metab. Dis. 37, 1–12. doi:10.1007/s10545-013-9613-3

Arias-Fuenzalida, J., Jarazo, J., Qing, X., Walter, J., Gomez-Giro, G., Nickels, S., Zaehres, H., Scholer, H., Schwamborn, J., 2017. FACS-Assisted CRISPR-Cas9 Genome Editing Facilitates Parkinson's Disease Modeling. Stem Cell Reports 9, 1423–1431. doi:http://dx.doi.org/10.1016/j.stemcr.2017.08.026

Ariza, L., Giménez-Llort, L., Cubizolle, A., Pagès, G., García-Lareu, B., Serratrice, N., Cots, D., Thwaite, R., Chillón, M., Kremer, E.J., Bosch, A., 2014. Central Nervous System Delivery of Helper-Dependent Canine Adenovirus Corrects Neuropathology and Behavior in Mucopolysaccharidosis Type VII Mice. Hum. Gene Ther. 25, 199–201. doi:10.1089/hum.2013.152

Ballabio, A., Gieselmann, V., 2009. Lysosomal disorders: from storage to cellular damage. Biochim. Biophys. Acta 1793, 684–696.

Bang, O.Y., Kim, E.H., Cha, J.M., Moon, G.J., 2016. Adult Stem Cell Therapy for Stroke: Challenges and Progress. J. Stroke 18, 256–266. doi:10.5853/jos.2016.01263

Bani-Yaghoub, M., Felker, J.M., Naus, C.C.G., 1999. Human NT2/D1 cells differentiate into functional astrocytes. Neuroreport 10, 3843–3846. doi:10.1097/00001756-199912160-00022

Birey, F., Andersen, J., Makinson, C., Islam, S., Wei, W., Huber, N., Fan, H., Metzler, K., Panagiotakos, G., Thom, N., O'Rourke, N., Steinmetz, L., Bernstein, J., J, H., JR, H., Pașca, S., 2017. Assembly of functionally integrated human forebrain spheroids. Nature. doi:10.1038/nature22330

Borger, D.K., McMahon, B., Roshan Lal, T., Serra-Vinardell, J., Aflaki, E., Sidransky, E., 2017. Induced pluripotent stem cell models of lysosomal storage disorders. Dis. Model. Mech. 10, 691–704. doi:10.1242/dmm.029009

Breier, J.M., Radio, N.M., Mundy, W.R., Shafer, T.J., 2008. Development of a high-throughput screening assay for chemical effects on proliferation and viability of immortalized human neural progenitor cells. Toxicol. Sci. 105, 119–33. doi:10.1093/toxsci/kfn115

Brennand, K.J., Simone, A., Jou, J., Gelboin-Burkhart, C., Tran, N., Sangar, S., Li, Y., Mu, Y., Chen, G., Yu, D., McCarthy, S., Sebat, J., Gage, F.H., 2011. Modelling schizophrenia using human induced pluripotent stem cells. Nature 473, 221–225. doi:10.1038/nature09915

Breslin, S., Driscoll, L.O., 2013. Three-dimensional cell culture : the missing link in drug discovery. Drug Discov. Today 18, 240–249.

Breslin, S., O'Driscoll, L., 2013. Three-dimensional cell culture: the missing link in drug discovery. Drug Discov. Today 18, 240–9. doi:10.1016/j.drudis.2012.10.003

Briggs, J., Sun, J., Shepherd, J., ..., Wolvetang, E., 2013. Integration-Free Induced Pluripotent Stem Cells Model Genetic and Neural Developmental Features of Down Syndrome Etiology. Stem Cells 31, 467–478. doi:10.1002/ stem.1297

Brodal, P., 2010. The Central Nervous System: Structure and Function. Oxford University Press.

Byrne, J., Heidelberger, R., Waxham, M., Byrne, J., Roberts, J., 2009. From Molecules to Networks: An Introduction to Cellular and Molecular Neuroscience. Academic Press.

Caiazzo, M., Dell'Anno, M.T., Dvoretskova, E., Lazarevic, D., Taverna, S., Leo, D., Sotnikova, T.D., Menegon, A., Roncaglia, P., Colciago, G., Russo, G., Carninci, P., Pezzoli, G., Gainetdinov, R.R., Gustincich, S., Dityatev, A., Broccoli, V., 2011. Direct generation of functional dopaminergic neurons from mouse and human fibroblasts. Nature 476, 224–227. doi:10.1038/nature10284

Caiazzo, M., Giannelli, S., Valente, P., Lignani, G., Carissimo, A., Sessa, A., Colasante, G., Bartolomeo, R., Massimino, L., Ferroni, S., Settembre, C., Benfenati, F., Broccoli, V., 2015. Direct Conversion of Fibroblasts into Functional Astrocytes by Defined Transcription Factors. Stem Cell Reports 4, 25–36. doi:http://dx.doi.org/10.1016/j.stemcr.2014.12.002

Calcoen, D., Elias, L., Yu, X., 2015. What does it take to produce a breakthrough drug? Nat. Rev. Drug Discov. 14, 161–162.

Canals, I., Soriano, J., Orlandi, J.G., Torrent, R., Richaud-Patin, Y., Jiménez-Delgado, S., Merlin, S., Follenzi, A., Consiglio, A., Vilageliu, L., Grinberg, D., Raya, A., 2015. Activity and high-order effective connectivity alterations in sanfilippo C patient-specific neuronal networks. Stem Cell Reports 5, 546–557. doi:10.1016/j.stemcr.2015.08.016

Carmona-Gutierrez, D., Hughes, A.L., Madeo, F., Ruckenstuhl, C., 2016. The crucial impact of lysosomes in aging and longevity. Ageing Res. Rev. 32, 2–12. doi:10.1016/j.arr.2016.04.009

Chambers, S.M., Craft, C.A., Papapetrou, E.P., Tomishima, M., Sadelain, M., Studer, L., 2009. Highly efficient neural conversion of human ES and iPS cells by dual inhibition of SMAD signaling. Nat Biotechnol 27, 275–280.

Chandrasekaran, A., Avci, H.X., Ochalek, A., Rösingh, L.N., Molnár, K., László, L., Bellák, T., Téglási, A., Pesti, K., Mike, A., Phanthong, P., Bíró, O., Hall, V., Kitiyanant, N., Krause, K.-H.,

Kobolák, J., Dinnyés, A., 2017. Comparison of 2D and 3D neural induction methods for the generation of neural progenitor cells from human induced pluripotent stem cells. Stem Cell Res. 25, 139–151. doi:10.1016/j.scr.2017.10.010

Choi, S., Kim, Y., Hebisch, M., Sliwinski, C., Lee, S., D'Avanzo, C., Chen, H., Hooli, B., Asselin, C., Muffat, J., Klee, J., Zhang, C., Wainger, B., Peitz, M., Kovacs, D., Woolf, C., Wagner, S., Tanzi, R., Kim, D., 2014. A three-dimensional human neural cell culture model of Alzheimer's disease. Nature 515, 274–278. doi:10.1038/nature13800

Choi, S.H., Tanzi, R.E., 2012. iPSCs to the rescue in Alzheimer's research. Cell Stem Cell 10, 235–6. doi:10.1016/j.stem.2012.02.011

Choi, Y., Kwak, E., Lee, J., Lee, Y., Cheong, I., Lee, H.J., Kim, S., Kim, M., Kwon, Y., Chun, W., 2011. Cytoprotective Effects of Docosyl Cafferate against tBHP- Induced Oxidative Stress in SH-SY5Y Human Neuroblastoma Cells 19, 195–200. doi:10.4062/biomolther.2011.19.2.195

Conti, L., Cattaneo, E., 2010. Neural stem cell systems: physiological players or *in vitro* entities? Nat. Rev. Neurosci. 11, 176–87. doi:10.1038/nrn2761

Conway, A., Vazin, T., Spelke, D.P., Rode, N.A., Healy, K.E., Kane, R.S., Schaffer, D. V., 2013. Multivalent ligands control stem cell behaviour *in vitro* and *in vivo*. Nat. Nanotechnol. 8, 831–838. doi:10.1038/nnano.2013.205

Coyle, D.E., Li, J., Baccei, M., 2011. Regional differentiation of retinoic acid-induced human pluripotent embryonic carcinoma stem cell neurons. PLoS One 6, e16174. doi:10.1371/journal.pone.0016174

Cubizolle, A., Serratrice, N., Skander, N., Colle, M.-A., Ibanes, S., Gennetier, A., Bayo-Puxan, N., Mazouni, K., Mennechet, F., Joussemet, B., Cherel, Y., Lajat, Y., Vite, C., Bernex, F., Kalatzis, V., Haskins, M.E., Kremer, E.J., 2013. Corrective GUSB transfer to the canine mucopolysaccharidosis VII brain. Mol. Ther. 181, 22–31. doi:10.1038/mt.2013.283

Cummings, J.L., Morstorf, T., Zhong, K., 2014. Alzheimer ' s disease drug-development pipeline : few candidates , frequent failures. Alzheimer's Res. Ther. 6, 1–7.

Darbinyan, A., Kaminski, R., White, M., Darbinian, N., Khalili, K., 2013. Isolation and propagation of primary human and rodent embryonic neural progenitor cells and cortical neurons. Methods Mol Bio 1078, 45–54. doi:10.1007/ 978-1-62703-640-5_5

Darmanis, S., Sloan, S.A., Zhang, Y., Enge, M., Caneda, C., Shuer, L.M., Hayden Gephart, M.G., Barres, B.A., Quake, S.R., 2015. A survey of human brain transcriptome diversity at the single cell level. Proc. Natl. Acad. Sci. 112, 201507125. doi:10.1073/pnas.1507125112

Del Barrio, L., Martín-de-Saavedra, M.D., Romero, A., Parada, E., Egea, J., Avila, J., McIntosh, J.M., Wonnacott, S., López, M.G., 2011. Neurotoxicity induced by okadaic acid in the human neuroblastoma SH-SY5Y line can be differentially prevented by α7 and β2* nicotinic stimulation. Toxicol. Sci. 123, 193–205. doi:10.1093/toxsci/kfr163

DeRosa, B., Van Baaren, J., Dubey, G., Vance, J., Pericak-Vance, M., Dykxhoorn, D., 2010. Derivation of autism spectrum disorder-specific induced pluripotent stem cells from peripheral blood mononuclear cells. Neurosci Lett. 516, 9–14. doi:10.1016/j.neulet.2012.02.086

Devillard, R., Pagès, E., Correa, M.M., Kériquel, V., Rémy, M., Kalisky, J., Ali, M., Guillotin, B., Guillemot, F., 2014. Cell patterning by laser-assisted bioprinting. Methods Cell Biol. 119, 159–74. doi:10.1016/B978-0-12-416742-1.00009-3

Dhara, S.K., Stice, S.L., 2008. Neural differentiation of human embryonic stem cells. J. Cell. Biochem. 105, 633–40. doi:10.1002/jcb.21891

DiLuca, M., Olesen, J., Gustavsson, A., McDaid, D., Ersek, K., Georges, J., Gulácsi, L., Karpati, K., Kenigsberg, P., Valtonen, H., Group, C., al., et, 2014. The Cost of Brain Diseases: A Burden or a Challenge? Neuron 82, 1205–1208. doi:10.1016/j.neuron.2014.05.044

Dodel, R., Balakrishnan, K., Keyvani, K., Deuster, O., Neff, F., Andrei-Selmer, L.-C., Roskam, S., Stuer, C., Al-Abed, Y., Noelker, C., Balzer-Geldsetzer, M., Oertel, W., Du, Y., Bacher, M., 2011. Naturally Occurring Autoantibodies against -Amyloid: Investigating Their Role in Transgenic Animal and *In Vitro* Models of Alzheimer's Disease. J. Neurosci. 31, 5847–5854. doi:10.1523/JNEUROSCI.4401-10.2011

Donato, R., Miljan, E., Hines, S., Aouabdi, S., Pollock, K., Patel, S., Edwards, F., Sinden, J., 2007. Differential development of neuronal physiological responsiveness in two human neural stem cell lines. BMC Neurosci. 8. doi:10.1186/1471-2202-8-36

Doudna, J.A., Charpentier, E., 2014. Genome editing. The new frontier of genome engineering with CRISPR-Cas9. Science (80). 346, 1258096–1258096. doi:http://dx.doi.org/10.1126/science.1258096

Dutta, D., Heo, I., Clevers, H., 2017. Disease Modeling in Stem Cell-Derived 3D Organoid Systems. Trends Mol. Med. 23, 393–410. doi:10.1016/j.molmed.2017.02.007

Efremova, L., Schildknecht, S., Adam, M., Pape, R., Gutbier, S., Hanf, B., Bürkle, A., Leist, M., 2015. Prevention of the degeneration of human dopaminergic neurons in an astrocyte co-culture system allowing endogenous drug metabolism. Br. J. Pharmacol. 172, 4119–4132. doi:10.1111/bph.13193

Eiraku, M., Watanabe, K., Matsuo-Takasaki, M., Kawada, M., Yonemura, S., Matsumura, M., Wataya, T., Nishiyama, A., Muguruma, K., Sasai, Y., 2008. Self-organized formation of polarized cortical tissues from ESCs and its active manipulation by extrinsic signals. Cell Stem Cell 3, 519–532.

Fang, B., Jia, L., Jia, J., 2006. Chinese Presenilin-1 V97L mutation enhanced Abeta42 levels in SH-SY5Y neuroblastoma cells. Neurosci Lett. 406, 33–37.

Fernandes, T.G., Duarte, S.T., Ghazvini, M., Gaspar, C., Santos, D.C., Porteira, A.R., Rodrigues, G.M.C., Haupt, S., Rombo, D.M., Armstrong, J., Sebastião, A.M., Gribnau, J.,

Garcia-Cazorla, À., Brüstle, O., Henrique, D., Cabral, J.M.S., Diogo, M.M., 2015. Neural commitment of human pluripotent stem cells under defined conditions recapitulates neural development and generates patient-specific neural cells. Biotechnol. J. 10, 1578–1588. doi:10.1002/biot.201400751

Fitzgerald, K., Malhotra, M., Curtinb, C., O' Brien, F., O' Driscoll, C., 2015. Life in 3D is never flat: 3Dmodels to optimise drug delivery. J. Control. Release 215, 39–54. doi:http://dx.doi.org/10.1016/j.jconrel.2015.07.020

Flanary, B., 2005. The role of microglial cellular senescence in the aging and Alzheimer diseased brain. Rejuvenation Res 8, 82–85.

Fraldi, A., Klein, A.D., Medina, D.L., Settembre, C., 2016. Brain Disorders Due to Lysosomal Dysfunction. Annu. Rev. Neurosci. 39, 277–295. doi:10.1146/annurev-neuro-070815-014031

Franze, K., Janmey, P., Guck, J., 2013. Mechanics in neuronal development and repair. Annu. Rev. Biomed. Eng. 15, 227–251.

Gerrard, L., Rodgers, L., Cui, W., 2005. Differentiation of Human Embryonic Stem Cells to Neural Lineages in Adherent Culture by Blocking Bone Morphogenetic Protein Signaling. Stem Cells 23, 1234–1241. doi:10.1634/stemcells.2005-0110

Giugliani, R., Federhen, A., Vairo, F., Vanzella, C., Pasqualim, G., da Silva, L.M.R., Giugliani, L., de Boer, A.P.K., de Souza, C.F.M., Matte, U., Baldo, G., 2016. Emerging drugs for the treatment of mucopolysaccharidoses. Expert Opin. Emerg. Drugs 21, 9–26. doi:10.1517/14728214.2016.1123690

Goodfellow, C.E., Graham, S.E., Dragunow, M., Glass, M., 2011. Characterization of NTera2/D1 cells as a model system for the investigation of cannabinoid function in human neurons and astrocytes. J. Neurosci. Res. 89, 1685–97. doi:10.1002/jnr.22692

Griffin, T., Anderson, H., Wolfe, J., 2015. Ex Vivo Gene Therapy Using Patient iPSC-Derived NSCs Reverses Pathology in the Brain of a Homologous Mouse Model. Stem Cell Reports 8, 831–842. doi:10.1016/j.stemcr.2017.02.007

Guilak, F., Cohen, D.M., Estes, B.T., Gimble, J.M., Liedtke, W., Chen, C.S., 2009. Control of stem cell fate by physical interactions with the extracellular matrix. Cell Stem Cell 5, 17–26. doi:10.1016/j.stem.2009.06.016

Gupta, K., Patani, R., Baxter, P., Serio, a, Story, D., Tsujita, T., Hayes, J.D., Pedersen, R. a, Hardingham, G.E., Chandran, S., 2012. Human embryonic stem cell derived astrocytes mediate non-cell-autonomous neuroprotection through endogenous and drug-induced mechanisms. Cell Death Differ. 19, 779–87. doi:10.1038/cdd.2011.154

Hargis, E., Blalock, E., 2018. Transcriptional signatures of brain aging and Alzheimer's disease: What are our rodent models telling us? Behav. Brain Res. 322, 311–328. doi:https://doi.org/10.1016/j.bbr.2016.05.007

Harper, S., 2014. Economic and social implications of aging societies. Science (80-.). 346, 587–91. doi:10.1126/science.1254405

Hay, M., Thomas, D.W., Craighead, J.L., Economides, C., Rosenthal, J., 2014. Clinical development success rates for investigational drugs. Nat. Biotechnol. 32, 40–51.

Higuchi, T., Kawagoe, S., Otsu, M., Shimada, Y., Kobayashi, H., 2014. The generation of induced pluripotent stem cells (iPSCs) from patients with infantile and late-onset types of Pompe disease and the effects of treatment with acid- α -glucosidase in Pompe iPSCs. Mol. Genet. Metab. 112, 44–48. doi:10.1016/j.ymgme.2014.02.012

Hill, E.J., Jiménez-González, C., Tarczyluk, M., Nagel, D. a, Coleman, M.D., Parri, H.R., 2012. NT2 derived neuronal and astrocytic network signalling. PLoS One 7, e36098. doi:10.1371/journal.pone.0036098

Hill, E.J., Woehrling, E.K., Prince, M., Coleman, M.D., 2008. Differentiating human NT2/D1 neurospheres as a versatile *in vitro* 3D model system for developmental neurotoxicity testing. Toxicology 249, 243–50. doi:10.1016/j.tox.2008.05.014

Hockemeyer, D., Jaenisch, R., 2016. Induced Pluripotent Stem Cells Meet Genome Editing. Cell Stem Cell 18, 573–586. doi:http://dx.doi.org/10. 1016/j.stem.2016.04.013

Hong, S., Stevens, B., 2016. Microglia: Phagocytosing to Clear, Sculpt, and Eliminate. Devlopmental cell 38, 126–128. doi:http://dx.doi.org/10.1016/j.devcel.2016.07.006

Hopkins, A.M., DeSimone, E., Chwalek, K., Kaplan, D.L., 2015. 3D *in vitro* modeling of the central nervous system. Prog. Neurobiol. 125, 1–25. doi:10.1016/j.pneurobio.2014.11.003

Humpel, C., 2015. Organotypic brain slices cultures: a review. Neuroscience 305, 86–98. doi:10.1016/j.neuroscience.2015.07.086.

Irons, H.R., Cullen, D.K., Shapiro, N.P., Lambert, N. a, Lee, R.H., Laplaca, M.C., 2008. Three-dimensional neural constructs: a novel platform for neurophysiological investigation. J. Neural Eng. 5, 333–41. doi:10.1088/1741-2560/5/3/006

Israel, M. a, Yuan, S.H., Bardy, C., Reyna, S.M., Mu, Y., Herrera, C., Hefferan, M.P., Van Gorp, S., Nazor, K.L., Boscolo, F.S., Carson, C.T., Laurent, L.C., Marsala, M., Gage, F.H., Remes, A.M., Koo, E.H., Goldstein, L.S.B., 2012. Probing sporadic and familial Alzheimer's disease using induced pluripotent stem cells. Nature 482, 216–20. doi:10.1038/nature10821

Jakel, R.J., Schneider, B.L., Svendsen, C.N., 2004. Using human neural stem cells to model neurological disease. Nat. Rev. Genet. 5, 136–144. doi:10.1038/nrg1268

Jones, V.C., Atkinson-Dell, R., Verkhratsky, A., Mohamet, L., 2017. Aberrant iPSC-derived human astrocytes in Alzheimer's disease. Cell Death Dis. 8, 1–11. doi:10.1038/cddis.2017.89

Kehoe, D.E., Jing, D., Lock, L.T., Tzanakakis, E.S., Ph, D., 2010. Scalable Stirred-Suspension Bioreactor Culture 16.

Kelava, I., Lancaster, M.A., 2017. Stem Cell Models of Human Brain Development. Cell Stem Cell 18, 736–748. doi:10.1016/j.stem.2016.05.022

Kesselheim, A.S., Hwang, T.J., Franklin, J.M., 2015. Two decades of new drug development for central nervous system disorders. Nat. Rev. Drug Discov. 1. doi:10.1038/nrd4793

Khan, F.I., Shahbaaz, M., Bisetty, K., Waheed, A., Sly, W.S., Ahmad, F., Hassan, M.I., 2016. Large scale analysis of the mutational landscape in b-glucuronidase: A major player of mucopolysaccharidosis type VII. Gene 576, 36–44. doi:10.1016/j.gene.2015.09.062

Kikuchi, T., Morizane, A., Doi, D., Magotani, H., Onoe, H., Hayashi, T., Mizuma, H., Takara, S., Takahashi, R., Inoue, H., Morita, S., Yamamoto, M., Okita, K., Nakagawa, M., Parmar, M., Takahashi, J., 2017. Human iPS cell-derived dopaminergic neurons function in a primate Parkinson's disease model. Nature 548, 592–596. doi:10.1038/nature23664

Kim, J. Bin, Stein, R., Hare, M.J.O., 2004. Three-dimensional *in vitro* tissue culture models of breast cancer – a review 281–291.

Kinney, M., Sargent, C.Y., McDevitt, T.C., 2011. The multiparametric effects of hydrodynamic environments on stem cell culture. Tissue Eng. Part B Rev 37, 249–262.

Kleinman, H.K., Martin, G.R., 2005. Matrigel: Basement membrane matrix with biological activity. Semin. Cancer Biol. 15, 378–386. doi:10.1016/j.semcancer.2005.05.004

Kondo, T., Asai, M., Tsukita, K., Kutoku, Y., Ohsawa, Y., Sunada, Y., Imamura, K., Egawa, N., Yahata, N, …., Yamanaka, S., Inoue, H., 2013. Modeling Alzheimer's disease with iPSCs reveals stress phenotypes associated with intracellular Aβ and differential drug responsiveness. Cell Stem Cell 12, 487–96. doi:10.1016/j.stem.2013.01.009

Kowalewski, B., Lamanna, W.C., Lawrence, R., Damme, M., Stroobants, S., Padva, M., Kalus, I., Frese, M.-A., Lubke, T., Lullmann-Rauch, R., D'Hooge, R., Esko, J.D., Dierks, T., 2012. Arylsulfatase G inactivation causes loss of heparan sulfate 3-O-sulfatase activity and mucopolysaccharidosis in mice. Proc. Natl. Acad. Sci. 109, 10310–10315. doi:10.1073/pnas.1202071109

Kunz-Schughart, L., Freyer, J., Hofstaedter, F., Ebner, R., 2004. The use of 3-D cultures for high-throughput screening: the multicellular spheroid model. J Biomol Screen 9, 273–285.

LaFerla, F., Green, K., 2012. Animal models of Alzheimer disease. Cold Spring Harb Perspect Med 2. doi:10.1101/cshperspect.a006320

Lancaster, M. a, Renner, M., Martin, C., Wenzel, D., Bicknell, S., Hurles, M.E., Homfray, T., Penninger, J.M., Andrew, P., 2013. Cerebral organoids model human brain development and microcephaly. Nature 501, 373–379. doi:10.1038/nature12517.Cerebral

Lancaster, M., Corsini, N., Wolfinger, S., Gustafson, E., Phillips, A., Burkard, T., Otani, T., Livesey, F., Knoblich, J., 2017. Guided self-organization and cortical plate formation in human brain organoids. Nat. Biotechnol. 35, 659–666.

Lau, L., Cua, R., Keough, M., Haylock-Jacobs, S., Yong, V., 2013. Pathophysiology of the brain extracellular matrix: a new target for remyelination. Nat. Rev. Neurosci. 14.

Lee, Y., Morrison, B.M., Li, Y., Lengacher, S., Farah, M.H., Hoffman, P.N., Liu, Y., et al, 2012. Oligodendroglia metabolically support axons and contribute to neurodegeneration. Nature 487, 443–448.

Lemke, K.A., Aghayee, A., Ashton, R.S., 2017. Deriving, regenerating, and engineering CNS tissues using human pluripotent stem cells. Curr. Opin. Biotechnol. 47, 36–42. doi:10.1016/j.copbio.2017.05.010

Lemonnier, T., Blanchard, S., Toli, D., Roy, E., Bigou, S., Froissart, R., Rouvet, I., Vitry, S., Heard, J.M., Bohl, D., 2011. Modeling neuronal defects associated with a lysosomal disorder using patient-derived induced pluripotent stem cells. Hum. Mol. Genet. 20, 3653–3666. doi:10.1093/hmg/ddr285

Llorens-Bobadilla, E., Martin-Villalba, A., 2017. Adult NSC diversity and plasticity: the role of the niche. Curr. Opin. Neurobiol. 42, 68–74. doi:10.1016/j.conb.2016.11.008

Lozano, R., Stevens, L., Thompson, B., Gilmore, K., Gorkin, R., Stewart, E., Panhuis, M., Romero-Ortega, M., Wallace, G., 2015. 3D printing of layered brain-like structures using peptide modified gellan gum substrates. Biomaterials 67, 264–273.

Ma, L., Hu, B., Liu, Y., Vermilyea, S.C., Liu, H., Gao, L., Sun, Y., Zhang, X., Zhang, S.C., 2012. Human embryonic stem cell-derived GABA neurons correct locomotion deficits in quinolinic acid-lesioned mice. Cell Stem Cell 10, 455–464. doi:10.1016/j.stem.2012.01.021

Mariani, J., Coppola, G., Pelphrey, K.A., Howe, J.R., Vaccarino Correspondence, F.M., 2015. FOXG1-Dependent Dysregulation of GABA/ Glutamate Neuron Differentiation in Autism Spectrum Disorders. Cell 162, 375–390. doi:10.1016/j.cell.2015.06.034

Mariani, J., Simonini, M.V., Palejev, D., Tomasini, L., Coppola, G., Szekely, A.M., Horvath, T.L., Vaccarino, F.M., 2012. Modeling human cortical development *in vitro* using induced pluripotent stem cells. Proc. Natl. Acad. Sci. U. S. A. 109, 12770–5. doi:10.1073/pnas.1202944109

Marks, D.M., 2003. Equipment design considerations for large scale cell culture 21–33.

Martins-Taylor, K., Xu, R.-H., 2012. Concise review: genomic stability of human induced pluripotent stem cells. Stem Cells 30.

Mattson, M., Rychlik, B., 1990. Cell culture of cryopreserved human fetal cerebral cortical and hippocampal neurons: neuronal development and responses to trophic factors. Brain Res 522, 204–214.

McCauley, H.A., Wells, J.M., 2017. Pluripotent stem cell-derived organoids: using principles of developmental biology to grow human tissues in a dish. Development 144, 958–962. doi:10.1242/dev.140731

Mertens, J., Marchetto, M., Bardy, C., Gage, F., 2016. Evaluating cell reprogramming, differentiation and conversion technologies in neuroscience. Nat. Rev. Neurosci. doi:10.1038/nrn.2016.46

Michell-Robinson, M.A., Touil, H., Healy, L.M., Owen, D.R., Durafourt, B.A., Bar-Or, A., Antel, J.P., Moore, C.S., 2015. Roles of microglia in brain development, tissue maintenance and repair. Brain 138, 1138–1159. doi:10.1093/brain/awv066

Middeldorp, J., Boer, K., Sluijs, J. a, De Filippis, L., Encha-Razavi, F., Vescovi, A.L., Swaab, D.F., Aronica, E., Hol, E.M., 2010. GFAPdelta in radial glia and subventricular zone progenitors in the developing human cortex. Development 137, 313–21. doi:10.1242/dev.041632

Miller, J., Horvath, S., Geschwind, D., 2010. Divergence of human and mouse brain transcriptome highlights Alzheimer disease pathways doi: Proc Natl Acad Sci USA 107, 12698–12703. doi:10.1073/pnas.0914257107

Molofsky, A.V., Deneen, B., 2015. Astrocyte development: A Guide for the Perplexed. Glia 63, 1320–1329. doi:10.1002/glia.22836

Molofsky, A. V, Krencik, R., Krenick, R., Ullian, E.M., Ullian, E., Tsai, H., Deneen, B., Richardson, W.D., Barres, B. a, Rowitch, D.H., 2012. Astrocytes and disease: a neurodevelopmental perspective. Genes Dev. 26, 891–907. doi:10.1101/gad.188326.112

Montaño, A.M., Lock-Hock, N., Steiner, R.D., Graham, B.H., Szlago, M., Greenstein, R., Pineda, M., Gonzalez-Meneses, A., Çoker, M., Bartholomew, D., Sands, M.S., Wang, R., Giugliani, R., Macaya, A., Pastores, G., Ketko, A.K., Ezgü, F., Tanaka, A., Arash, L., Beck, M., Falk, R.E., Bhattacharya, K., Franco, J., White, K.K., Mitchell, G.A., Cimbalistiene, L., Holtz, M., Sly, W.S., 2016. Clinical course of sly syndrome (mucopolysaccharidosis type VII). J. Med. Genet. jmedgenet-2015-103322-. doi:10.1136/jmedgenet-2015-103322

Muffat, J., Li, Y., Yuan, B., Mitalipova, M., Omer, A., Corcoran, S., Bakiasi, G., Tsai, L.-H., Aubourg, P., Ransohoff, R.M., Jaenisch, R., 2016. Efficient derivation of microglia-like cells from human pluripotent stem cells. Nat Med 22, 1358–1367. doi:10.1038/nm.4189

Murrow, L.M., Weber, R.J., Gartner, Z.J., 2017. Dissecting the stem cell niche with organoid models: an engineering-based approach. Development 144, 998–1007. doi:10.1242/dev.140905

Najm, F.J., Lager, A.M., Zaremba, A., Wyatt, K., Caprariello, A. V., Factor, D.C., Karl, R.T., Maeda, T., Miller, R.H., Tesar, P.J., 2013. Transcription factor-mediated reprogramming of fibroblasts to expandable, myelinogenic oligodendrocyte progenitor cells. Nat. Biotechnol. 31, 426–433. doi:10.1038/nbt.2561

Nasello, M., Schirò, G., Crapanzano, F., Balistreri, C., 2017. Stem cells and other emerging agents as innovative “drugs” in neurodegenerative diseases: benefits and limitations. Rejuvenation Res. doi:10.1089/rej.2017.1946

O'Collins, V., Macleod, M., Donnan, G., Horky, L., van der Worp, B., Howells, D., 2006. 1,026 experimental treatments in acute stroke. Ann Neurol 59, 67–477.

O'Connor, D.M., Boulis, N.M., 2015. Gene therapy for neurodegenerative diseases. Trends Mol. Med. 21, 504–512. doi:10.1016/j.molmed.2015.06.001

Oberheim, N.A., Takano, T., Han, X., He, W., Lin, J.H.C., Wang, F., Xu, Q., Wyatt, J.D., Pilcher, W., Ojemann, J.G., Ransom, B.R., Goldman, S. a, Nedergaard, M., 2009. Uniquely hominid features of adult human astrocytes. J. Neurosci. 29, 3276–87. doi:10.1523/JNEUROSCI.4707-08.2009

Olmer, R., Lange, A., Selzer, S., Kasper, C., Haverich, A., Martin, U., Zweigerdt, R., 2012. Suspension Culture of Human Pluripotent Stem Cells in Controlled, Stirred Bioreactors. Tissue Eng. Part C Methods 18, 772–784. doi:10.1089/ten.tec.2011.0717

Olson, H., Betton, G., Robinson, D., Al, E., 2000. Concordance of the toxicity of pharmaceuticals in humans and in animals. Regul Toxicol Pharmacol 32, 56–67. doi:10.1006/rtph.2000.1399

Ostenfeld, T., Caldwell, M., Prowse, K.R., Linskens, M.H., Jauniaux, E., Svendsen, C.N., 2000. Human neural precursor cells express low levels of telomerase *in vitro* and show diminishing cell proliferation with extensive axonal outgrowth following transplantation. Exp. Neurol 164, 215–226.

Pal, R., Ravindran, G., 2006. Assessment of pluripotency and multilineage differentiation potential of NTERA-2 cells as a model for studying human embryonic stem cells 585–598.

Pampaloni, F., Reynaud, E.G., Stelzer, E.H.K., 2007. The third dimension bridges the gap between cell culture and live tissue 8, 839–845.

Pang, Z., Yang, N., Vierbuchen, T., Ostermeier, A., Fuentes, D., Yang, T., Citri, A., Sebastiano, V., Marro, S., Südhof, T., Wernig, M., 2011. Induction of human neuronal cells by defined transcription factors. Nature 26, 220–223.

Paşca, A.M., Sloan, S.A., Clarke, L.E., Tian, Y., Makinson, C.D., Huber, N., Kim, C.H., Park, J.-Y., O'Rourke, N.A., Nguyen, K.D., Smith, S.J., Huguenard, J.R., Geschwind, D.H., Barres, B.A., Paşca, S.P., 2015. Functional cortical neurons and astrocytes from human pluripotent stem cells in 3D culture. Nat. Methods 12, 671–678. doi:10.1038/nmeth.3415

Pauklin, S., Vallier, L., 2015. Activin / Nodal signalling in stem cells 607–619. doi:10.1242/dev.091769

Payne, N.L., Sylvain, A., O'Brien, C., Herszfeld, D., Sun, G., Bernard, C.C. a, 2015. Application of human induced pluripotent stem cells for modeling and treating neurodegenerative diseases. N. Biotechnol. 32, 212–228. doi:10.1016/j.nbt.2014.05.001

Perrier, A.L., Tabar, V., Barberi, T., Rubio, M.E., Bruses, J., Topf, N., Harrison, N.L., Studer, L., 2004. Derivation of midbrain dopamine neurons from human embryonic stem cells. Proc.

Natl. Acad. Sci. 101, 12543–12548. doi:10.1073/pnas.0404700101

Picollet-D'hahan, N., Dolega, M.E., Liguori, L., Marquette, C., Le Gac, S., Gidrol, X., Martin, D.K., 2016. A 3D Toolbox to Enhance Physiological Relevance of Human Tissue Models. Trends Biotechnol. 1–13. doi:10.1016/j.tibtech.2016.06.012

Pleasure, S., Lee, V., 1993. NTera 2 cells: a human cell line which displays characteristics expected of a human committed neuronal progenitor cell. J. Neurosci. Res. 35, 585–602.

Plotegher, N., Duchen, M.R., 2017. Mitochondrial Dysfunction and Neurodegeneration in Lysosomal Storage Disorders. Trends Mol. Med. 23, 116–134. doi:S1471-4914(16)30188-5 [pii]

Podrygajlo, G., Tegenge, M. a, Gierse, A., Paquet-Durand, F., Tan, S., Bicker, G., Stern, M., 2009. Cellular phenotypes of human model neurons (NT2) after differentiation in aggregate culture. Cell Tissue Res. 336, 439–52. doi:10.1007/s00441-009-0783-0

Presgraves, S., Ahmed, T., Borwege, S., Joyce, J., 2004. Terminally differentiated SH-SY5Y cells provide a model system for studying neuroprotective effects of dopamine agonists. Neurotox. Res. 5, 579–598.

Preynat-Seauve, O., Suter, D.M., Tirefort, D., Turchi, L., Virolle, T., Chneiweiss, H., Foti, M., Lobrinus, J.-A., Stoppini, L., Feki, A., Dubois-Dauphin, M., Krause, K.H., 2009. Development of Human Nervous Tissue upon Differentiation of Embryonic Stem Cells in Three-Dimensional Culture. Stem Cells 27, 509–520. doi:10.1634/stemcells.2008-0600

Price, D.J., Jarman, A.P., Mason, J.O., Kind, P.C., 2011. Building Brains: An Introduction to Neural Development, Wiley-Blackwell.

Qian, X., Nguyen, H.N., Jacob, F., Song, H., Ming, G., 2017. Using brain organoids to understand Zika virus-induced microcephaly. Development 144, 952–957. doi:10.1242/dev.140707

Quadrato, G., Nguyen, T., Macosko, E.Z., Sherwood, J.L., Min Yang, S., Berger, D.R., Maria, N., Scholvin, J., Goldman, M., Kinney, J.P., Boyden, E.S., Lichtman, J.W., Williams, Z.M., McCarroll, S.A., Arlotta, P., 2017. Cell diversity and network dynamics in photosensitive human brain organoids. Nature. doi:10.1038/nature22047

Ranga, A., Girgin, M., Meinhardt, A., Eberle, D., Caiazzo, M., Tanaka, E., Lutolf, M., 2016. Neural tube morphogenesis in synthetic 3D microenvironments. Proc. Natl. Acad. Sci. U. S. A. E6831–E6839.

Ray, B., Chopra, N., Long, J.M., Lahiri, D.K., 2014. Human primary mixed brain cultures: Preparation, differentiation, characterization and application to neuroscience research. Mol. Brain 7, 1–15. doi:10.1186/s13041-014-0063-0

Rigamonti, A., Repetti, G., Sun, C., Price, F., Reny, D., Rapino, F., Weisinger, K., Benkler, C., Peterson, Q., Davidow, L., Hansson, E., Rubin, L., 2016. Large-Scale Production of Mature

Neurons from Human Pluripotent Stem Cells in a Three-Dimensional Suspension Culture System. Stem Cell Reports 6, 993–1008. doi:http://dx.doi.org/10.1016/j.stemcr.2016.05.010

Ring, K., Tong, L., Balestra, M., Javier, R., Andrews-Zwilling, Y., Li, G., Walker, D., Zhang, W., Kreitzer, A., Huang, Y., 2012. Direct Reprogramming of Mouse and Human Fibroblasts into Multipotent Neural Stem Cells with a Single Factor. Cell Stem Cell 11, 100–109. doi:10.1016/j.stem.2012.05.018

Rosemann, A., 2015. Stem cell treatments for neurodegenerative diseases: challenges from a science, business and healthcare perspective. Neurodegener. Dis. Manag. 5, 85–87. doi:10.2217/nmt.15.2

Ross, C. a, Akimov, S.S., 2014. Human-induced pluripotent stem cells: potential for neurodegenerative diseases. Hum. Mol. Genet. 1–10. doi:10.1093/hmg/ddu204

Saha, K., Keung, A.J., Irwin, E.F., Li, Y., Little, L., Schaffer, D.V., Healy, K.E., 2008. Substrate modulus directs neural stem cell behavior. Biophys. J. 95, 4426–4438.

Salazar, D., Rodríguez-López, A., Herreño, A., Barbosa, H., Herrera, J., Ardila, A., Barreto, G., González, J., Alméciga-Díaz, C., 2016. Systems biology study of mucopolysaccharidosis using a human metabolic reconstruction network. Mol. Genet. Metab. 117, 129–139. doi:http://dx.doi.org/10.1016/j.ymgme.2015.08.001

Scholz, D., Pöltl, D., Genewsky, A., Weng, M., Waldmann, T., Schildknecht, S., Leist, M., 2011. Rapid, complete and large-scale generation of post-mitotic neurons from the human LUHMES cell line. J. Neurochem. 119, 957–971. doi:10.1111/j.1471-4159.2011.07255.x

Schuldiner, M., Eiges, R., Eden, A., Yanuka, O., Itskovitz-eldor, J., 2001. Induced neuronal differentiation of human embryonic stem cells 913, 201–205.

Sena, E., van der Worp, H., Bath, P., Howells, D., Macleod, M., 2010. Publication bias in reports of animal stroke studies leads to major overstatement of efficacy. PLoS Biol 8.

Serra, M., Brito, C., Correia, C., Alves, P.M., 2012. Process engineering of human pluripotent stem cells for clinical application. Trends Biotechnol. 1–10. doi:10.1016/j.tibtech.2012.03.003

Serra, M., Brito, C., Costa, E.M., Sousa, M.F.Q., Alves, P.M., 2009. Integrating human stem cell expansion and neuronal differentiation in bioreactors 14, 1–14. doi:10.1186/1472-6750-9-82

Shaltouki, A., Peng, J., Liu, Q., Rao, M.S., Zeng, X., 2013. Efficient generation of astrocytes from human pluripotent stem cells in defined conditions. Stem Cells 31, 941–952. doi:10.1002/stem.1334

Shi, Y., Kirwan, P., Livesey, F.J., 2012. Directed differentiation of human pluripotent stem cells to cerebral cortex neurons and neural networks. Nat. Protoc. 7, 1836–46. doi:10.1038/nprot.2012.116

Shipley, M., Mangold, C., Szpara, M., 2016. Differentiation of the SH-SY5Y Human Neuroblastoma Cell Line. J Vis Exp 108. doi:10.3791/53193

Simão, D., Arez, F., Terasso, A.P., Pinto, C., Sousa, M.F.Q., Brito, C., Alves, P.M., 2016. Perfusion Stirred-Tank Bioreactors for 3D Differentiation of Human Neural Stem Cells. Methods Mol. Biol. doi:10.1007/7651_2016_333

Simão, D., Pinto, C., Piersanti, S., Weston, A., Peddie, C.J., Bastos, A.E.P., Licursi, V., Schwarz, S.C., Collinson, L.M., Salinas, S., Serra, M., Teixeira, A.P., Saggio, I., Lima, P.A., Kremer, E.J., Schiavo, G., Brito, C., Alves, P.M., 2014. Modeling human neural functionality *in vitro*: 3D culture for dopaminergic differentiation. Tissue enginnering, Part A. 21. doi: 10.1089/ten.TEA.2014.0079

Simão, D., Silva, M.M., Terrasso, A.P., Arez, F., Sousa, M.F., Mehrjardi, N.Z., Šarić, T., Gomes-Alves, P., Raimundo, N., Alves, P.M., Brito, C., 2018. 3D differentiation of iPSC-derived NPC recapitulates human brain microenvironment. Stem Cell Reports, *under review*

Simão, D., Terrasso, A.P., Teixeira, A.P., Brito, C., Sonnewald, U., Alves, P.M., 2016. Functional metabolic interactions of human neuron-astrocyte 3D *in vitro* networks. Sci. Rep. 6. doi:10.1038/srep33285

Smirnova, L., Harris, G., Delp, J., Valadares, M., Pamies, D., Hogberg, H.T., Waldmann, T., Leist, M., Hartung, T., 2016. A LUHMES 3D dopaminergic neuronal model for neurotoxicity testing allowing long-term exposure and cellular resilience analysis. Arch. Toxicol. 90, 2725–2743. doi:10.1007/s00204-015-1637-z

Sofroniew, M. V, Vinters, H. V, 2010. Astrocytes : biology and pathology 7–35. doi:10.1007/s00401-009-0619-8

Soleman, S., Filippov, M.A., Dityatev, A., Fawcett, J.W., 2013. Targeting the neural extracellular matrix in neurological disorders. Neuroscience 253, 194–213. doi:10.1016/j.neuroscience.2013.08.050

Spaethling, J.M., Na, Y., Lee, J., Sul, J., Kim, J., Eberwine, J.H., Spaethling, J.M., Na, Y., Lee, J., Ulyanova, A. V, Baltuch, G.H., Bell, T.J., Kung, D.K., Lucas, T.H., Rourke, D.M.O., Stefanik, D., Wang, J., Wolf, J.A., 2017. Primary Cell Culture of Live Neurosurgically Resected Aged Adult Human Brain Cells and Single Cell Transcriptomics. Cell Rep. 18, 791–803. doi:10.1016/j.celrep.2016.12.066

Spittau, B., 2017. Aging microglia-phenotypes, functions and implications for age-related neurodegenerative diseases. Front. Aging Neurosci. 9, 1–9. doi:10.3389/fnagi.2017.00194

Stern, M., Gierse, A., Tan, S., Bicker, G., 2013. Human Ntera2 cells as a predictive *in vitro* test system for developmental neurotoxicity. Arch. Toxicol. doi:10.1007/s00204-013-1098-1

Takahashi, K., Tanabe, K., Ohnuki, M., Narita, M., Ichisaka, T., Tomoda, K., Yamanaka, S., 2007. Induction of pluripotent stem cells from adult human fibroblasts by defined factors. Cell 131, 861–72. doi:10.1016/j.cell.2007.11.019

Tapia, N., Scholer, H.R., 2016. Molecular obstacles to clinical translation of iPSCs. Cell Stem Cell 19, 298–309.

Terrasso, A.P., Pinto, C., Serra, M., Filipe, A., Almeida, S., Ferreira, A.L., Pedroso, P., Brito, C., Alves, P.M., 2015. Novel scalable 3D cell based-model for *in vitro* neurotoxicity testing: combining human differentiated neurospheres with gene expression and functional endpoints. J. Biotechnol. 205, 82–92. doi:10.1016/j.jbiotec.2014.12.011

Terrasso, A.P., Silva, A.C., Filipe, A., Pedroso, P., Ferreira, A.L., Alves, P.M., Brito, C., 2017. Human neuron-astrocyte 3D co-culture-based assay for evaluation of neuroprotective compounds. J. Pharmacol. Toxicol. Methods 83. doi:10.1016/j.vascn.2016.10.001

Thomson, J.A., Itskovitz-Eldor, J., Shapiro, S.S., Waknitz, M.A., Swiergiel, J.J., Marshall, V.S., Jones, J.M., 1998. Embryonic stem cell lines derived from human blastocysts. Science (80-.). 282, 1145–1147.

Tian, E., Sun, G., Sun, G., Chao, J., Ye, P., Warden, C., Riggs, A.D., Shi, Y., 2016. Small-Molecule-Based Lineage Reprogramming Creates Functional Astrocytes. Cell Rep. 16, 781–792. doi:10.1016/j.celrep.2016.06.042

Tomatsu, S., Montaño, A.M., Dung, V.C., Grubb, J.H., Sly, W.S., 2009. Mutations and Polymorphisms in GUSB Gene in Mucopolysaccharidosis VII (Sly Syndrome). Hum Mutat. 30, 511–519. doi:10.1002/humu.20828

Vasile, F., Dossi, E., Rouach, N., 2017a. Human astrocytes: structure and functions in the healthy brain. Brain Struct. Funct. doi:10.1007/s00429-017-1383-5

Vasile, F., Dossi, E., Rouach, N., 2017b. Human astrocytes: structure and functions in the healthy brain. Brain Struct. Funct. doi:10.1007/s00429-017-1383-5

Vitner, E.B., Platt, F.M., Futerman, A.H., 2010. Common and uncommon pathogenic cascades in lysosomal storage diseases. J Biol Chem 285, 20423–20427. doi:10.1074/jbc.R110.134452

von Bartheld, C.S., Bahney, J., Herculano-Houzel, S., 2016. The search for true numbers of neurons and glial cells in the human brain: A review of 150 years of cell counting. J. Comp. Neurol. 524, 3865–3895. doi:10.1002/cne.24040

Walsh, K., Megyesi, J., Hammond, R., 2005. Human central nervous system tissue culture: a historical review and examination of recent advances. Neurobiol. Dis. 18, 2–18. doi:10.1016/j.nbd.2004.09.002

Wheeler, H., Wing, C., Delaney, S., Komatsu, M., Dolan, M., 2015. Modeling chemotherapeutic neurotoxicity with human induced pluripotent stem cell-derived neuronal cells. PLoS One 10, e0118020.

Xing, E.M., Wu, S., Ponder, K.P., 2015. The effect of Tlr4 and/or C3 deficiency and of neonatal gene therapy on skeletal disease in mucopolysaccharidosis VII mice. Mol. Genet.

Metab. 114, 209–216. doi:10.1016/j.ymgme.2014.12.305

Yang, N., Zuchero, J.B., Ahlenius, H., Marro, S., Ng, Y.H., 2013. Generation of oligodendroglial cells by direct lineage conversion. Nat. Biotechnol. 31, 434–439. doi:10.1038/nbt.2564.

Zhang, N., An, M., Montoro, D., Ellerby, L., 2010. Characterization of Human Huntington's Disease Cell Model from Induced Pluripotent Stem Cells. PLoS Curr 2, 10.1371/currents.RRN1193.

Zhang, S.-C., 2006. Neural Subtype Specification from Embryonic Stem Cells. Brain Pathol.

Zhang, S.-C., Wernig, M., Duncan, I.D., Brustle, O., Thomson, J.A., 2001. *In vitro* differentiation of transplantable neural precursors from human embryonic stem cells. Nat Biotechnol 19, 1129–1133. doi:http://dx.doi.org/10.1038/ nbt1201-1129

Zhang, X., Zhang, S., 2010. Differentiation of Neural Precursors and Dopaminergic Neurons from Human Embryonic Stem Cells. Methods Mol Biol. 584, 355–366. doi:10.1007/978-1-60761-369-5_19

Zhang, X.M., Yin, M., Zhang, M.H., 2014. Cell-based assays for Parkinson's disease using differentiated human LUHMES cells. Acta Pharmacol. Sin. 35, 945–956. doi:10.1038/aps.2014.36

Zhang, Y., Sloan, S.A., Clarke, L.E., Caneda, C., Plaza, C.A., Blumenthal, P.D., Vogel, H., Steinberg, G.K., Edwards, M.S.B., Li, G., Duncan, J.A., Cheshier, S.H., Shuer, L.M., Chang, E.F., Grant, G.A., Gephart, M.G.H., Barres, B.A., 2016. Purification and Characterization of Progenitor and Mature Human Astrocytes Reveals Transcriptional and Functional Differences with Mouse NeuroResource Purification and Characterization of Progenitor and Mature Human Astrocytes Reveals Transcriptional and. Neuron 89, 37–53. doi:10.1016/j.neuron.2015.11.013

Zirra, A., Wiethoff, S., Patani, R., 2016. Neural Conversion and Patterning of Human Pluripotent Stem Cells: A Developmental Perspective. Stem Cells Int. 2016. doi:10.1155/2016/8291260

CHAPTER 2

Novel scalable 3D cell-based model for *in vitro* neurotoxicity testing:
Combining human differentiated neurospheres with gene expression and functional endpoints

This chapter was adapted from:

Terrasso AP, Pinto C, Serra M, Filipe A, Almeida S, Ferreira AL, Predroso P, Brito C, Alves PM. 2015. Novel scalable 3D cell based-model for *in vitro* neurotoxicity testing: combining human differentiated neurospheres with gene expression and functional endpoints. Journal of Biotechnology, 205, 82–92, doi: 10.1016/j.jbiotec.2014.12.011.

Table of contents

Abstract

There is an urgent need for new *in vitro* strategies to identify neurotoxic agents with speed, reliability and respect for animal welfare. Cell models should include distinct brain cell types and represent brain microenvironment to attain higher relevance. The main goal of this study was to develop and validate a human 3D neural model containing both neurons and glial cells, applicable for toxicity testing in high-throughput platforms. To achieve this, a scalable bioprocess for neural differentiation of human NTera2/cl.D1 cells in stirred culture systems was developed. Endpoints based on neuronal- and astrocytic-specific gene expression and functionality in 3D were implemented in multi-well format and used for toxicity assessment. The prototypical neurotoxicant acrylamide affected primarily neurons, impairing synaptic function; our results suggest that gene expression of the presynaptic marker synaptophysin can be used as sensitive endpoint. Chloramphenicol, described as neurotoxicant affected both cell types, with cytoskeleton markers' expression significantly reduced, particularly in astrocytes. In conclusion, a scalable and reproducible process for production of differentiated neurospheroids enriched in mature neurons and functional astrocytes was obtained. This 3D approach allowed efficient production of large numbers of human differentiated neurospheroids, which in combination with gene expression and functional endpoints are a powerful cell model to evaluate human neuronal and astrocytic toxicity.

1. Introduction

Human brain is a critical target organ of xenobiotics due to its developmental, structural and functional features that make it an extremely complex organ with highly elaborate physical, communicative and metabolic interactions between neurons and glial cells (Allen and Barres, 2009; Moors et al., 2009).

Given the insufficient information available on neurotoxicity and the growing number of chemicals to be tested, new testing strategies are required to identify neurotoxic agents with speed, reliability and respect for animal welfare. Moreover, generate *in vitro* tests with an increased high-throughput is needed to provide mechanistic data and evaluate more efficiently the toxics that may cause adverse effect in humans (Breier et al., 2010; Breslin and O'Driscoll, 2013; Tralau and Luch, 2012).

Numerous studies demonstrated that screens focusing solely on the direct effect of compounds on isolated neurons may not model consistently the basic Central Nervous System (CNS) functions and environment and will overlook potentially important neuroprotective and/or neurotoxic activities that act via astrocytes or other non-neuronal cells (Chen and Swanson, 2003; Gupta et al., 2012; Sofroniew and Vinters, 2010). Moreover, cell differentiation and tissue development and homeostasis *in vivo* are strongly dependent on cell spatial arrangement, essential for correct trafficking and communication between neurons and astrocytes and directional cues, so extracellular context profoundly affects cell behavior (Irons et al., 2008). Neurospheres, free-floating aggregates of neural progenitors (Conti and Cattaneo, 2010), allow formation of a complex 3D network of cell-cell and cell-extracellular matrix interactions, being potentially relevant in the penetration and action of drugs (Breslin and O'Driscoll, 2013). Despite research with neurospheres largely focused on their application for neuronal regeneration in CNS diseases, a few studies utilized neurospheres for *in vitro* developmental toxicity studies, providing support for their use in neurotoxic compounds identification (Breier et al., 2010). Furthermore, differentiated neurospheroids

fabrication procedures have been described by our laboratory and others (Brito et al., 2012; Moors et al., 2009; Serra et al., 2009), using different cell sources, however, none of these systems generates neurospheroids enriched in functional astrocytes. Since the use of human origin tissues is limited due to availability issues, an insufficient potential to generate the necessary number of cells and ethical concerns, efforts should focus on creating affordable and sensitive methods to develop alternative human-cell based *in vitro* models that closely reconstruct the *in vivo* situation for investigation of neurotoxic effects in human neural cells (Hill et al., 2008; Moors et al., 2009).

A wide range of cell systems have been under investigation for their suitability for inclusion in neurotoxicity test batteries (Mori and Hara, 2013). In recent years, protocols have been developed for the isolation and *in vitro* culture of human neural stem cells (NSC) or neural progenitor cells as well as for the derivation of human neurons and astrocytes from pluripotent stem cells (PSC), both embryonic (ESC) and induced (iPSC) (Molofsky et al., 2012; Mori and Hara, 2013). Although the use of the latter holds great promise and remarkable advances have been made in expansion, differentiation and characterization, numerous challenges must be overcome before the use of this technology can be widespread (Mori and Hara, 2013; Serra et al., 2010).

Human pluripotent embryonic carcinoma cell lines, such as NTera-2/cloneD1 (NT2), represent an alternative that can provide an unlimited number of cells, with less time-consuming and well characterized neuronal differentiation protocols (Brito et al., 2007; Serra et al., 2009). NT2-derived neurons have been shown to be a valuable model for *in vitro* developmental neurotoxicity testing (Laurenza et al., 2013; Stern et al., 2013), demonstrating advantages regarding the identification of potential neurotoxicants. A few works described astrocytic differentiation of NT2 cell line, based on RA neural induction and increased differentiation times, in 2D culture systems (Bani-Yaghoub et al., 1999; Goodfellow et al., 2011).

The present work focused on the development of a robust process for generation of a human 3D cellular model, enriched in functional neurons and astrocytes and suitable to feed high-throughput neurotoxicity studies, using the human pluripotent NT2 cell line as cell source. Having as starting point a scalable process based on stirred suspension culture system previously developed by us for NT2 neuronal differentiation (Serra et al., 2009, 2007), we have extended differentiation in order to allow astrocytic differentiation and maturation. The feasibility of using these differentiated neurospheroids as 3D human neural cell model for high-throughput neurotoxicity testing was attained by performing neurotoxicity assays in multi-well formats. The effect of neurotoxic compounds in differentiated neurospheroids was evaluated by gene expression and functional endpoints, allowing distinguishing between neuronal and astrocytic toxicity.

2. Materials and Methods

2.1. Cell culture and 2D differentiation

Undifferentiated NT2 cells from American Type Culture Collection (ATCC) were routinely cultivated in DMEM (Invitrogen) supplemented with 10% (v/v) fetal bovine serum (FBS, Invitrogen) and 1% (v/v) penicillin-streptomycin (P/S, Invitrogen), as previously described (Brito et al., 2007).

2.2. Stirred suspension culture

NT2 cells were cultured in stirred suspension culture systems in a humidified atmosphere of 5% CO_2 in air, at 37◦C. Undifferentiated NT2 cells were inoculated as single cell suspension in a silanized 125 mL spinner vessel (from Wheaton) equipped with ball impeller, at a density of 6.7×10^5 cell/mL in 75 mL DMEM, 10% FBS, 1% P/S. On day 2, 50 mL of fresh medium were added and cells allowed to aggregate for additional 2 days *in vitro* (DIV). After this aggregation period, at day 3 differentiation induced by RA was initiated, by performing 50% medium exchange which was repeated every2–3 days for 3 weeks (until 24DIV). The medium composition during this period was DMEM supplemented with 10% FBS, 1% P/S

and 20 M retinoic acid (RA, Fig. 2.1a). Following this period (from 24DIV onwards), the medium was composed by DMEM, 5% FBS, 1% P/S. Cultures were maintained up to 50DIV and applied in neurotoxicity assays (from 38 to 50 DIV). The agitation rate was increased along culture to avoid aggregate clumping and to control aggregate size (from initial 40 rpm, to 60 rpm during RA induction phase and up to 100 rpm by the end of this period).

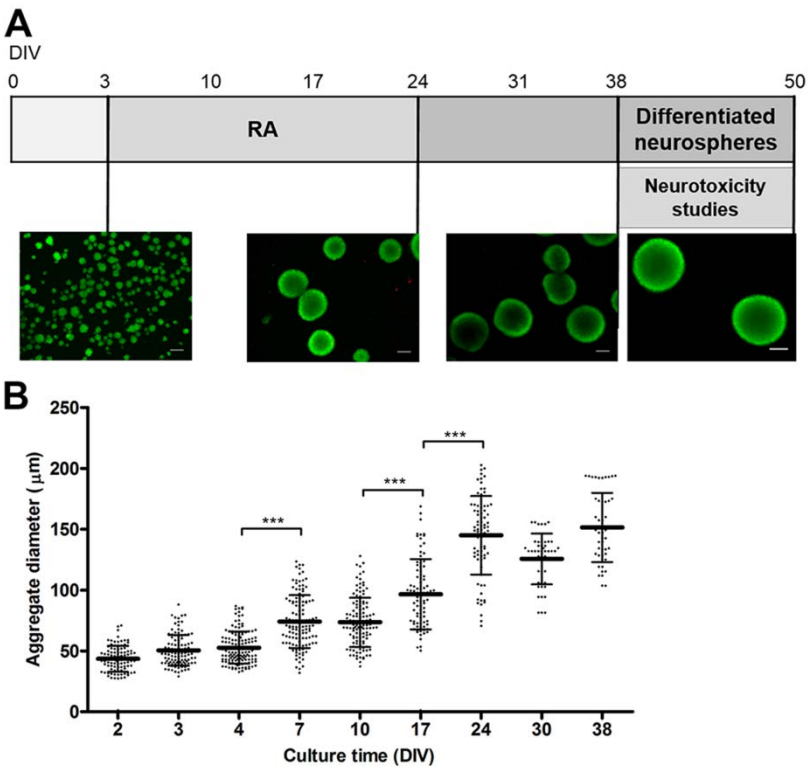

Figure 2.1: Neurospheroid culture. (a) Schematic workflow of stirred suspension culture. Cells were inoculated in a stirred suspension culture system and aggregated for 3 days. Neural differentiation was induced by retinoic acid (RA) for 3 weeks (3–24 DIV), followed by 2 weeks (until 38 DIV) without RA. Neurotoxicity studies were performed between 38 and 50 DIV. Images representative of the culture status at the indicated time points: fluorescent live/dead assay using fluorescein diacetate for identification of live cells (green) and propidium iodide for identification of dead cells (red). (b) Aggregate diameter profile along culture time; data are mean ± SD of three independent cultures. ***indicate significant difference with $P < 0.001$ by one-way ANOVA analysis with Tukey's post multiple comparison test.

2.3. Neurotoxicity assays

Neurospheroids were collected between 38-50 DIV, distributed in 96 or 6 well plates and incubated in DMEM, 5% FBS, 1% P/S, supplemented with increasingly

concentrations of test compounds, for 48–72 h, before carrying out the assay endpoints. Six wells were used per toxicant concentration and medium was used as untreated control. The induced toxicity of tert-buthyl hydroperoxide (tBHP;0.008–2 mM), acrylamide (Acr; 1 µM-1 mM) and chloramphenicol (39 µM–10 mM) (all purchased from Sigma-Aldrich) was evaluated by performing dose-response curves using cell viability as end-point, measured by the Presto blue viability assay (Invitrogen),based on resazurin reduction, following the manufacturer's instructions (calibration curves with neurospheroids Fig. 2.2). Based on these results the concentrations of Acr and chloramphenicol for further analysis were selected.

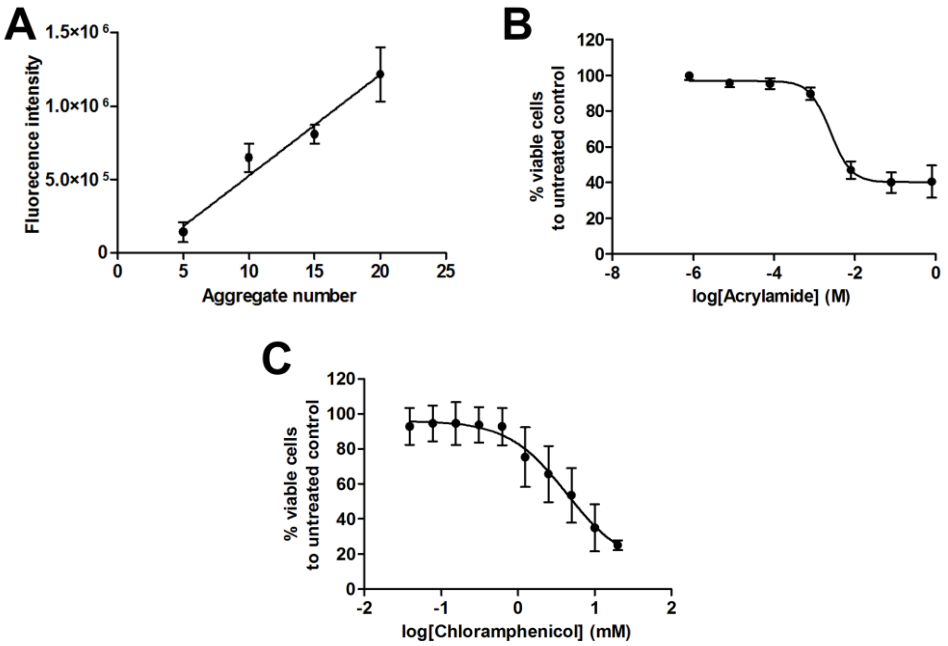

Figure 2.2: Neurotoxicity assays – dose-response curves. (a) Calibration curve performed to validate Presto blue cell viability assay. 5 to 20 neurospheroids were distributed per well, with 6 replicates per neurospheroids number and incubated for 72 hours before carrying out Presto blue cell viability assay. (b) Dose-response curve of 1 µM–1M acrylamide induced lesion for 72 hours in differentiated neurospheroids, determined by Presto blue assay. (c) Dose-response curve of 39 µM-10 mM chloramphenicol induced lesion for 48 hours in differentiated neurospheroids, determined by Presto blue assay; data are mean ± SD of three independent experiments.

2.4. Astrocytic functionality

Neurospheroids were collected at 38DIV, distributed in 6-well plates and incubated with DMEM without glutamate (Glu) and glutamine (Gln; Invitrogen). Glu transporters and Gln synthetase (GS) activities were stimulated adding 5 mM Glu (Sigma) to culture medium. As control medium was added to empty wells and processed together with those containing neurospheroids. Samples were collected at 0, 24, 48 at 72 h and Glu and Gln concentrations in culture medium were evaluated using a YSI 7100 MBS equipment (YSI Incorporated, USA).

2.5. Synaptic vesicle trafficking assay

Synaptic vesicles trafficking assay was based in Gaffield, 2006. Neurospheroids were plated in poly-d-lysine (PDL) – coated glass coverslips and incubated with 100 mM KCl buffer (5 mM HEPES-NaOH, pH 7.4; 10 mM glucose; 2.5 mM calcium chloride; 1 mM magnesium chloride; 100 mM potassium chloride; 37 mM sodium chloride) for 5 min. Afterwards, 100 mM KCl buffer was removed and neurospheroids incubated with 10 M FM-1-43 dye (Invitrogen)in 5 mM KCl buffer (5 mM HEPES-NaOH, pH 7.4; 10 mM glucose;2.5 mM calcium chloride; 1 mM magnesium chloride; 5 mM potassium chloride; 37 mM sodium chloride) for 15 min. Neurospheroids were washed for 1 min with 5 mM KCl buffer with ADVASEP-7(Sigma), followed by three washes with 5 mM KCl buffer. Exocytosis was stimulated with 100 mM KCl buffer and samples were visualized live using a fluorescence microscope (Leica DMI6000) in order to monitor the decreasing of fluorescence intensity overtime. Fluorescence intensity was measured using ImageJ software version 1.47m (*http://rsbweb.nih.gov/ij/*).

2.6. Fluorescence microscopy

Neurospheroids were collected at several time points and processed for immunofluorescence staining according to Serra et al. (2009). Briefly, neurospheroids were fixed in 4% (w/v) paraformaldehyde (Sigma) solution in PBS with 4% (w/v) sucrose and processed directly for immunostaining. Primary

antibodies used for cell characterization were: anti-nestin (Millipore), anti-βIII-tubulin (βIII-Tub, Millipore), anti-microtubule associated protein 2 (MAP2, Millipore), anti-synaptophysin (Syn, Millipore), anti-Glu descarboxilase 65/67 (GAD65/67, Chemicon), anti-vesicular Glu transporter 1 (VGluT1, Abcam), anti-glial fibrillary acidic protein (GFAP, DAKO), and anti-Glu transporter 1 (GLT-1, Millipore). Secondary antibodies were goat anti-mouse IgG-AlexaFluor 594, goat anti-mouse IgG-AlexaFluor 488 and goat anti-rabbit IgG-AlexaFluor 594 (Invitrogen). Cell nuclei were counterstained with 4',6-diamidino-2-phenylindole (DAPI, Invitrogen). Preparations were visualized using a point scan confocal (Leica SP5) microscope. Merge between channels, maximum z-projections and orthogonal projections, as well as linear brightness and contrast adjustments of the images, were created using the ImageJ software version 1.47m. The number of positively labeled cells was quantified by counting 10–20 randomly selected fields of at least three independent experiments.

2.7. Western blot

Neurospheroids were lysed in TX-100 lysis buffer (50 mM Tris, 5 mM EDTA, 150 mM NaCl, 1% Triton X-100 and 1× complete protease inhibitors cocktail (Roche)) and protein quantification was carried out using the Micro BSA^{TM} Protein Assay Kit (Thermo Scientific). Protein samples were subjected to a gel electrophoresis using a NuPAGE 4-12% Bis–Tris Gel with MES running buffer (Invitrogen) and electrophoretically transferred to polyvinylidene difluoride (PVDF) membrane. Membranes were blocked with PBS with 0.1% (w/v) Tween 20 and 5% non-fat dried milk powder (blocking solution) for 1 h, followed by incubation with primary antibodies overnight at RT, diluted in blocking solution with 0.1% sodium azide and then with secondary antibodies (horseradish peroxidase-conjugated, ECL anti-mouse IgG or anti-rabbit IgG; GE Healthcare) diluted 1:5000 in blocking solution, for 2 h at RT. Anti-α-tubulin antibody (Millipore) was used as control to confirm equal loading of total protein. Membranes were developed using Amersham ECL Prime Western Blotting Detection Reagent (GE Healthcare) and visualized using a

ChemiDoc™ XRS+ System (BioRad). Primary antibodies used for protein detection were anti- βIII-Tub, anti-syn, anti-GFAP, anti-GAD65/67 and anti-VGluT1 described above as well as anti-tyrosine hydroxylase (TH, SantaCruz Biotechnology).

2.8. qRT-PCR

Real-time quantitative PCR analysis (qRT-PCR) was performed as described in Brito et al. (2012). Briefly, total RNA was extracted with High Pure RNA Isolation kit (Roche) and quantified using a NanoDrop 2000c (ThermoScientific). Reverse transcription was performed with Transcriptor High Fidelity cDNA Synthesis kit (Roche), using Anchored-oligo(dT)18 Primer. qRT-PCR analysis was performed in a LightCycler 480 Multiwell Plate 96 (Roche), according to Light-Cycler 480 SYBR Green I Master Kit (Roche). cDNA was diluted 1:2 and primers were used in a concentration of 5 M, in20 L reactions; each sample was performed in triplicates. The list of used primers and its sequence is presented in Table 1. Cycles threshold (Ct's) and melting curves were determined using LightCycler 480 software, version 1.5 (Roche) and results were processed using the $2^{-\Delta\Delta Ct}$ method for relative gene expression analysis (Brito et al., 2012; Livak and Schmittgen, 2001). Changes in gene expression were normalized using the house-keeping gene RPL22 (coding for ribosomal protein L22) as internal control.

2.9. Statistical analysis

Statistical analysis was carried out using GraphPad Prism 5 software. Data are mean ± SD from at least three independent experiments performed in triplicates (qRT-PCR) or six replicates (neurotoxicity assays). One-way ANOVA analysis with Tukey's post multiple comparison test was performed to assess differences between time points (aggregate's diameter and qRT-PCR) or treated and control in neurotoxicity assays. Statistical significance was indicated as follows *P < 0.05, **P < 0.01, and ***P < 0.001.

Table 2.1: List of primers used in NT2 neurospheroids qRT-PCR analysis.

Gene	Cell type	Primers forward (top) and reverse (bottom)
RPL22	-	CACGAAGGAGGAGTGACTGG TGTGGCACACCACTGACATT
Nestin	Undifferentiated NT2 cells and neural progenitors	TAAGGTGAAAAGGGGTGTGG GCAAGAGATTCCCTTTGCAG
βIII-tubulin	Neurons	GGGCCTTTGGACATCTCTTC CCTCCGTGTAGTGACCCTTG
Synaptophysin	Neurons	TTTGTGAAGGTGCTGCAATG GCTGAGGTCACTCTCGGTCT
ChAT	Cholinergic neurons	AGCTGATCCGAGCAGACTCC TTTCTGCCGAGGAGGCTAAG
GAD 67	GABAergic neurons	ACCAGAAAACTGGGGCTCAA GCAGGTTCTTGGAGGATTGC
TH	Dopaminergic neurons	AGCCCTACCAAGACCAGACG GCGTGTACGGGTCGAACTT
GFAP	Astrocytes	AGAGAGGTCAAGCCAGGAG GGTCACCCACAACCCCTACT
S-100β	Astrocytes	GGAGACGGCGAATGTGACTT GAACTCGTGGCAGGCAGTAGTAA
GLAST	Astrocytes	TACCATCCATGGAGCACGAG ACCTGGTGACCACCACACAC
GLT-1	Astrocytes	CCAGGAAAAACCCCTTCTCC TCTTCCAGGCAACGAAAGGT
Glutamine synthetase	Astrocytes	CGTAGCTATCCGGACAGAGC CCCAACCCCTACCTTCTCTC

3. Results

3.1 Characterization of 3D neural cultures along differentiation in stirred culture systems

NT2 neuronal and astrocytic differentiation as 3D aggregates in stirred suspension systems was optimized in order to obtain a very reproducible and robust process, without significant batch-to-batch variation: typically cultures with high concentration of aggregates were obtained (888 ± 194 aggregates/mL by 38DIV) which maintained their structural integrity along the entire culture period, with high cell viability and no evidences of necrotic core formation, as indicated by generalized FDA staining and few PI-positive cells scattered through the aggregates (Fig. 2.1a).

Aggregate size gradually increased until 24DIV (end of the RA induction period) and was kept stable during the remaining time of the cultures (Fig. 2.1b), with an average diameter of 179.0 ± 76.5 μm. Initially, neurospheroids had a ragged

appearance; however, as differentiation progressed the aggregate shape became uniform, forming compact and spherical structures (Fig. 2.1a, 24DIV), typical of neurospheroid cultures (Serra et al., 2009). In order to accurately characterize the NT2-derived 3D neural model, cultures were monitored along the differentiation process, including phenotypic and functional assessment of neurons and astrocytes. Along differentiation the expression of neuronal marker βIII-tubulin was upregulated (Fig. 2.3a), with an eight-fold increase in gene expression at 10DIV, compared to undifferentiated cells.

Thereafter, maintenance of high levels of expression was observed, indicating an efficient differentiation into the neuronal lineage. In accordance, the expression of nestin, a marker of undifferentiated NT2 cells and early neuroepithelial progenitors, was downregulated in differentiated cultures (two-fold decrease at38DIV), while an initial four-fold increase was observed at 10DIV, probably corresponding to the proliferation of nestin^{+} neural progenitors (Michalczyk and Ziman, 2005).

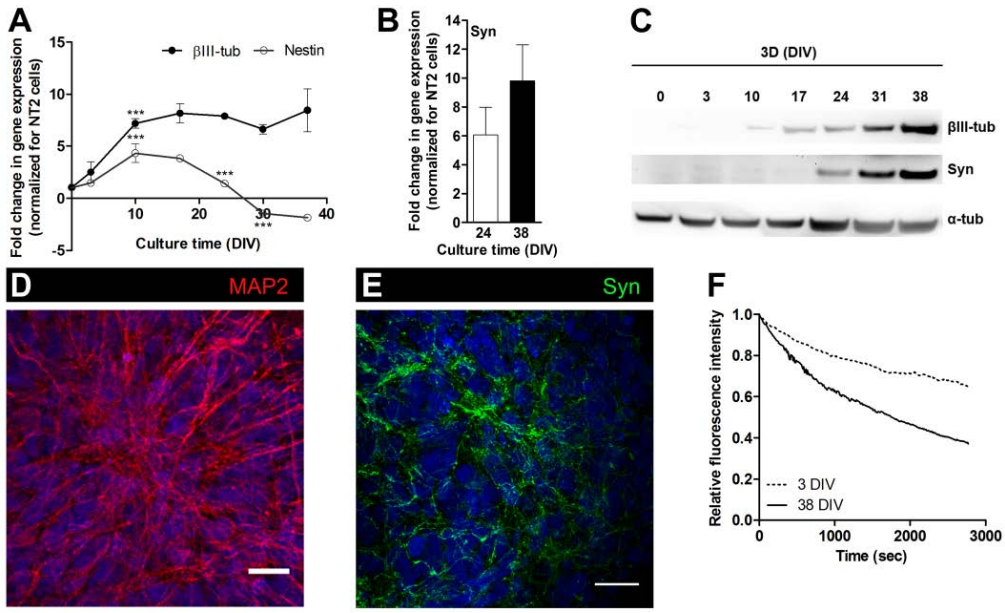

Figure 2.3: Characterization of the neuronal population in neurospheroids. (a) qRT-PCR analysis of βIII-tubulin and nestin gene expression; fold increase in gene expression of neuro-spheres along culture relatively to NT2 undifferentiated cells; data are mean ± SD of two independent cultures.***indicate significant difference with P < 0.001 by one-way ANOVA analysis with Tukey's

post multiple comparison test. (b) qRT-PCR analysis of synaptophysin gene expression; fold increase in gene expression of neurospheroids at 24 and 38 DIV normalized for NT2 undifferentiated cells; data are mean ± SD of three independent cultures. (c) Detection of βIII-tubulin (βIII-tub) and synaptophysin (syn) by Western blot analysis; β-tub was used as loading control. (d) Immunofluorescence microscopy of neurospheroids (38 DIV); scale bar: 20 µm; MAP2 (red) and DAPI (blue). (e) Immunofluorescence microscopy of neurospheroids (38DIV); scale bar: 20 µm; Synaptophysin (green) and DAPI (blue). For (d) and (e) data are from one representative experiment of three independent cultures. (f) Relative decrease in fluorescence intensity evaluated by FM-1-43 dye assay performed for undifferentiated aggregates at 3DIV and neurospheroids at 38DIV.

At 38DIV, an extensive network of $MAP2^+$ cells was detected throughout the neurospheroids (Fig. 2.3d), indicating that mature neurons were present in culture at this time point. Concomitantly, synaptophysin, a presynaptic vesicle glycoprotein, was detected in a typical vesicular pattern across the differentiated neurospheroids (38DIV, Fig. 2.3e), with a 10-fold increase in synaptophysin gene expression (Fig. 2.3b). Although synaptophysin was already detected at 24DIV, protein levels increased till 38DIV (Fig. 2.3c). The neurotransmitter-specific phenotype of neurons in differentiated neurospheroids was further evaluated. By 38DIV, high expression levels of the GABAergic marker GAD67 were observed, as well as gene expression of the dopaminergic marker TH and cholinergic marker ChAT (Fig. 2.4a). These correlated with the detection of VGluT1, GAD65/67 and TH proteins (Fig. 3b). Immunofluorescence co-localization allowed identification of βIII-$tubulin^+$/$GAD65/67^+$ GABAergic neurons (Fig. 2.4c), as well as βIII-$tubulin^+$/$VGluT1^+$ glutamatergic neurons (Fig. 2.4d). Moreover, VGluT1 was detected in a vesicular punctate pattern (inset in Fig. 2.4d), suggesting its localization in presynaptic vesicles (Alonso-Nanclares and Defelipe, 2005). These results indicated that the two main neurotransmitters in human brain – Glu and GABA (γ-aminobutyric acid) – were present in NT2 differentiated neurospheroids, as well as dopaminergic and cholinergic neurons.

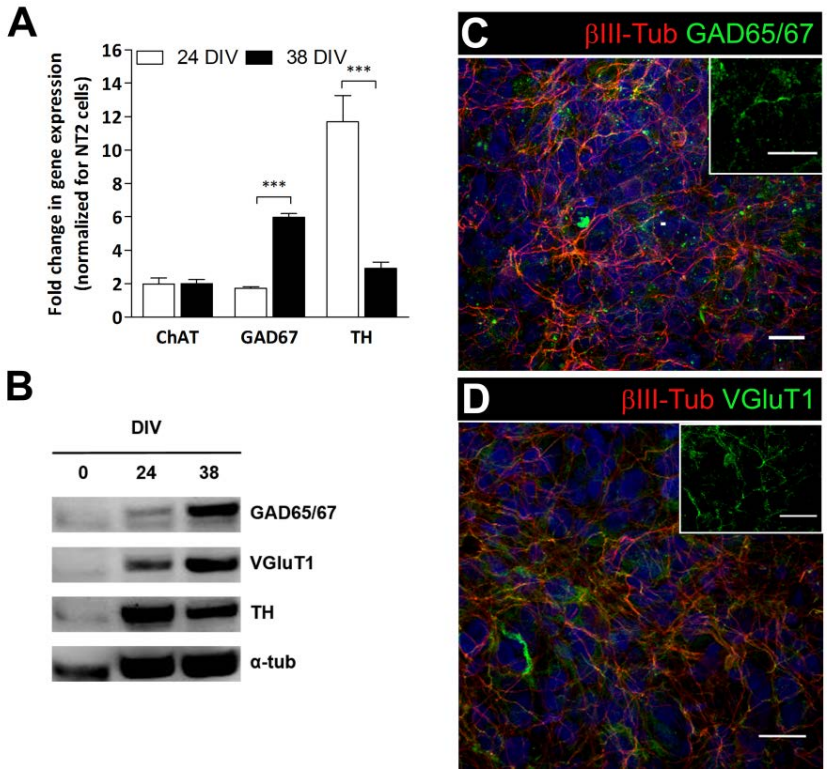

Figure 2.4: Characterization of neurotransmitter phenotype of neuronal population in neurospheroids. (a) qRT-PCR analysis of ChAT, GAD67 and TH gene expression; fold increase in gene expression of neurospheroids at 24 and 38 DIV relatively to NT2 undifferentiated cells; data are mean ± SD of three independent cultures;***indicate significant difference with $P < 0.001$ by one-way ANOVA analysis with Tukey's post multiple comparison test. (b) Detection of TH, VGluT1 and GAD65/67 by Western blot analysis; β-tubulin (β-tub) was used as loading control. (c) Immunofluorescence microscopy of neurospheroids (38 DIV); scale bar: 20 µm; βIII-tubulin (βIII-tub) (red), GAD65/67 (green) and DAPI (blue). (d) Immunofluorescence microscopy of neurospheroids (38DIV); scale bar: 20 µm; βIII-tubulin (red), VGluT1 (green) and DAPI (blue). For (b), (c) and (d) data are from one representative experiment of three independent cultures.

In terms of astrocytic differentiation, expression of GFAP significantly increased from 24 to 38DIV (Fig. 2.5a). In accordance, GFAP protein reached detectable levels by 38DIV (Fig. 2.5b), with $GFAP^+$ cells homogeneously distributed across the neurospheroids (Fig. 2.5c) and being 77.5 ± 4.9% of total cells in culture. These results indicated that the extended period implemented (Fig. 2.1a) was essential to obtain NT2 astrocytic cells expressing GFAP. Expression of the astrocytic markers S100-β, GLAST and GLT-1 was evaluated in order to confirm the astrocytic nature of

these cells (Cantini et al., 2012). Expression of S100- β increased during differentiation until 38DIV (Fig. 2.5a).

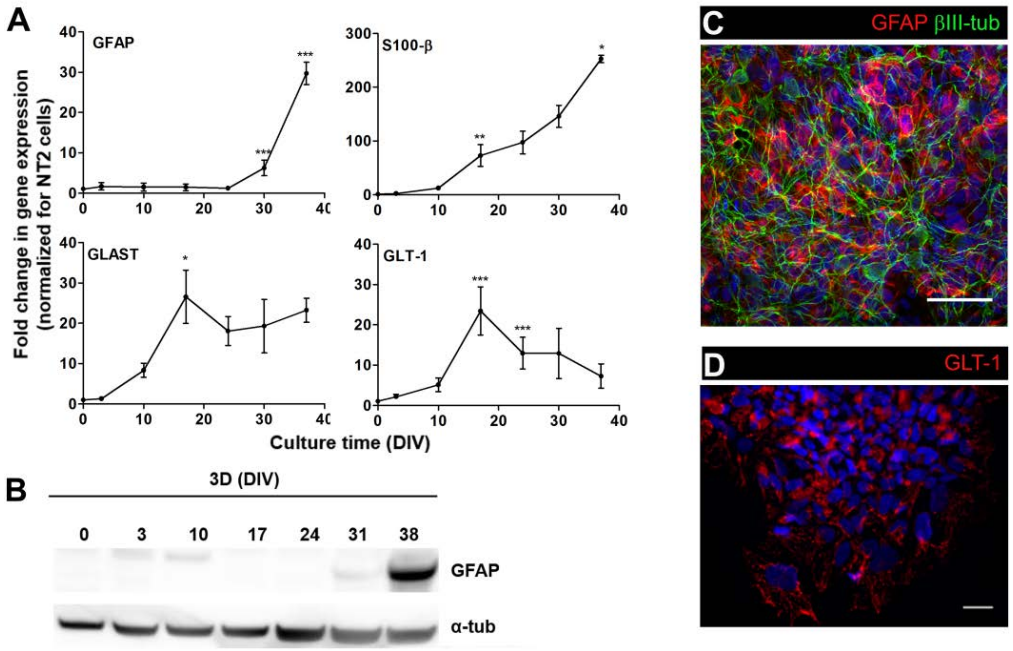

Figure 2.5: Characterization of astrocytic population in neurospheroids. (a) qRT-PCR analysis of GFAP, S100-β, GLAST and GLT-1 gene expression; fold increase in gene expression of neurospheroids along culture relatively to NT2 undifferentiated cells; data are mean ± SD of three independent cultures. Asterisks indicate significant difference (*P < 0.05, **P < 0.01 and***P < 0.001) by one-way ANOVA analysis with Tukey's post multiple comparison test. (b) Detection of GFAP by Western blot analysis; β-tubulin (β-tub) was used as loading control (c) Immunofluorescence microscopy of neurospheroids (38DIV); scale bar: 20 m; βIII-tubulin (green), GFAP (red) and DAPI (blue). (d) Immunofluorescence microscopy of neurospheroids (38DIV); scale bar: 20 µm; GLT-1 (red) and DAPI (blue). For (b), (c) and (d) data are from one representative experiment of three independent cultures.

Upregulation of the two main Glu transporters, GLAST and GLT-1, was observed until 17DIV, with maintenance of high levels of expression thereafter (Fig. 2.5a), with GLT-1$^+$ cells detected at 38DIV (Fig. 2.5d). Altogether, these results indicated that culture time extension besides the 3-weeks RA induction was essential to attain differentiated neurospheroids, which by 38DIV were enriched in GFAP$^+$ astrocytes, as well as MAP2$^+$ mature neurons with several neurotransmitter phenotypes. Neurospheroids from 38DIV onwards were referred as differentiated neurospheroids (Fig. 2.1a) and applied in neurotoxicity studies.

3.2. Characterization of 3D neural cell cultures by neuronal and astrocytic-specific endpoints

Neuronal and astrocytic specific functional endpoints were implemented in differentiated neurospheroids in multi-well plate format. To assess neuronal synaptic activity, the ability of differentiated neurospheroids to respond to depolarizing stimuli was evaluated using the fluorescent probe FM-1-43 which allows labeling and monitoring synaptic vesicle exocytosis (Gaffield and Betz, 2006). Undifferentiated aggregates (3DIV) and differentiated neurospheroids (38DIV) were loaded with FM-1-43 dye and loss of fluorescence upon a depolarizing stimulus triggered a steeply decrease in fluorescence intensity of differentiated neurospheroids, when compared to undifferentiated aggregates (Fig. 2.3f), suggesting that these neurospheroids contained mature neurons with functional synaptic terminals able to fuse the synaptic vesicles with the plasma membrane and perform exocytosis and neurotransmitters release. Concerning astrocytic features, a four-fold increase in GS gene expression was observed at 38DIV (Fig. 2.6a).

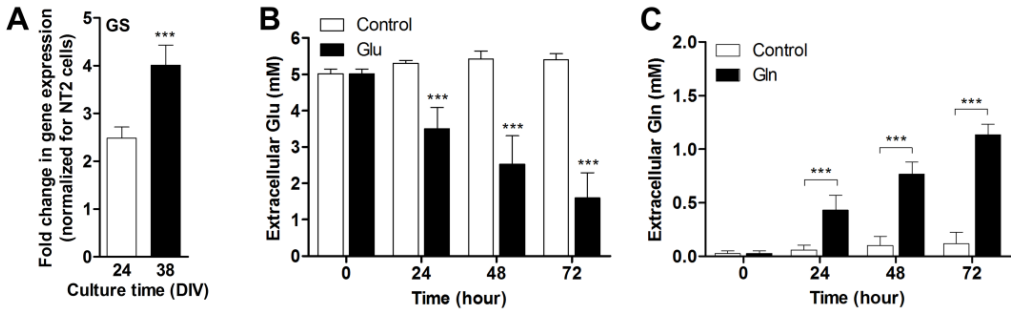

Figure 2.6: Functional characterization of astrocytic population in neurospheroids. (a) qRT-PCR analysis of glutamine synthetase (GS) gene expression; fold increase in gene expression of neurospheroids at day 24 and 38 normalized for NT2 undifferentiated cells. (b) Extracellular glutamate (Glu) clearance. Neurospheroids were incubated with5 mM Glu for 72 h and Glu concentration was measured at 0, 24, 48 and 72 h; medium without cells was used as control. (c) Extracellular glutamine (Gln) concentration. Neurospheroids were incubated with only medium (control) or medium with 5 mM Glu for 72 h and Gln concentration was measured at 0, 24, 48 and 72 h. In (a), (b) and (c) results are mean ± SD of three independent experiments;***indicate significant difference with $P < 0.001$ by one-way ANOVA analysis with Tukey's post multiple comparison test.

Moreover, when differentiated neurospheroids were challenged with medium containing Glu (5 mM), clearance of the metabolite was observed for 72 h (Fig. 2.6c), with an average Glu uptake rate of 0.385 ± 0.137 mol mg $prot^{-1}$ h^{-1}; concomitantly, increased Gln concentrations were detected in cell supernatant for 72 h (Fig. 2.6d), with a seven-fold increase in Gln secretion rate in Glu challenged neurospheroids (0.092 ± 0.026 against 0.013 ± 0.007 mol mg $prot^{-1}$ h^{-1}). Altogether, these results indicate that neurospheroids were capable of Glu internalization, and Gln efflux, suggesting the activity of Glu and Gln transporters, as well as of GS in astrocytes within neurospheroids.

3.3. Neurotoxicity assays

The applicability of the human 3D neural cell model generated in a scalable stirred culture system to feed high-throughput neuro-toxicity studies was evaluated. As a proof of concept, differentiated neurospheroids were used to feed 96-well plates for neurotoxicity assays with toxic compounds: tBHP, an oxidant (Holownia et al., 2009), Acr, a prototypical neurotoxicant (Lopachin and Gavin, 2012) and chloramphenicol, described as neurotoxicant (Grill and Maganti, 2011; Ramilo et al., 1988) and recently suggested to be astrotoxicant (Woehrling et al., 2011). Cellular viability was evaluated as first endpoint for IC50 determination. Initially, in order to set-up assay conditions, a calibration curve was performed distributing 0–100 neurospheroids per well; linearity was observed between 5 and 20 neurospheroids per well (Fig. 2.2). To validate the assay setup in 96-well plates a general oxidant compound was used. Neurospheroids were exposed to 0.008–2 mM tBHP, for 48 h and a dose-response curve was generated based on cellular viability evaluation (determined IC50 of 246 ± 1 µM, Fig. 2.7a).

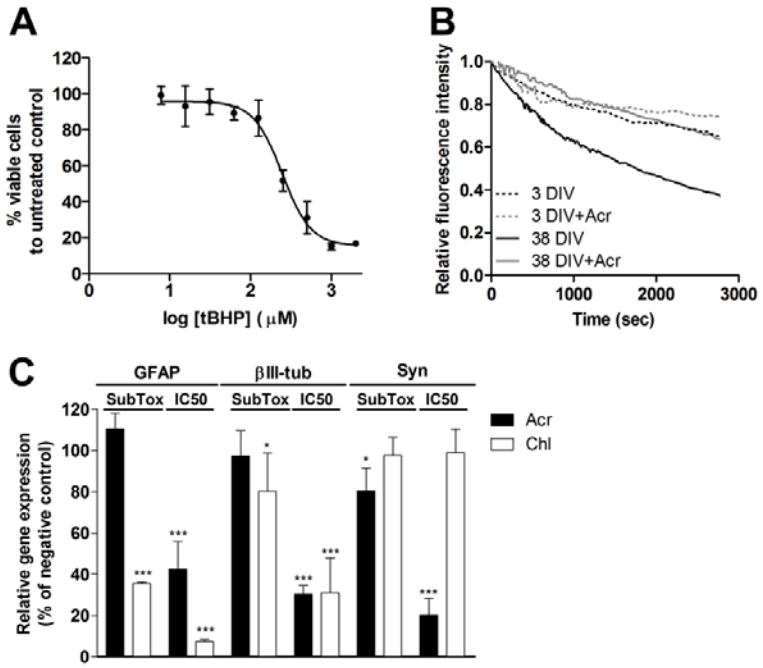

Figure 2.7: Neurotoxicity assays – functional and gene expression endpoints. (a) Dose-response curve of 0.008 - 2 mM tert-buthyl hydroperoxide (tBHP) induced lesion for 48 h, determined by Presto blue assay. (b) FM-1-43 dye assay performed for 3DIV (undifferentiated aggregates) and 38DIV (differentiated neurospheroids) with and without acrylamide incubation (2.47 mM) for 72 h. (c) qRT-PCR analysis of GFAP, βIII-tubulin and synaptophysin gene expression; Relative gene expression of neurospheroids after incubation with acrylamide (0.10 and 2.47 mM)and chloramphenicol (1 and 4.31 mM) for 72 and 48 h (respectively) normalized to negative control; data are mean ± SD of three independent cultures; asterisks indicate significant difference to negative control, with $P < 0.001$ by one-way ANOVA analysis with Tukey's post multiple comparison test.

Dose-response curves were obtained for Acr and chloramphenicol (Fig. 2.2b and 2.2c). Overall, the inter-assay coefficient of variation (%CV) was of 15.8 ± 3.51%, for 12 independent experiments, indicating that evaluation of toxicity using differentiated neurospheroids was a reproducible and robust assay setup. The IC50 and a subtoxic concentration in which cellular viability was affected less than 5% were selected for gene expression and functional endpoints.

3.3.1. Acrylamide neurotoxicity

Differentiated neurospheroids were exposed to Acr in concentrations ranging between 1 µM and 1 M for 72 h and cellular viability was affected in a dose-dependent manner in concentrations above 0.1 mM (Fig. 2.2b). The dose–response

curve of Acr presented a plateau around 40% of cellular viability and the determined IC50 was 2.47 ± 0.45 mM. Evaluation of gene expression of specific cell-makers was used as endpoint (Laurenza et al., 2013). Differentiated neurospheroids were distributed in 6-well plates, incubated with Acr at IC50 and one subtoxic concentration (2.47 and 0.10 mM, respectively) and recovered for qRT-PCR analysis. Exposure to 2.47 mM Acr led to a significant decrease in gene expression of the evaluated neuronal and astrocytic markers (30.3 ± 4.2, 22.7 ± 3.3 and 42.3 ± 13.5% of control for βIII-tubulin, synaptophysin and GFAP, respectively, Fig. 2.7c). The subtoxic concentration of 0.10 mM Acr did not affect gene expression of cytoskeletal neuronal marker βIII-tubulin and the astrocytic marker GFAP; noteworthy, for synaptophysin a significant decrease in gene expression (80.4 ± 7.2% of control, Fig. 2.7c) was observed, indicating that expression of this pre-synaptic marker was affected before further cellular effects could be detected. In order to determine if the toxicant impaired synaptic functionality, the ability of Acr (2.47 mM)-treated neurospheroids to respond to depolarizing stimuli was evaluated. This stimulus triggered a smaller decrease in fluorescence intensity of differentiated neuro-spheres exposed to Acr than differentiated neurospheroids without treatment (Fig. 2.7b) and comparable to undifferentiated aggregates. The data obtained suggested that Acr affected synaptic activity of neurons and that this assay could be used as a functional endpoint for neurotoxicity evaluation.

3.3.2. Chloramphenicol neurotoxicity

Differentiated neurospheroids were exposed to chloramphenicol in concentrations ranging between 39 µM and 10 mM, for 48 h. Cellular viability was affected in a dose-dependent manner in concentrations above 0.1 mM (Fig. 2.2c) and the determined IC50 was 4.31 ± 0.85 mM. Upon exposure of neurospheroids to the IC50 concentration (4.31 mM), gene expression of both βIII-tubulin neuronal and GFAP astrocytic markers was affected (31 ± 16.7 and 7.3 ± 1 % of negative control, respectively, Fig. 2.7c). Exposure to a subtoxic concentration (1 mM) was sufficient to induce dramatic changes in expression of astrocytic GFAP, but only

minor changes in the neuronal βIII-tubulin (35.4 ± 0.7 and 80.1 ± 18.4 % of negative control, respectively, Fig. 2.7c). These results indicated that the changes in gene expression induced by chloramphenicol treatment were dose-dependent, with higher impact on astrocytic GFAP; therefore these can be used as sensitive endpoints for chloramphenicol-mediated toxicity, particularly in astrocytes.

4. Discussion

In this work we developed a scalable 3D culture strategy using stirred suspension culture systems for robust and reproducible differentiation of NT2 cells, which allow efficient production of high numbers of stable neurospheroids containing not only mature and functional human neurons but also astrocytes, in a 50% less time-consuming process when compared with the 2D culture systems (Goodfellow et al., 2011). This was accomplished having as starting point a protocol forNT2 neuronal differentiation in stirred suspension culture systems previously developed in our laboratory (Serra et al., 2009, 2007), which increased 10-fold the final yields of NT2 neurons, favoring cell–cell interactions and promoting an increased synchrony in response of undifferentiated cells to RA (Tonge et al., 2010). Herein, an extended culture time was introduced to obtain neurospheroid enrichment in functional astrocytes, as well as mature neurons, modeling more consistently the basic CNS unit and increasing neurospheroid reliability on neurotoxicity assessment. The applicability of the human 3D neural cell model generated to feed high-throughput neurotoxicity studies was evaluated by using neurospheroids obtained to feed multi-well plates. From one 125 mL culture, we are able to feed more than one hundred 96-well plates (typically 10 neurospheroids/ well). Moreover, the use of a scalable culture system allows easy scale-up if higher numbers of neurospheroids are required for even higher throughput. Therefore, our differentiated neurospheroids production process, in combination with automated measurement of fluorescence-based endpoints, is applicable for first screening high-throughput neurotoxicity assays. The culture

system described herein allowed obtaining differentiated neurospheroids by 38DIV; these neurospheroids were composed mainly of $GFAP^+$ cells (77.5 ± 4.9% of total cells), βIII-$tubulin^+$/$MAP2^+$ neurons and few $nestin^+$ cells, with the different cells types homogeneously distributed through the neurospheroids. Similarly, astrocytes greatly outnumber neurons *in vivo*, depending on the brain region, often 10:1 (Allen and Barres, 2009). Moreover, differentiated neurospheroids composition was kept stable for at least 12 additional DIV (up to 50DIV, not shown), allowing to start several assays during this time interval with reproducible results. Notably, the proportion of $GFAP^+$ cells in the neurospheroids was maintained between different batches, indicating a small batch-to-batch variation in differentiation efficiencies. Neurospheroid concentration and size (Fig. 2.1b) were also maintained through different batches, highlighting the reproducibility and robustness of the process. βIII-$tubulin^+$ neurons were detected early in culture, around10DIV, while $GFAP^+$ astrocytes were only detected by 31DIV. This is in line with *in vivo* prenatal neural development where neurogenesis is followed by astrocytic differentiation and also with ESC *in vitro* differentiation that generate neurons in the first month and astrocytes after 2–3 months (Hu et al., 2010). Together, these results indicate that the order of neuronal and astrocytic differentiation of NT2 cells resembles those in normal brain development and therefore this model could also be applied to developmental neurotoxicity studies. Importantly, NT2 cell differentiation has the advantage of being a much simpler and less time-consuming process than ESC or NSC differentiation (Gupta et al., 2012; Schwarz, 2007), as it requires only RA as differentiation factor, thus providing a more amenable and cost-effective cell model to be used in high-throughput platforms. Excitatory glutamatergic neurons and inhibitory GABAergic neurons, the main neuronal phenotypes in brain, were detected in differentiated neurospheroids. Furthermore, detection of $MAP2^+$ neurons, and the increase in synaptophysin gene expression during differentiation, with accumulation of $synaptophysin^+$ vesicles detected in a punctate pattern along neuronal processes

suggest that neuronal maturation occurred within neurospheroids. The ability of neurospheroids to respond with exocytosis of vesicles to depolarizing stimuli confirmed that mature neurons with functional synapses were present within neurospheroids, presenting the ability of synaptic vesicle fusion with the plasma membrane and neurotransmitter release. Concerning astrocytic differentiation, expression of S100-β was detected earlier than GFAP, probably because this calcium-binding protein is present in neural precursor cells committed to the astrocytic lineage (Donato et al., 2009). The presence of GLT-1 along differentiation suggest that astrocytic maturation occurred within neurospheroids since it is the predominant Glu transporter in astrocytes, being responsible for 90% of total Glu uptake by all excitatory aminoacid transporters in adult brain (Kim et al., 2011). Furthermore, astrocytic maturation was confirmed by the ability of neurospheroids to perform Glu uptake from the extracellular media and Gln production upon Glu challenge. These results suggested the presence of functional Glu transporters, which are the main mediators of Glu clearance by astrocytes; active GS, which is an astrocyte-specific enzyme responsible for conversion of Glu into Gln (Zou et al., 2010); and Gln efflux into the extracellular space via Gln transporters. These are essential steps of the well-described Gln–Glu cycle, involved in supply of Gln to neurons (Amaral et al., 2011; Zou et al., 2010). Furthermore, the Gln secretion rates after Glu challenge (0.092 ± 0.026 μmol mg $prot^{-1}$ h^{-1}) were in line with those previously determined for primary cultures of pure astrocytes (0.049 ± 0.005 μmol mg $prot^{-1}$ h^{-1}; Amaral et al., 2011), which might be explained by the high astrocyte : neuron cell ratio observed in differentiated neurospheroids. The developed cell model was validated for neurotoxicity assays by evaluating the response of neurospheroids to exposure to Acr and chloramphenicol, previously described as neurotoxicants (Grill and Maganti, 2011; Lopachin and Gavin, 2012; Ramilo et al., 1988). Acr is a widely used industrial chemical with proved neurodegenerative effects in humans, with nerve terminals being described as a primary site of Acr action (Lopachin and Gavin, 2012). We observed Acr effects on cellular viability

with an IC50 of 2.47 mM, within the range of previously reported for murine cells and animal studies; IC50s of 2.68 and 1.90 mM were reported for differentiated PC12 and primary cultures of cerebellum cells, respectively (Gartlon et al., 2006) and average LD50 values of 160.8 mg/kg (i.e., 2.26 mmol/kg; Hoffmann et al., 2010), for rodents. Acr affected synaptophysin gene expression, which was significantly decreased in Acr-treated neurospheroids even at subtoxic concentrations, while changes in commonly used toxicity endpoints such as cytoskeletal genes expression (βIII-tubulin) and cellular viability (Laurenza et al., 2013; Stern et al., 2013) could not be detected at these concentrations. Furthermore, the response of Acr-treated neurospheroids to depolarizing stimuli decreased to levels similar to those of undifferentiated aggregates, indicating loss of ability of synaptic vesicles to fuse with plasma membrane and perform exocytosis. Altogether, our results suggest that Acr neurotoxicity mechanism involves impairment of synaptic activity, in particular presynaptic function. This is in line with previous reports that showed that Acr inhibits proteins involved in synaptic vesicle cycle, as N-ethylmaleimide-sensitive factor and some SNARE proteins (Barber and LoPachin, 2004) and consequently interfere with membrane fusion processes and impairs neurotransmitter release (Exon, 2006; Lopachin and Gavin, 2012). Moreover, our results suggested that gene expression analysis of the neuronal marker synaptophysin can be used as a high sensitive endpoint for neuronal toxicity. Chloramphenicol is a widely used broad spectrum antibiotic known to be neurotoxic (Grill and Maganti, 2011; Ramilo et al., 1988). We observed that chloramphenicol affects cellular viability, with an IC50 of 4.31 mM, which is within the range of the LD50 previously reported for rodents – 2270 mg/kg (i.e., 7.02 mmol/kg; Hoffmann et al., 2010). Concerning specific neural markers, chloramphenicol affected neuronal βIII-tubulin but not synaptophysin gene expression and, to a major extent, astrocytic GFAP gene expression. Altogether, our results suggested that chloramphenicol toxicity mechanism involves impairment of cytoskeletal proteins βIII-tubulin and GFAP. Although chloramphenicol

neurotoxicity mechanisms are not well known, this is in line with a previous report that described that chloramphenicol induces cytoskeletal injury, including degeneration of neurofilaments in neuronal cells and, more significantly, GFAP in astrocytic cells, being more toxic to astrocytes than to neurons (Woehrling et al., 2011). Moreover, our results suggested that gene expression analysis can be used as a high sensitive endpoint to distinguish between neuronal and astrocytic toxicity. Cell viability within neurospheroids was affected by the oxidant tBHP (Holownia et al., 2009), in a dose-dependent manner. In brain, oxygen free radicals are constantly produced and can damage neural cells and oxidative stress is known to be involved in most neurodegenerative diseases (Federico et al., 2012). Therefore, our model can also be used as model to neurodegeneration-related oxidative stress. Overall, our results showed that human NT2-derived differentiated neurospheroids are compatible with multi-well plate assay formats for high-throughput neurotoxicity evaluation campaigns, with clear advantages in terms of relevance when compared with standard 2D culture systems (Hill et al., 2008; Moors et al., 2009). Taking into account the typical workflow of high-throughput assays (from cell counting and seeding, to data acquisition and analysis), all steps are amenable to be performed in automated high-throughput screening platforms applying recent advances in robotic systems for high-throughput campaigns (Fennema et al., 2013; Trumpi et al., 2014). Moreover, complementary to cellular viability, the specific endpoints implemented – gene expression and functionality, presented high sensitivity, allowing early detection of disturbed neuronal or astrocytic functions and their correlation with mechanisms of toxicity. The use of a larger set of known neurotoxic test compounds, such as methylmercury or hydroxyurea (Mundy et al., 2009), as well as the performance of neuroprotection assays will provide additional validation of the relevance and robustness of this 3Dhuman brain *in vitro* cell model for neurotoxicity evaluation. For repeated dose applications, neurospheroids can be distributed into microfluidic devices such as

multi-organ chip platforms, which will allow long-term cultures in miniaturized controlled environments (Materne et al., 2015).

5. Conclusion

Differentiation of NT2 cell line using stirred suspension culture systems with integration of a maturation step allowed obtaining a 3D co-culture enriched in mature and functional human neurons and astrocytes, homogeneously distributed throughout neurospheroids, modeling more consistently the CNS composition. This efficient and robust scalable culture strategy generates large numbers of human differentiated neurospheroids, providing an amenable and cost-effective cell model. Moreover, the feasibility of using this culture strategy to feed high-throughput neurotoxicity studies was demonstrated by the determination of the neurotoxicity of several toxicants. The implementation of specific endpoints such as gene expression analysis of cell-specific markers and functional assays allowed detection of specific neuronal and astrocytic effects of tested compounds with improved sensibility.

6. Acknowledgements

This work was partially supported by Fundação para a Ciência e Tecnologia (FCT), Portugal, under the scope of the projects PTDC/EBB-BIO/112786/2009 and PTDC/EBB-BIO/119243/2010 and by the PhD fellowships to APT, PD/BD/52473/2014 and to CP, PD/BD/52202/2013. Tecnimede - Sociedade Técnico Medicinal S.A. sponsored the work that lead to the development of the cell model described. The authors acknowledge Ana Teixeira for fruitful discussion concerning neural metabolism and Lorena Ardaya for technical support in neurotoxicity assays.

7. References

Allen, N.J., Barres, B.A., 2009. Glia—more than just brain glue. Neuroscience 457,675–677.

Alonso-Nanclares, L., Defelipe, J., 2005. Vesicular glutamate transporter 1 immuno-staining in the normal and epileptic human cerebral cortex. Neuroscience 134, 59–68,

http://dx.doi.org/10.1016/j.neuroscience.2005.03.038.

Amaral, A.I., Teixeira, A.P., Håkonsen, B.I., Sonnewald, U., Alves, P.M., 2011. A comprehensive metabolic profile of cultured astrocytes using isotopic transient metabolic flux analysis and C-labeled glucose. Front. Neuroenergetics 3 (5), http://dx.doi.org/10.3389/fnene.2011.00005.

Bani-Yaghoub, M., Felker, J.M., Naus, C.C.G., 1999. Human NT2/D1 cells differentiate into functional astrocytes. Neuroreport 10, 3843–3846, http://dx.doi.org/10.1097/00001756-199912160-00022.

Barber, D.S., LoPachin, R.M., 2004. Proteomic analysis of acrylamide-protein adduct formation in rat brain synaptosomes. Toxicol. Appl. Pharmacol. 201, 120–136, http://dx.doi.org/10.1016/j.taap.2004.05.008.

Breier, J.M., Gassmann, K., Kayser, R., Stegeman, H., De Groot, D., Fritsche, E., Shafer,T.J., 2010. Neural progenitor cells as models for high-throughput screens of developmental neurotoxicity: state of the science. Neurotoxicol. Teratol. 32, 4–15, http://dx.doi.org/10.1016/j.ntt.2009.06.005.

Breslin, S., Driscoll, L.O., 2013. Three-dimensional cell culture: the missing link indrug discovery. Drug Discov. Today 18, 240–249.

Brito, C., Escrevente, C., Reis, C.A., Lee, V.M., Trojanowski, J.Q., Costa, J., 2007.Increased levels of fucosyltransferase IX and carbohydrate lewis X adhesion determinant in human NT2N neurons. J. Neurosci. Res. 1270, 1260–1270, http://dx.doi.org/10.1002/jnr.

Brito, C., Simão, D., Costa, I., Malpique, R., Pereira, C.I., Fernandes, P., Serra, M.,Schwarz, S.C., Schwarz, J., Kremer, E.J., Alves, P.M., 2012. Generation and genetic modification of 3D cultures of human dopaminergic neurons derived from neural progenitor cells. Methods 56, 452–460.

Cantini, G., Pisati, F., Pessina, S., Finocchiaro, G., Pellegatta, S., 2012. Immunotherapy against the radial glia marker GLAST effectively triggers specific anti-tumor effectors without autoimmunity. Oncoimmunology, 1–10.

Chen, Y., Swanson, R.A., 2003. Astrocytes and Brain Injury, 137–149, http://dx.doi.org/10.1097/01.WCB.0000044631.80210.3C.

Conti, L., Cattaneo, E., 2010. Neural stem cell systems: physiological players or *in vitro* entities? Nat. Rev. Neurosci. 11, 176–187, http://dx.doi.org/10.1038/nrn2761.

Donato, R., Sorci, G., Riuzzi, F., Arcuri, C., Bianchi, R., Brozzi, F., Tubaro, C.,Giambanco, I., 2009. S100B's double life: intracellular regulator and extracellular signal. Biochim. Biophys. Acta 1793, 1008–1022, http://dx.doi.org/10.1016/j.bbamcr.2008.11.009.

Exon, J.H., 2006. A review of the toxicology of acrylamide. J. Toxicol. Environ. Health.B. Crit. Rev. 9, 397–412, http://dx.doi.org/10.1080/10937400600681430.

Federico, A., Cardaioli, E., Da Pozzo, P., Formichi, P., Gallus, G.N., Radi, E., 2012. Mitochondria, oxidative stress and neurodegeneration. J. Neurol. Sci. 322, 254–262, http://dx.doi.org/10.1016/j.jns.2012.05.030.

Fennema, E., Rivron, N., Rouwkema, J., van Blitterswijk, C., de Boer, J., 2013. Spheroid culture as a tool for creating 3D complex tissues. Trends Biotechnol. 31, 108–115, http://dx.doi.org/10.1016/j.tibtech.2012.12.003.

Gaffield, M.a., Betz, W.J., 2006. Imaging synaptic vesicle exocytosis and endocytosis with FM dyes. Nat. Protoc. 1, 2916–2921, http://dx.doi.org/10.1038/nprot.2006.476.

Gartlon, J., Kinsner a, Bal-Price a, Coecke S., Clothier R.H., 2006. Evaluation of a proposed *in vitro* test strategy using neuronal and non-neuronal cell systems for detecting neurotoxicity. Toxicol. *In Vitro* 20, 1569–1581, http://dx.doi.org/10.1016/j.tiv.2006.07.009.

Goodfellow, C.E., Graham, S.E., Dragunow, M., Glass, M., 2011. Characterizationof NTera2/D1 cells as a model system for the investigation of cannabinoid function in human neurons and astrocytes. J. Neurosci. Res. 89, 1685–1697,http://dx.doi.org/10.1002/jnr.22692.

Grill, M.F., Maganti, R.K., 2011. Neurotoxic effects associated with antibi-otic use: management considerations. Br. J. Clin. Pharmacol. 72, 381–393, http://dx.doi.org/10.1111/j. 1365-2125.2011.03991.x.

Gupta, K., Patani, R., Baxter, P., Serio, A., Story, D., Tsujita, T., Hayes, J.D., Peder-sen, R.A., Hardingham, G.E., Chandran, S., 2012. Human embryonic stem cell-derived astrocytes mediate non-cell-autonomous neuroprotection through endogenous and drug-induced mechanisms. Cell Death Differ. 19, 779–787,http://dx.doi.org/10.1038/cdd.2011.154.

Hill, E.J., Woehrling, E.K., Prince, M., Coleman, M.D., 2008. Differentiating humanNT2/D1 neurospheres as a versatile *in vitro* 3D model system for developmental neurotoxicity testing. Toxicology 249, 243–250, http://dx.doi.org/10.1016/j.tox.2008.05.014.

Hoffmann, S., Kinsner-Ovaskainen, A., Prieto, P., Mangelsdorf, I., Bieler, C., Cole,T., 2010. Acute oral toxicity: variability, reliability, relevance and inter-species comparison of rodent LD50 data from literature surveyed for the Acute-Tox project. Regul. Toxicol. Pharmacol. 58, 395–407, http://dx.doi.org/10.1016/j.yrtph.2010.08.004.

Holownia, A., Mroz, R.M., Wielgat, P., Skiepko, A., Sitko, E., Jakubow, P., Kolodziejczyk,A., Braszko, J.J., 2009. Propofol protects rat astroglial cells against tert-butylhydroperoxide—induced cytotoxicity; the effect on histone and cAMP-response element-binding protein (CREB). Signaling, 63–69.

Hu, B., Weick, J.P., Yu, J., Ma, L., Zhang, X., Thomson, J.A., 2010. Neural differentiation of human induced pluripotent stem cells follows developmental principles but with variable potency 1, http://dx.doi.org/10.1073/pnas.0910012107.

Irons, H.R., Cullen, D.K., Shapiro, N.P., Lambert, N. a, Lee, R.H., Laplaca, M.C.,2008. Three-

dimensional neural constructs: a novel platform for neuro-physiological investigation. J. Neural Eng. 5, 333–341, http://dx.doi.org/10.1088/1741-2560/5/3/006.

Kim, K., Lee, S.-G., Kegelman, T.P., Su, Z.-Z., Das, S.K., Dash, R., Dasgupta, S., Barral,P.M., Hedvat, M., Diaz, P., Reed, J.C., Stebbins, J.L., Pellecchia, M., Sarkar, D., Fisher,P.B., 2011. Role of excitatory amino acid transporter-2 (EAAT2) and glutamate in neurodegeneration: opportunities for developing novel therapeutics. J. Cell.Physiol. 226, 2484–2493, http://dx.doi.org/10.1002/jcp.22609.

Laurenza, I., Pallocca, G., Mennecozzi, M., Scelfo, B., Pamies, D., Bal-Price, A., 2013.A human pluripotent carcinoma stem cell-based model for *in vitro* developmental neurotoxicity testing: effects of methylmercury, lead and aluminum evaluated by gene expression studies. Int. J. Dev. Neurosci. 31, 679–691, http://dx.doi.org/10.1016/j.ijdevneu.2013.03.002.

Livak, K.J., Schmittgen, T.D., 2001. Analysis of relative gene expression data usingreal-time quantitative PCR and the 2(-Delta Delta C(T)) Method. Methods 25, 402–408, http://dx.doi.org/10.1006/meth.2001.1262.

Lopachin, R.M., Gavin, T., 2012. Review molecular mechanism of acrylamide neuro-toxicity: lessons learned from organic chemistry 1650–1657.

Materne, E.-M., Ramme, A.P., Terrasso, A.P., Serra, M., Alves, P.M., Brito, C., Sakharov, D.A., Tonevitsky, A.G., Lauster, R., Marx, U., 2014. A multi-organ chip co-culture of neurospheres and liver equivalents for long-term substance testing. J. Bio-technol., 205, http://dx.doi.10.1016/j.jbiotec.2015.02.002.

Michalczyk, K., Ziman, M., 2005. Nestin structure and predicted function in cellular cytoskeletal organization, 665–671.

Molofsky, A.V., Krencik, R., Krenick, R., Ullian, E.M., Ullian, E., Tsai, H.,Deneen, B., Richardson, W.D., Barres, B. a, Rowitch, D.H., 2012. Astrocytes and disease: a neurodevelopmental perspective. Genes Dev. 26, 891–907, http://dx.doi.org/10.1101/gad.188326.112.

Moors, M., Rockel, T.D., Abel, J., Cline, J.E., Gassmann, K., Schreiber, T., Schuwald, J., Weinmann, N., Fritsche, E., 2009. Human neurospheres as three-dimensional cellular systems for developmental neurotoxicity testing. Environ. Health Perspect. 117, 1131–1138, http://dx.doi.org/10.1289/ehp.0800207.

Mori, H., Hara, M., 2013. Cultured stem cells as tools for toxicological assays. J. Biosci.Bioeng. 116, 647–652, http://dx.doi.org/10.1016/j.jbiosc.2013.05.028.

Mundy, W., Padilla, S., Shafer, T., Gilbert, M., Breier, J., Cowden, J., Crofton, K., Herr,D., Jensen, K., Raffaele, K., Radio, N., Schumacher, K., Epa, N.D.U.S., Toxicology, C., Chapel, N.C., Hill, C., Ord, N., Epa, U.S., City, K., 2009. Building a database of developmental neurotoxicants: evidence from human and animal studies. Toxicologist 108.

Ramilo, O., Kinane, B., McCracken, G., 1988. Chloramphenicol neurotoxicity. Pediatr. Infect. Dis. J. 7, 358.

Schwarz, J., 2007. Developmental perspectives on human midbrain-derived neural stem cells 13, 466–468.

Serra, M., Brito, C., Costa, E.M., Sousa, M.F.Q., Alves, P.M., 2009. Integrating human stem cell expansion and neuronal differentiation in bioreactors, 14, 1–14. doi:10.1186/1472-6750-9-82.

Serra, M., Brito, C., Sousa, M.F.Q., Jensen, J., Tostões, R., Clemente, J., Strehl, R., Hyll-ner, J., Carrondo, M.J.T., Alves, P.M., 2010. Improving expansion of pluripotent human embryonic stem cells in perfused bioreactors through oxygen control .J. Biotechnol. 148, 208–215, http://dx.doi.org/10.1016/j.jbiotec.2010.06.015.

Serra, M., Leite, S.B., Brito, C., Carrondo, M.J.T., Alves, P.M., 2007. Novel culturestrategy for human stem cell proliferation and neuronal differentiation 3566,3557–3566. doi:10.1002/jnr.

Sofroniew, M. V, Vinters, H. V, 2010. Astrocytes: biology and pathology 7–35. doi:10.1007/s00401-009-0619-8.

Stern, M., Gierse, A., Tan, S., Bicker, G., 2013. Human Ntera2 cells as a predictive *in vitro* test system for developmental neurotoxicity. Arch. Toxicol., http://dx.doi.org/10.1007/s00204-013-1098-1.

Tonge, P.D., Andrews, P.W., 2010. Retinoic acid directs neuronal differentiation of human pluripotent stem cell lines in a non-cell-autonomous manner. Differentiation 80, 20–30, http://dx.doi.org/10.1016/j.diff.2010.04.001.

Tralau, T., Luch, A., 2012. Drug-mediated toxicity: illuminating the bad in the test tube by means of cellular assays? Trends Pharmacol. Sci., 1–12, http://dx.doi.org/10.1016/j.tips.2012.03.015.

Trumpi, K., Egan, D.A., Vellinga, T.T., Rinkes, I.H. B., Kranenburg, O.W., 2014. Highthroughput toxicity assay for three-dimensional cell cultures, in: AACR AnnualMeeting 2014; April 5–9, 2014; San Diego, CA.

Woehrling, E.K., Hill, E.J., Torr, E.E., Coleman, M.D., 2011. Single-cell ELISA and flow-cytometry as methods for highlighting potential neuronal and astrocytic toxicant specificity 472–483. doi:10.1007/s12640-010-9202-2.

Zou, J., Wang, Y.-X., Dou, F.-F., Lü, H.-Z., Ma, Z.-W., Lu, P.-H., Xu, X.-M., 2010. Glutamine synthetase down-regulation reduces astrocyte protection against glutamate excitotoxicity to neurons. Neurochem. Int. 56, 577–584, http://dx.doi.org/10.1016/j.neuint.2009.12.021.

CHAPTER 3

Human neuron-astrocyte 3D co-culture-based assay for evaluation of neuroprotective compounds

This chapter was adapted from:

Terrasso AP, Silva AC, Filipe A, Pedroso P, Ferreira AL, Alves PM, Brito C. 2017. Human neuron-astrocyte 3D co-culture-based assay for evaluation of neuroprotective compounds. Journal of pharmacological and toxicological methods, 83, 72–79, doi: 10.1016/j.vascn.2016.10.001.

Table of Contents

Abstract

Central nervous system drug development has registered high attrition rates, mainly due to the lack of efficacy of drug candidates, highlighting the low reliability of the models used in early-stage drug development and the need for new *in vitro* human cell-based models and assays to accurately identify and validate drug candidates. 3D human cell models can include the different tissue cell types and represent the spatiotemporal context of the original tissue (co-cultures), allowing the establishment of biologically-relevant cell-cell and cell-extracellular matrix interactions. Nevertheless, exploitation of these 3D models for neuroprotection assessment has been limited due to the lack of data to validate such 3D co-culture approaches.

In this work we combined a 3D human neuron-astrocyte co-culture with a cell viability endpoint for the implementation of a novel *in vitro* neuroprotection assay, over an oxidative insult. Neuroprotection assay robustness and specificity were evaluated. The applicability of Presto blue, MTT and CytoTox-Glo viability assays to the 3D co-culture was evaluated. Presto Blue was the adequate endpoint as it is non-destructive and is a simpler and reliable assay. Semi-automation of the cell viability endpoint was performed, indicating that the assay setup is amenable to be transferred to automated screening platforms. Finally, the neuroprotection assay setup was applied to a series of 36 test compounds and several candidates with higher neuroprotective effect than the positive control, Idebenone, were identified.

The robustness and simplicity of the implemented neuroprotection assay with the cell viability endpoint enables the use of more complex and reliable 3D *in vitro* cell models to identify and validate drug candidates.

1. Introduction

There is an increased social, clinical and economical need for new therapies targeting central nervous system (CNS) neurodegenerative diseases. CNS drug development slowed down since 1990 and high attrition rates have been registered, with CNS drugs more likely to fail in late-stage clinical trials than others (Kesselheim et al., 2015). The most common reason for failure was the lack of efficacy, highlighting the low reliability of the models used in early-stage development and the need for new preclinical *in vitro* cell-based models and assays to accurately identify and validate new drug candidates (Astashkina and Grainger, 2014; Kesselheim et al., 2015).

Human neural *in vitro* models typically consist of 2D cultures of neuronal-like cells, such as neuroblastoma cell lines (Choi et al., 2011; Del Barrio et al., 2011) or, more recently, pluripotent stem cell-derived neurons (Avior, Sagi, & Benvenisty, 2016). However, to achieve a significant level of mimicry of the *in vivo* tissue, cell models must include the different tissue cell types and be able to represent the spatiotemporal context of the original tissue.

Human *in vitro* 3D models allow the establishment of biologically relevant cell-cell and cell-extracellular matrix interactions, which recapitulate the tissue microenvironment (Edmondson, Broglie, Adcock, & Yang, 2014). In the last years, 3D models have undergone rapid development and gained increased attention as complementary tools for pre-clinical research which bridge the gap between animal models and human clinical trials (Breslin and Driscoll 2013; Astashkina and Grainger 2014). Nevertheless, exploitation of these 3D models for neuroprotection assessment has been limited due to the lack of validated, robust and user-friendly assays.

Cell viability assays have been developed and widely used in standard 2D cultures as simple and robust endpoints (Burroughs et al., 2012). The most commonly used cell viability assays are based on cell metabolic activity, such as tetrazolium- and resazurin-based methods. MTT (3-(4,5-dimethylthiazol-2-yl)-2,5-

diphenyltetrazolium bromide) is an endpoint tetrazolium-based assay that quantifies the cellular metabolic activity through the formation of blue formazan crystals after the cleavage of the tetrazolium ring by mitochondrial dehydrogenases; such crystals can then be solubilized and quantified in cell lysates (Riss et al., 2004). Assays based on tetrazolium reduction that originates water-soluble tetrazolium salts, such as MTS, XTT and WTS are also commercially available. Nevertheless, all of these assays are toxic to the cells (Riss et al., 2004). Resazurin-based methods quantify the cellular metabolic activity by measuring the fluorescence of the water soluble, non-toxic resofurin. This compound is formed through the metabolization of resazurin by live cells and diffuses from the cells into the surrounding medium; therefore cell lysis is not required and cell cultures can be maintained after the measurement (Riss et al., 2004; Sonnaert, Papantoniou, Luyten, & Schrooten, 2014). Alternatively, cell viability can be evaluated by plasma membrane integrity assays that include trypan blue or nucleic acid staining, by ATP determination or by assays that measure the activity of an intracellular enzyme that has been released from cells with damaged membrane integrity (Niles, 2007); these latter can be lactate dehydrogenase (LDH), or cytosolic, lysosomal or transmembrane-bound proteases whose activities are measured using luminogenic peptide substrates. However, the use of these assays in 3D cultures for drug screening requires its validation.

Herein we describe the implementation of an assay setup for neuroprotection evaluation in a 3D human co-culture of neurons and astrocytes over an oxidative insult. We describe the evaluation of several cell viability assays and semi-automation of the endpoint as a proof-of-concept that the neuroprotection assay setup is amenable for high-throughput screening platforms. We have used a scalable 3D human neuron-astrocyte co-culture previously developed, based on the 3D differentiation of the pluripotent embryonic carcinoma-derived NTera-2/ clone D1 (NT2) cell line into neurospheroids, in an agitation-based culture system (Terrasso et al., 2015). This 3D co-culture is an amenable and cost-effective cell

model to feed high-throughput screening platforms and to evaluate human neuronal and astrocytic toxicity with improved sensitivity due to the functional neuron-astrocyte metabolic interactions (Simão et al., 2016; Terrasso et al., 2015).

Finally, we have applied the neuroprotection assay setup implemented in this work to a series of 36 compounds, where several candidates with higher neuroprotective effect than the positive control, Idebenone, were identified.

2. Materials and Methods

2.1. Cell culture and 3D neural differentiation

Undifferentiated NTera-2/ clone D1 (NT2) cells from the American Type Culture Collection (ATCC) were routinely propagated in 2D culture systems (Brito et al., 2007); 3D neural differentiation was performed in an agitation-based culture system as previously described (Terrasso et al., 2015). Briefly, undifferentiated NT2 cells were inoculated as a single cell suspension in 125 mL spinner vessels equipped with a ball impeller (Wheaton) in DMEM, 10% (v/v) fetal bovine serum (FBS) and 1% (v/v) penicillin-streptomycin (P/S; all from Life Technologies). After 3 days of aggregation, neuronal and astrocytic differentiation was induced by addition of 10 µM RA, with a 50% media exchange every 2-3 days for 21 days. Following this period, a neurospheroid 3D neuron-astrocyte co-culture was obtained and maintained in DMEM, 5% (v/v) FBS, 1% (v/v) P/S up to day 50 and applied in neurotoxicity assays between days 38 and 50 of culture.

2.2. Cell viability endpoint

Presto blue™ cell viability assay (Life Technologies) was performed following the manufacturer's instructions. Briefly, Presto blue cell viability reagent was diluted 1:10 in culture media and incubated with neurospheroids for 40 min. at 37ºC and 5% CO_2. The fluorescence intensity was evaluated using a FluoroMax®-4 spectrofluorometer, with excitation and emission wavelengths of 580/ 595 nm, respectively.

A stock solution of 3-(4,5-dimethylthiazol-2-yl)-2,5-diphenyltetrazolium bromide (MTT; Sigma-Aldrich) 5mg/ mL in PBS was diluted 1:10 in culture media and incubated with neurospheroids for 3 hours, at 37ºC and 5% CO_2. Afterwards, blue formazan crystals were dissolved in dimethyl sulfoxide (DMSO), for 15 min. at RT, under shaking conditions, and the absorbance was read at 570 nm.

CytoTox-Glo™ Cytotoxicity Assay (Promega) was performed accordingly to manufacturer's instructions. Briefly, CytoTox-Glo ™ cytotoxicity assay reagent was added to the neurospheroids and incubated for 15 min. at RT, in an orbital shaker. Afterwards, the lysis reagent was added and further incubated for additional 15 min. in agitation before luminescence measurement.

2.3. Semi-automation of cell viability endpoint

Semi-automation of cell viability endpoint was performed using a Hamilton® Microlab STARlet workstation (Hamilton) equipped with 8 independent pipetting channels, a reagent container carrier, a plate carrier (5 positions) and a disposable tip carrier (5 trays with 5 racks). The workstation has an integrated plate storage module with 64 positions and a Biotek Synergy 2 multimode microplate reader controlled by a computer using the MicroLab Star software. A program for the automation of the steps of (1) addition of Presto blue reagent, (2) transfer of medium from assay plate to fluorescence reading plate and (3) fluorescence reading was implemented.

2.4. Neurotoxicity and neuroprotection assays

Neurospheroids were collected from spinner vessels between days 38 and 50 of culture, where aggregate diameter was kept stable, typically with approximately 180 µm, distributed in 96-well plates at 10 neurospheroid/ well and incubated in DMEM, 5% (v/v) FBS, 1% (v/v) P/S, before carrying out neurotoxicity or neuroprotection assays. Six wells were used per test condition and the culture medium was used as an untreated control. Cell viability, evaluated by the Presto blue assay, was used as an endpoint. The neurotoxicity of Idebenone (provided by

Grupo Tecnimede) was evaluated for concentrations between 0.01 nM-100 µM. Thirty-six (36) test compounds were evaluated for their neuroprotective effects on 3D neuron-astrocyte cultures over an oxidative insult. The test compounds were added to the cultures under different regimens: 24 or 48 h pre-incubation, 24 or 48 h pre-incubation followed by 48 h of co-incubation together with tert-butyl hydroperoxide (tBHP) or chloramphenicol, 48 h co-incubation, 48 h co-incubation followed by 24 h post-incubation (Fig. 3.1). tBHP- and chloramphenicol-induced insults were performed by exposure to its half maximal inhibitory concentration (IC50; 280 µM and 4.3 mM, respectively) for 48 h (Terrasso et al., 2015). Negative (medium), insult and test compound neurotoxicity controls have been performed. Cell viability was accessed before exposure to test compound, before tBHP insult and 48h after insult. Final cell viability was calculated as a percentage of cell viability before insult.

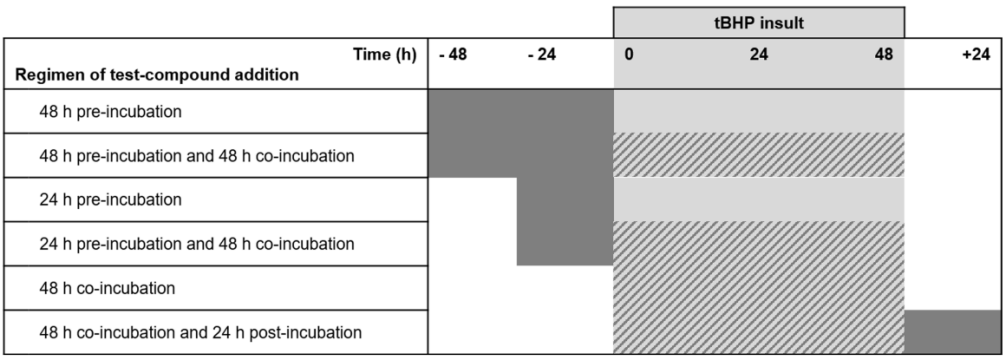

Figure 3.1: Schematic workflow for the addition of test compounds in neuroprotection assay over tBHP insult in 3D human neuron-astrocyte co-culture. Schematic workflow for regimens of test compounds addition for neuroprotection evaluation: tBHP insult (light grey), incubation with test compound (dark grey) and co-incubation of tBHP and test compound (stripes).

2.5. Immunofluorescence microscopy

3D neuron-astrocyte co-cultures were collected at day 38 and processed for immunofluorescence staining, accordingly to (Terrasso et al., 2015). Briefly, the neurospheroids were fixed in 4% (w/v) paraformaldehyde (Sigma) solution in PBS with 4% (w/v) sucrose and processed directly for immunostaining. The primary antibodies used for cell characterization were anti-βIII-tubulin (Millipore) and anti-

glial fibrillary acidic protein (GFAP, DAKO). The secondary antibodies used were goat anti-mouse IgG-AlexaFluor 488 and goat anti-rabbit IgGAlexaFluor 594 (Life Technologies). Cell nuclei were counterstained with 4',6-diamidino-2- phenylindole (DAPI, Life Technologies). Preparations were visualized using a point-scan confocal (Leica SP5) microscope. Merge between channels, maximum z-projections, and orthogonal projections, as well as linear brightness and contrast adjustments of the images were created using the ImageJ software version 1.47 m (http://rsbweb.nih.gov/ij/).

2.6. Statistical Analysis

Statistical analysis was carried out using GraphPad Prism 5 software. Neurotoxicity and neuroprotection data are mean ± SD from at least three independent experiments performed with six replicates. D'Agostino & Pearson omnibus normality test was performed to test if the data follows a normal distribution. One-way ANOVA analysis with Tukey's post multiple comparison test was performed to assess statistical differences between samples and controls in neuroprotection assays. $P < 0.001$ was chosen as the level of significance.

3. Results

3.1. Neurospheroids cultured in 96 well plates are amenable for cell viability and neuroprotection assays

For the implementation of a viability readout in neurospheroids (Fig. 3.2a, b) we have evaluated three different viability assays: a resazurin-based cell viability assay (Presto Blue™) and MTT, which measure cell metabolic activity based on resazurin reduction and on tetrazolium salt formation, respectively, and CytoTox-Glo, which measures cell death based on the activity of an intracellular protease in the cell culture supernatant.

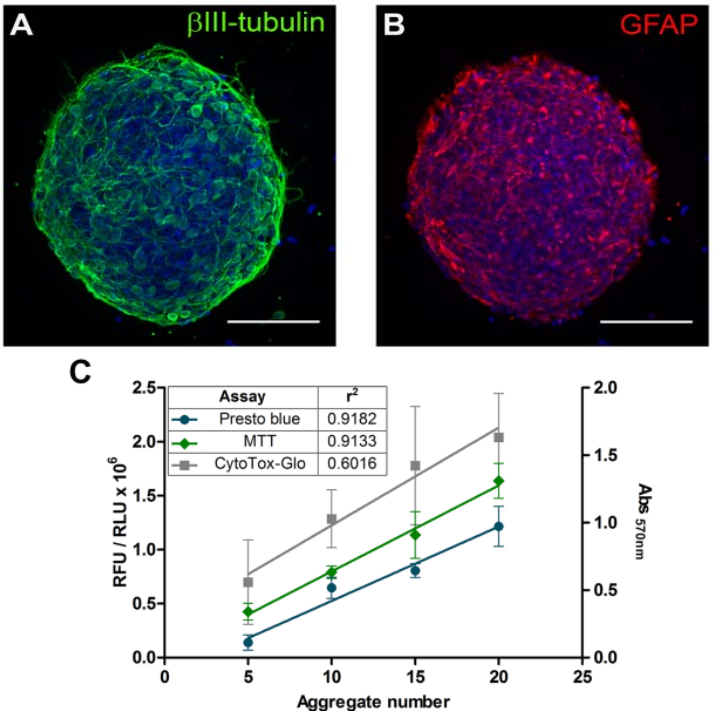

Figure 3.2: Cell viability assays in 3D human neuron-astrocyte co-culture. Immunofluorescence microscopy of 3D human neuron-astrocyte co-culture. βIII-tubulin (green) and DAPI (blue) (a);GFAP (red) and DAPI (blue) (b); scale bars: 100 µm. (c) Calibration curves performed for the cell viability assays Presto blue (blue; data in relative fluorescence units (RFU)), MTT (green; Abs 570nm) and CytoTox-Glo (grey; data in relative luminescence units (RLU)). 5 to 20 neurospheroids were distributed per well and incubated for 72 h before carrying out the viability assay; data are mean ± SD of at least two independent experiments per aggregate number, all with six technical replicates.

Differentiated neurospheroids, composed of neurons and astrocytes (Fig. 3.2 a,b), were generated in stirred-tank culture system as previously described (Terrasso et al., 2015). Neurospheroids were distributed in 96-well plates at increasing concentrations, ranging from 5 to 100 neurospheroids/ well. For the three cell viability methods, signal intensity correlated linearly with the aggregate number (Fig 3.2c) from 5 to 20 aggregate/ well. Nonetheless, the coefficients of determination (r^2) were higher for Presto Blue (0.92) and MTT (0.91) assays than for CytoTox-Glo (0.60; Fig 2c). Moreover, higher standard deviations were obtained for the latter, indicating higher intra-assay variability, compared with the Presto Blue and MTT assays. This might have been due to a heterogeneous aggregate lysis,

a step required in CytoTox-Glo assay for data normalization. Thus, the Presto Blue assay was chosen to measure the cell viability in the neuroprotection assays.

For the implementation of the neuroprotection assay, we have chosen tBHP as the neurotoxic agent, a widely used oxidative lesion inducer in neuronal cultures (Choi et al., 2011; Kaja et al., 2012). The incubation of neurospheroids with 280 µM of tBHP for 48h resulted in approximately 50% reduction of cell viability, measured by Presto Blue (Fig 3.3a,b).

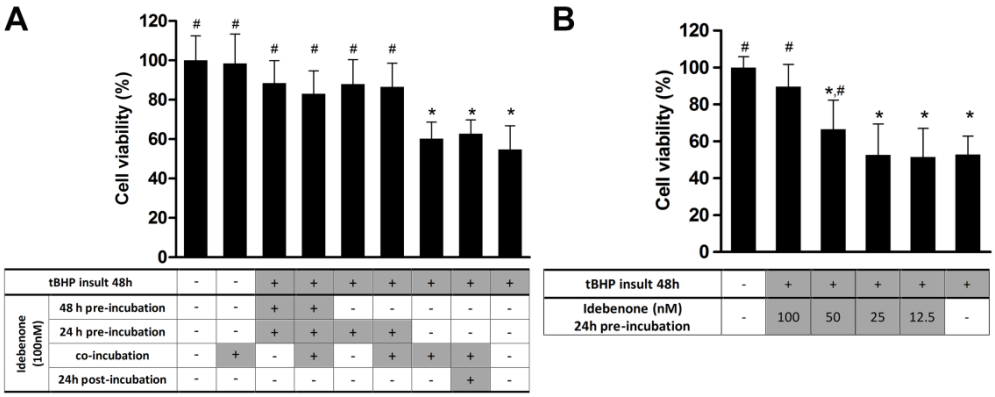

Figure 3.3: Idebenone neuroprotective effect over tBHP insult in 3D human neuron-astrocyte co-culture. (a) Idebenone (100 nM) neuroprotective effect over the tBHP insult in 3D human neuron-astrocyte co-culture evaluated at several regimens: 24 or 48 h pre-incubation, 24 or 48 h pre-incubation and 48 h co-incubation, 48 h co-incubation, 48 h co-incubation and 24 h post-incubation. (b) Idebenone (12.5–100 nM) neuroprotective effect over the tBHP insult in 3D human neuron-astrocyte co-culture evaluated at 24 h pre-incubation. Cell viability was determined 48 h after insult, relatively to cell viability before insult, by Presto blue assay; data are mean ± SD of at least three independent experiments; * indicates significant difference ($P < 0.001$) to negative control (no tBHP insult and no test compound), # indicates significant difference ($P < 0.001$) to insult control (tBHP) by One-way ANOVA analysis with Tukey's post multiple comparison test.

This loss in cell viability was mitigated by a pre-incubation with 100 nM of Idebenone (Fig 3.3a), an analogue of the prototypical anti-oxidant co-enzyme Q10 (Erb et al., 2012), but not by the incubation of the same Idebenone concentration during or after the induction of the insult (Fig 3.3a). Moreover, Idebenone showed a dose-dependent neuroprotection in the 24 h pre-incubation assay layout, with a significant difference from insult control at 50 nM (Fig. 3.3b). Idebenone was not toxic at 100 nM (Fig. 3.3a).

The specificity of the neuroprotective effect of Idebenone over the oxidative insult was evaluated by testing the effect of the compound on a different type of insult. Chloramphenicol, an antibiotic proposed to have neurotoxic effects was chosen. Nevertheless, the mechanisms by which it causes neurotoxicity are not fully described (Wiest, Cochran, & Tecklenburg, 2012). Incubation with 4.3 mM of Chloramphenicol for 48h resulted in approximately 50% reduction in cell viability (Fig. 3.4).

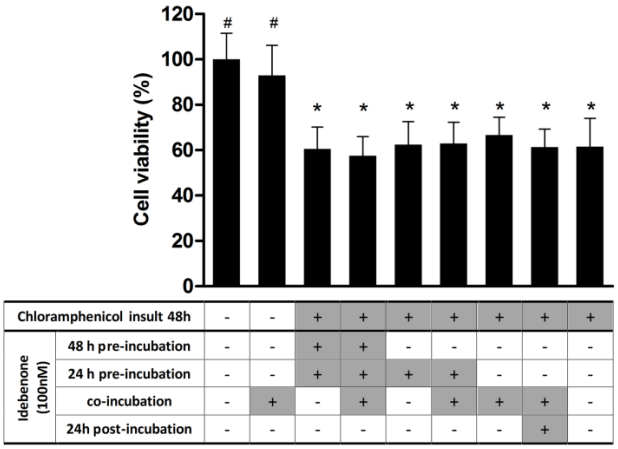

Figure 3.4: Idebenone neuroprotective effect over the chloramphenicol insult in 3D human neuron-astrocyte co-culture. Idebenone (100 nM) neuroprotective effect over the chloramphenicol (4.3 mM) insult in 3D human neuron-astrocyte co-culture evaluated at several regimens: 24 or 48 h pre-incubation, 24 or 48 h pre-incubation and 48 h co-incubation, 48 h co-incubation, 48 h co-incubation and 24 h post-incubation. Cell viability was determined 48 h after insult, relatively to cell viability before insult, by Presto blue assay; data are mean ± SD of three independent experiments; * indicates significant difference (P b 0.001) to negative control (no chloramphenicol-induced insult and no test compound) and # indicates significant difference (P b 0.001) to insult control (chloramphenicol) by One-way ANOVA analysis with Tukey's post multiple comparison test.

Idebenone (100 nM) was not able to revert this loss in cell viability in any of the regimens evaluated (Fig. 3.4), contrary to what was observed over a tBHP insult.

As a proof-of-concept that the implemented assay setup is amenable to be transferred to high-throughput screening platforms, the Presto blue cell viability assay was semi-automated. The Hamilton® Microlab STARlet workstation was used to read the cell viability endpoint semi-automatically and thus evaluate the neuroprotective effect of Idebenone with 24h pre-incubation. The cell viabilities

measured were not significantly different when using the manual or semi-automated methods, for all controls and Idebenone (Fig. 3.5).

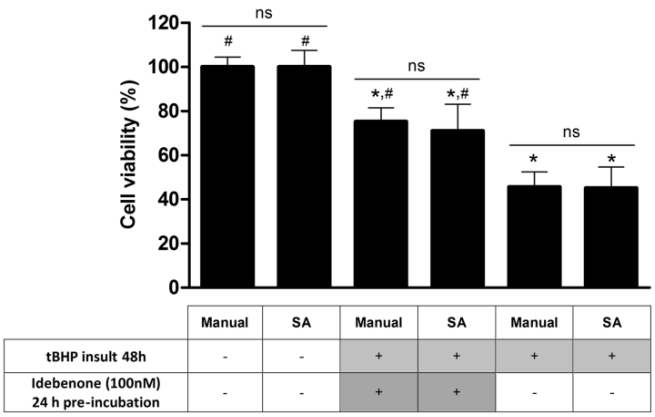

	Manual	SA	Manual	SA	Manual	SA
tBHP insult 48h	-	-	+	+	+	+
Idebenone (100nM) 24 h pre-incubation	-	-	+	+	-	-

Figure 3.5: Semi-automation of Presto blue cell viability endpoint. Idebenone (100 nM) neuroprotective effect over tBHP-insult in 3D human neuron-astrocyte co-culture evaluated at 24 h pre-incubation performing the final step of Presto blue assay and fluorescence reading manually (standard) or semi-automated (SA; using the Hamilton® Microlab STARlet workstation). Cell viability was determined 48 h after insult, relatively to cell viability before insult, by Presto blue assay; data are mean ± SD of at least three independent experiments; * indicates significant difference (P b 0.001) to negative control (no tBHP insult and no test compound), # indicates significant difference (P b 0.001) to insult control (tBHP), ns indicates no significant difference by One-way ANOVA analysis with Tukey's post multiple comparison test.

We showed that all steps of the Presto blue viability assay are amenable to be performed on the workstation and that it was possible to conclude likewise about the neuroprotective effect of Idebenone. This demonstrates the feasibility of transferring the neuroprotection assay to an automated platform.

3.2. Evaluation of the neuroprotective effect of test-compounds over tBHP insult

The implemented assay setup was applied to evaluate the neuroprotective effect of a series of 36 test-compounds, ranging from chemically synthesized compounds (Fig. 3.6) to natural extracts (data not shown).

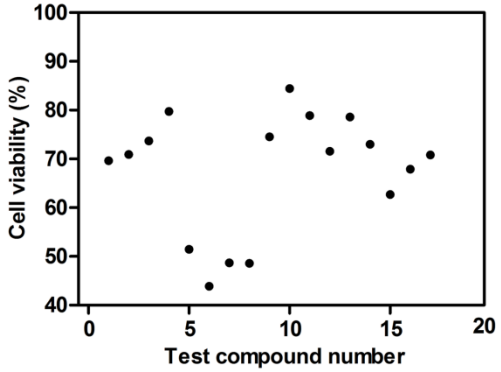

Figure 3.6: Neuroprotective effect of chemically synthesized test compounds over the tBHP insult in human neuron-astrocyte co-culture. The average cell viability is plotted against the test compounds tested at 5 µM with 24 pre-incubation. Cell viability 48 h after insult, relatively to cell viability before insult, determined by Presto blue assay; data are mean of at least three independent experiments. The threshold of a hit compound was set as ≥65% cell viability.

The positive hits (cell viability ≥ 65%) were further tested in different incubation regimens and in dose-response validation assays. For Nicotinamide and Linezolid (compounds 1 and 2 in Fig. 3.6, respectively) the results are presented in Fig. 3.7, where non-toxic concentrations of both compounds were used (Fig 3.7 a-d).

Nicotinamide and Linezolid were assayed at 1 and 5 µM and displayed neuroprotective effect in pre-incubation regimens only, with no significant differences between the two concentrations tested (Fig. 3.7 a-d). A significantly higher neuroprotection was detected in 24 h pre-incubation in comparison to 48 h pre-incubation. Nicotinamide and Linezolid were further tested at lower concentrations (1 nM and 1 pM) and there were no significant differences between all tested concentrations (Fig. 3.7e and f), although a slight decrease in cell viability was observed at such lower concentrations.

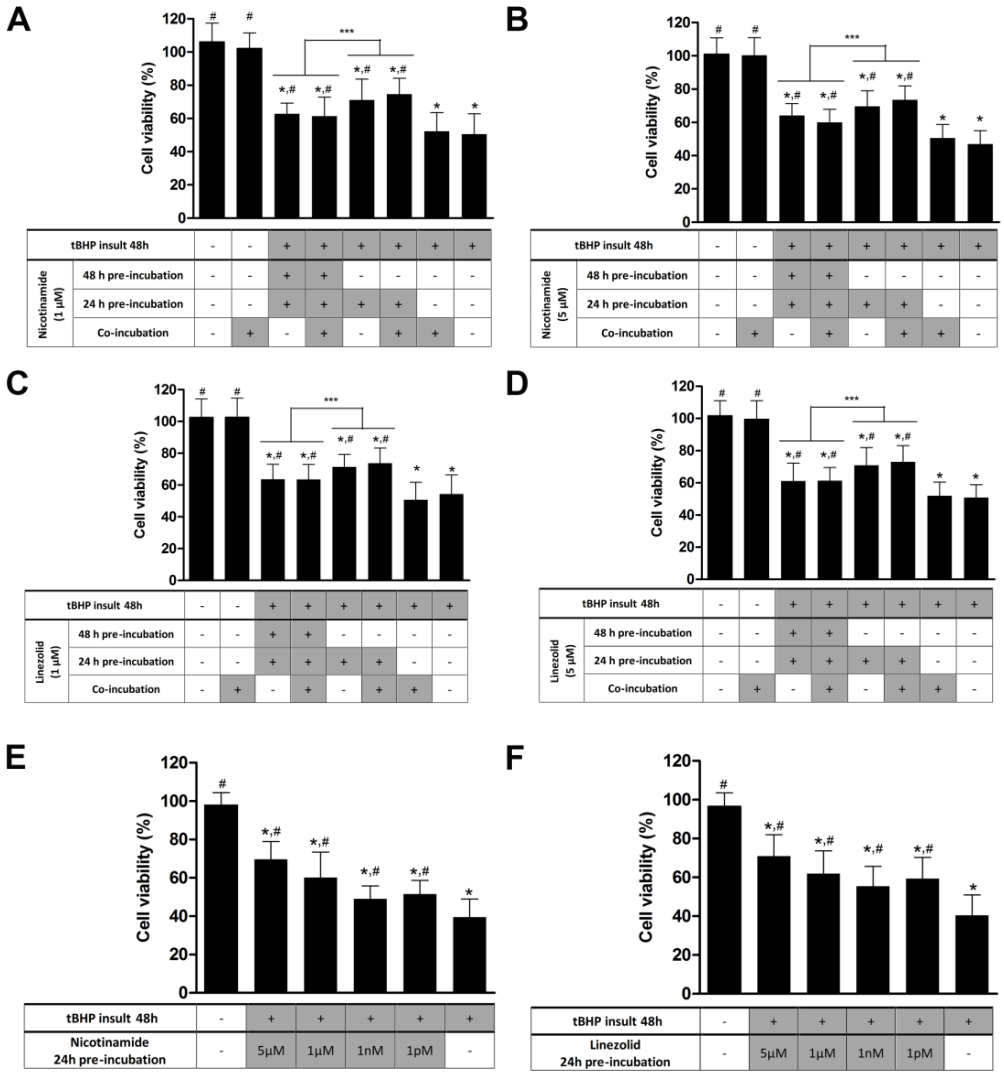

Figure 3.7: Nicotinamide and Linezolid neuroprotective effect over the tBHP insult in 3D human neuron-astrocyte co-culture. (a, b, c and d) Neuroprotective effect over tBHP insult in 3D human neuron-astrocyte co-culture evaluated at several regimens: 24 or 48 h pre-incubation, 24 or 48 h pre-incubation and 48 h co-incubation, 48 h co-incubation, 48 h co-incubation and 24 h post-incubation. (a) and (b) Nicotinamide, 1 and 5 µM, respectively. (c) and (d) Linezolid, 1 and 5 µM, respectively. Nicotinamide (e) and Linezolid (f) (1 pM, 1 nM, 1 µM, 5 µM) neuroprotective effect over tBHP insult in 3D human neuron-astrocyte co-culture evaluated at 24 h pre-incubation. (a–f) Cell viability was determined 48 h after insult, relatively to cell viability before insult, by Presto blue assay; data are mean ± SD of at least three independent experiments; * indicates significant difference (P b 0.001) to negative control (no tBHP-insult and no test compound), # indicates significant difference (P b 0.001) to insult control (tBHP) and *** indicates significant difference (P b 0.001) by One-way ANOVA analysis with Tukey's post multiple comparison test.

4. Discussion

In this work we describe the implementation of a new *in vitro* assay setup combining a 3D human neuron-astrocyte co-culture with a cell viability endpoint for screening of neuroprotective compounds. We have shown that this assay is amenable to be transferred to high-throughput platforms.

There is a need for human cell-based models in early-stage drug development which can accurately identify and validate new drug candidates. We evaluated the applicability of Presto blue, MTT and CytoTox-Glo viability assays to evaluate the cell viability of a 3D human neural co-culture. For this, we took advantage of the 3D human neuron-astrocyte co-culture previously developed by us in an agitation-based culture system (Terrasso et al., 2015) which yields large numbers of differentiated neurospheroids, in a scalable culture system. These are mainly composed of glial cells (approximately 80 % of total cells) and neurons, homogeneously distributed throughout the neurospheroids. Aggregate size increased during retinoic acid-induced differentiation period (until day 24), up to an average diameter of approximately 180 µm and was kept stable during the remaining culture time, with low batch-to-batch variation. The application of the 3D culture system for NT2 neural differentiation allowed reducing in 50% culture time and increasing 2.4-fold and 10-fold the final yields of astrocytes and neurons, respectively, in comparison with the standard 2D cultures. Moreover, in 2D co-cultures neurons bundle in small aggregates on top of astrocytes, so cell-cell interactions are minimized, while the 3D culture favours cell-cell and cell-extracellular matrix interactions, closely recapitulating target tissue environment and increasing neurospheroids reliability in neurotoxicity assessment (Hopkins, DeSimone, Chwalek, & Kaplan, 2015; Picollet-D'hahan et al., 2016; Schmidt et al., 2016; Woehrling, Hill, & Coleman, 2010). Thus, the 3D co-culture used herein represents an amenable and cost-effective human neural cell model for neurotoxicity and neuroprotection studies. Moreover, the presence of functional human astrocytes provides an extra layer of complexity to this model, with impact

on the response to neurotoxic and neuroprotective chemicals, as many of these act via astrocytes (Gupta et al., 2012; Sofroniew & Vinters, 2010).

Presto blue was the chosen cell viability assay to be used as an endpoint in the neuroprotection assay as it is a non-destructive assay that can be used to evaluate viability at several time points in the same sample. This allows the data to be normalized relatively to the total cell number in each well and consequently minimize the variability of the replicates, which is generally higher in 3D culture assays than in 2D cultures. Moreover, it is simpler than the MTT assay as the dye could be directly added to the culture and the fluorescence is evaluated in the cell supernatant, with no need for crystal solubilisation as in MTT. The CytoTox-Glo assay requires an additional lysis step and consequently optimization steps are required to implement it when using 3D cell cultures.

We designed a neuroprotection assay setup that allows the screening of test compounds in different regimens of addition (pre-, co- and post-incubation with the insult), in a single 96-well plate. The neuroprotection assay setup was based on the induction of an oxidative lesion over the 3D human neuron-astrocyte co-cultures, using the oxidant tBHP (Choi et al., 2011; Kaja et al., 2012). The neuroprotective effect of the test-compounds over the tBHP insult was assessed based on cell viability compared with the positive and negative controls. In the human brain, reactive oxygen species (ROS) are constantly produced and are involved in protein misfolding and glial cell activation, leading to apoptosis and neurodegeneration (Federico et al., 2012). Oxidative stress is known to be implicated in most neurodegenerative diseases, such as Alzheimer's disease and Parkinson's disease (Yan, Wang, & Zhu, 2013). Therefore, reliable methods to evaluate novel neuroprotective compounds that can suppress ROS-induced neuronal damages might provide novel insights on chemicals that could be promising therapeutic molecules for numerous neurodegenerative disorders. For the assay validation, we have used Idebenone, an antioxidant benzoquinone, short-chain analogue of coenzyme Q10 (ubiquinone; (Erb et al., 2012)) and positive

control for neuroprotection over the tBHP insult. We have evaluated the robustness and specificity of the assay setup. The antioxidant function of Idebenone is dependent on its two-electron reduction to Idebenol, catalyzed by the cytoplasmic NAD(P)H:quinone oxidoreductase (Jaber & Polster, 2015). It has been widely investigated for the treatment of Friedreich's ataxia, caused by a deficiency in the protein frataxin, which is involved in iron metabolism and redox homeostasis, where the Idebenone treatment led to a reduction in oxidative stress markers (Jaber & Polster, 2015). Consistently with its antioxidant activity, Idebenone prevents lipid peroxidation in isolated brain mitochondria, synaptosomes and human hepatic cells (Erb et al., 2012). It was also shown to protect against ROS-induced damage in several *in vitro* cultures, as primary cortical neurons and immortalized neural cells (Jaber & Polster, 2015). We observed a dose-dependent neuroprotective effect over tBHP insult when Idebenone is administrated in pre-incubation.

The specificity of the neuroprotective effect observed for Idebenone over tBHP insult was evaluated using a non-oxidative lesion induced by chloramphenicol. Chloramphenicol is a known neurotoxic broad spectrum antibiotic (Grill & Maganti, 2011; Ramilo, Kinane, & McCracken, 1988). We and others have shown that the neurotoxicity mechanism of Chloramphenicol involves cytoskeletal injury, including degeneration of neurofilaments in neuronal cells and, to a major extent, degeneration of GFAP in astrocytic cells (Terrasso et al., 2015; Woehrling, Hill, Torr, & Coleman, 2011). Idebenone did not confer a neuroprotective effect over the chloramphenicol insult indicating that the neuroprotection observed for tBHP is specific and not an assay artefact.

Assay automation can significantly increase its throughput and accuracy, while decreasing variability (Wingfield, 2009). We have implemented a semi-automated procedure for the cell viability assay endpoint in an available Hamilton® Microlab STARlet workstation. Our results indicated that it was possible to perform the cell viability assay in automated high-throughput screening platforms. Thus, a 3D

human co-culture can be easily collected from an agitation-based culture system, distributed in 96-well plates and subject to neuroprotection assays performed in a high-throughput setup. The robustness and simplicity of the neuroprotection assay, combined with the easy evaluation of the fluorescence-based cell viability endpoint makes this a versatile assay setup suitable for early-stage drug screening.

As a proof-of-concept, 36 compounds from different origins, ranging from chemically-synthetized compounds to natural extracts, have been assayed using the neuroprotection assay setup implemented. As an example, the results obtained with the first two compounds - Nicotinamide and Linezolid are presented. Nicotinamide and Linezolid presented a partial neuroprotective effect when applied in concentrations between 1 pM and 5µM. Therefore, these compounds are potentially more potent over an oxidative insult than Idebenone, that in our assay setup did not present neuroprotective effect bellow the nanomolar range. Interestingly, for Nicotinamide and Linezolid, the effect was more pronounced when cells were exposed to the compounds 24h before insult than for 48h pre-incubation regimen; these differences were not observed for any of the other test compounds. This effect is not expected to be due to compound half-life, as Nicotinamide and Linezolid are stable in aqueous solutions, at 37ºC, for the assay period (our unpublished data). The differences observed for the 24 and 48h pre-incubation regimens may be related with the metabolization of these compounds by neural cells or with the mechanism of action of the compounds; additional studies are required to further evaluate these hypotheses.

Nicotinamide (vitamin B3) is the amide form of nicotinic acid (niacin) and is a precursor of β-nicotinamide adenine dinucleotide (NAD+), a coenzyme essential to the cellular energy metabolism (Klaidman, Mukherjee, & Adams, 2001; Shear et al., 2015). Moreover, the brain has an active uptake mechanism for Nicotinamide (Klaidman et al., 2001). Concomitantly with our results, Klaidman and colleagues have shown that the administration of tBHP to Nicotinamide pre-treated animals results in higher brain NADH, NADP and NADPH levels in some regions, compared

to control groups, indicating an upregulation of their synthesis during oxidative stress (Klaidman et al., 2001). Thus, Nicotinamide had already been described as playing a protective role in oxidative stress injury and as effectively preventing cell damage by free radicals due to their action in reductive reactions and energetics (Klaidman et al., 2001; Y. Wang & Zuo, 2015). In neurodegenerative diseases, Nicotinamide could affect the regulation of cell survival and death during activation of oxidative stress pathways (Y. Wang & Zuo, 2015). Thus, nicotinamide may become a promising therapeutic molecule for neurodegeneration.

Linezolid is a prototypical oxazolidinone antibiotic, highly effective against multi-drug resistant Gram-positive bacteria (Bobylev, Maru, Joshi, & Lehmann, 2016; Kombian & Phillips, 2011; T. Wang, Guo, Dong, & Mu, 2014). This compound has been reported to have good CNS penetration, making it a good antibiotic to treat CNS infections (Kombian & Phillips, 2011). Use of Linezolid at high concentrations or after prolonged treatments has been associated with severe side effects that include peripheral, central and optical neuropathies, however, the cellular mechanism by which it may alter neuronal function is not yet clearly understood (Bobylev et al., 2016; Kombian & Phillips, 2011). *In vitro* studies showed that the exposure of Schwann cells and sensory neurons to low concentration of linezolid did not change cell survival, while high concentrations induced toxicity, with reduction of axonal length in neurons, by a non-cell-specific toxic mechanism that may include mitochondrial dysfunction (Bobylev et al., 2016). It was also shown that Linezolid at low concentrations (below 10 µM) had minimal effects on excitatory and inhibitory synaptic transmission and on neuronal excitability in mammalian CNS; however, at higher concentrations (100 µM) it depressed NMDA receptor mediated synaptic response (Kombian & Phillips, 2011). In another study, linezolid decreased superoxide dismutase and catalase enzymatic activities inducing oxidative stress, in a time- and dose-dependent manner (T. Wang et al., 2014). Herein we observed that at lower concentrations (1 pM – 5 µM) linezolid was not toxic to 3D co-cultures of neurons and astrocytes and that the pre-

treatment with linezolid rescued the reduction in cell viability induced by tBHP. A biphasic dose-response characterized by a low dose beneficial effect and a high dose toxic effect have been described for some compounds (Calabrese et al., 2007; Mattson, 2008). The exposure to low concentrations of a compound that is toxic at higher doses could induce an adaptive beneficial effect on the cell and increase its resistance to more severe toxic effects caused by higher concentrations of the compound or to other types of stress (Calabrese et al., 2007). The molecular mechanisms of these responses typically involve the increase of cytoprotective proteins, including growth factors and antioxidant enzymes (Mattson, 2008). Thus, cells subjected to moderate levels of oxidative stress can respond by enhancing their ability to tolerate higher amounts of oxidative stress (Arumugam, Gleichmann, Tang, & Mattson, 2006). This could possibly explain the neuroprotective effect observed for low concentration linezolid over tBHP-induced oxidative lesion. Nevertheless, further studies are required to confirm the neuroprotective effect of linezolid and the mechanism by which this compound has an antioxidant effect at low concentrations.

5. Conclusion

We developed a novel assay setup for neuroprotection evaluation over several oxidative insults that are amenable to be transferred to a high-throughput screening automated platform. Moreover, the same general protection assay setup could be applied to other 3D cell models, using different cell sources and different insults affecting humans. The combination of 3D human co-cultures and an easy to perform cell viability endpoint with the utilization of an automated high-throughput screening platform would allow simplifying the application of the more reliable 3D *in vitro* cell models for compound screening.

6. Acknowledgements

We acknowledge Ligia O. Martins and Vânia Brissos for the support with the Hamilton® Microlab STARlet workstation and Rui M. Tostões for critically revising of the manuscript. The work was supported by Tecnimede – Sociedade Técnico Medicinal S.A. (Abrunheira, Sintra, Portugal), the European Regional Development Fund (FEDER) and the System of Incentives for the Research and Technological Development (QREN) of the Portuguese Government (project n.º 33913 – acronym PROiNEURO) and by Fundação para a Ciência e Tecnologia (FCT), Portugal, by the PhD fellowship to APT, PD/BD/52473/2014.

7. References

Arumugam, T. V., Gleichmann, M., Tang, S. C., & Mattson, M. P. (2006). Hormesis/ preconditioning mechanisms, the nervous system and aging. Ageing Research Reviews, 5(2), 165–178. http://dx.doi.org/10.1016/j.arr.2006.03.003.

Astashkina, A., & Grainger, D.W. (2014). Critical analysis of 3-D organoid *in vitro* cell culture models for high-throughput drug candidate toxicity assessments. Advanced Drug Delivery Reviews, 69–70, 1–18. http://dx.doi.org/10.1016/j.addr.2014.02.008.

Avior, Y., Sagi, I., & Benvenisty, N. (2016). Pluripotent stem cells in disease modelling and drug discovery. Molecular Cell Biology. http://dx.doi.org/10.1038/nrm.2015.27.

Bobylev, I., Maru, H., Joshi, A. R., & Lehmann, H. C. (2016). Toxicity to sensory neurons and Schwann cells in experimental linezolid-induced peripheral neuropathy. Journal of Antimicrobial Chemotherapy, 71(3), 685–691. http://dx.doi.org/10.1093/jac/dkv386.

Breslin, S., & Driscoll, L. O. (2013). Three-dimensional cell culture: the missing link in drug discovery. Drug Discovery Today, 18(March), 240–249.

Brito, C., Escrevente, C., Reis, C. A., Lee, V. M., Trojanowski, J. Q., & Costa, J. (2007). Increased levels of fucosyltransferase IX and carbohydrate Lewis x adhesion determinant in human NT2N neurons. Journal of Neuroscience Research, 1270, 1260–1270. http://dx.doi.org/10.1002/jnr.

Burroughs, S. L., Duncan, R. S., Rayudu, P., Kandula, P., Payne, J., Clark, J. L., ... Kaja, S. (2012). Plate reader-based assays for measuring cell viability, neuroprotection and calcium in primary neuronal cultures. Journal of Neuroscience Methods, 203(1), 141–145. http://dx.doi.org/10.1016/j.jneumeth.2011.09.007.

Calabrese, E. J., Bachmann, K. A., Bailer, A. J., Bolger, P. M., Borak, J., Cai, L., ... Mattson, M. P. (2007). Biological stress response terminology: Integrating the concepts of adaptive

response and preconditioning stress within a hormetic dose-response framework. Toxicology and Applied Pharmacology, 222(1), 122–128. http://dx.doi.org/10.1016/j.aap.2007.02.015.

Choi, Y., Kwak, E., Lee, J., Lee, Y., Cheong, I., Lee, H. J., ... Chun,W. (2011). Cytoprotective Effects of Docosyl Cafferate against tBHP- Induced Oxidative Stress in SH-SY5Y Human Neuroblastoma Cells 19 (2). (pp. 195–200), 195–200. http://dx.doi.org/10.4062/biomolther.2011.19.2.195.

Del Barrio, L., Martín-de-Saavedra, M. D., Romero, A., Parada, E., Egea, J., Avila, J., ... López, M. G. (2011). Neurotoxicity induced by okadaic acid in the human neuroblastoma SH-SY5Y line can be differentially prevented by α7 and β2* nicotinic stimulation. Toxicological Sciences, 123(1), 193–205. http://dx.doi.org/10.1093/toxsci/kfr163.

Edmondson, R., Broglie, J. J., Adcock, A. F., & Yang, L. (2014). Three-dimensional cell culture systems and their applications in drug discovery and cell-based biosensors. Assay and Drug Development Technologies, 12(4), 207–218. http://dx.doi.org/10.1089/adt.2014.573.

Erb, M., Hoffmann-Enger, B., Deppe, H., Soeberdt,M., Haefeli, R. H., Rummey, C., ... Gueven, N. (2012). Features of idebenone and related short-chain quinones that rescue ATP levels under conditions of impaired mitochondrial complex I. PloS One, 7(4), e36153. http://dx.doi.org/10.1371/journal.pone.0036153.

Federico, A., Cardaioli, E., Da Pozzo, P., Formichi, P., Gallus, G. N., & Radi, E. (2012). Mitochondria, oxidative stress and neurodegeneration. Journal of the Neurological Sciences, 322(1–2), 254–262. http://dx.doi.org/10.1016/j.jns.2012.05.030.

Grill, M. F., & Maganti, R. K. (2011). Neurotoxic effects associated with antibiotic use: management considerations. British Journal of Clinical Pharmacology, 72(3), 381–393. http://dx.doi.org/10.1111/j.1365-2125.2011.03991.x.

Gupta, K., Patani, R., Baxter, P., Serio, A., Story, D., Tsujita, T., ... Chandran, S. (2012). Human embryonic stem cell derived astrocytes mediate non-cell-autonomous neuroprotection through endogenous and drug-induced mechanisms. Cell Death and Differentiation, 19(5), 779–787. http://dx.doi.org/10.1038/cdd.2011.154.

Hopkins, A. M., DeSimone, E., Chwalek, K., & Kaplan, D. L. (2015). 3D *in vitro* modeling of the central nervous system. Progress in Neurobiology, 125, 1–25. http://dx.doi.org/10.1016/j.pneurobio.2014.11.003.

Jaber, S., & Polster, B. M. (2015). Idebenone and neuroprotection: antioxidant, pro-oxidant or electron carrier? Journal of Bioenergetics and Biomembranes, 111–118. http://dx.doi.org/10.1007/s10863-014-9571-y.

Kaja, S., Duncan, R. S., Longoria, S., Hilgenberg, J. D., Payne, A. J., Desai, N. M., ... Koulen, P. (2012). NIH Public Access1(816). (pp. 281–291), 281–291. http://dx.doi.org/10.1016/j.neuroscience.2010.11.010.Novel.

Kesselheim, A. S., Hwang, T. J., & Franklin, J.M. (2015). Two decades of new drug development for central nervous system disorders. Nature Reviews Drug Discovery, 1 (November). http://dx.doi.org/10.1038/nrd4793.

Klaidman, L. K., Mukherjee, S. K., & Adams, J. D. (2001). Oxidative changes in brain pyridine nucleotides and neuroprotection using nicotinamide. Biochimica et Biophysica Acta - General Subjects, 1525(1–2), 136–148. http://dx.doi.org/10.1016/S0304-4165(00)00181-1.

Kombian, S. B., & Phillips, O. A. (2011). *In vitro* electrophysiological investigations of the acute effects of linezolid and novel oxazolidinones on central nervous system neurons. Neuroscience, 180, 53–63. http://dx.doi.org/10.1016/j.neuroscience.2011.01.062.

Mattson, M. P. (2008). Hormesis defined. Ageing Research Reviews, 7(1), 1–7.

Niles, A. L., et al. (2007). A homogeneous assay to measure live and dead cells in the same sample by detecting different protease markers. Analytical Biochemistry, 366, 197–206.

Picollet-D'hahan, N., Dolega, M. E., Liguori, L., Marquette, C., Le Gac, S., Gidrol, X., &Martin, D. K. (2016). A 3D toolbox to enhance physiological relevance of human tissue models. Trends in Biotechnology, xx(9), 1–13. http://dx.doi.org/10.1016/j.tibtech.2016.06.012.

Ramilo, O., Kinane, B., & McCracken, G. (1988). Chloramphenicol neurotoxicity. Pediatric Infectious Disease Journal, 7(5), 358.

Riss, T. L., Moravec, R. A., Niles, A. L., Benink, H. A., Worzella, T. J., & Minor, L. (2004). Cell Viability Assays. Assay Guidance Manual. Eli Lilly & Company and the National Center for Advancing Translational Sciences.

Schmidt, B. Z., Lehmann, M., Gutbier, S., Nembo, E., Noel, S., Smirnova, L., ... Dinnyés, A. (2016). *In vitro* acute and developmental neurotoxicity screening: an overview of cellular platforms and high-throughput technical possibilities. Archives of Toxicology, 1–33. http://dx.doi.org/10.1007/s00204-016-1805-9.

Shear, D. A., Bramlett, H. M., Dixon, C. E., Dietrich, W. D., Deng-Bryant, Y., Schmid, K. E., ... Tortella, F. C. (2015). Nicotinamide treatment in traumatic brain injury: operation brain trauma therapy. Journal of Neurotrauma, 537(June). http://dx.doi.org/10.1089/neu.2015.4115.

Simão, D., Terrasso, A., Teixeira, A., Brito, C., Sonnewald, U., & Alves, P. M. (2016). Functional metabolic interactions of human neuron-astrocyte 3D *in vitro* networks. Scientific Reports, 6, 33285. http://dx.doi.org/10.1038/srep33285.

Sofroniew, M. V., & Vinters, H. V. (2010). Astrocytes: Biology and Pathology, 7–35. http://dx.doi.org/10.1007/s00401-009-0619-8.

Sonnaert, M., Papantoniou, I., Luyten, F. P., & Schrooten, J. (2014). Quantitative validation of the Presto Blue™ metabolic assay for on-line monitoring of cell proliferation in a 3D perfusion bioreactor system. Tissue Engineering Part C, 1, 1–34.

Terrasso, A. P., Pinto, C., Serra, M., Filipe, A., Almeida, S., Ferreira, A. L., ... Alves, P. M. (2015). Novel scalable 3D cell based-model for *in vitro* neurotoxicity testing: combining human differentiated neurospheres with gene expression and functional endpoints. Journal of Biotechnology, 205, 82–92. http://dx.doi.org/10.1016/j.jbiotec.2014.12.011.

Wang, Y., & Zuo, M. (2015). Nicotinamide improves sevoflurane-induced cognitive impairment through suppression of inflammation and anti-apoptosis in rat. International Journal of Clinical and Experimental Medicine, 8(11), 20079–20085.

Wang, T., Guo, D., Dong, X., & Mu, L. (2014). Effect of linezolid on hematological and oxidative parameters in rats. The Journal of Antibiotics, 67(6), 433–437. http://dx.doi.org/10.1038/ja.2014.21.

Wiest, D. B., Cochran, J. B., & Tecklenburg, F. W. (2012). Chloramphenicol toxicity revisited: a 12-year-old patient with a brain abscess. Journal of Pediatric Pharmacology and Therapeutics, 17(2), 182–188. http://dx.doi.org/10.5863/1551- 6776-17.2.182.

Wingfield, J. (2009). Modular automation for screening a cost/ benefit analysis. Drug Discovery World Summer, 65–70. Woehrling, E. K., Hill, E. J., & Coleman,M. D. (2010). Evaluation of the importance of astrocytes when screening for acute toxicity in neuronal cell systems. Neurotoxicity Research, 17, 103–113. http://dx.doi.org/10.1007/s12640-009-9084-3.

Woehrling, E. K., Hill, E. J., Torr, E. E., & Coleman, M. D. (2011). Single-Cell ELISA and Flow Cytometry as Methods for Highlighting Potential Neuronal and Astrocytic Toxicant Specificity, 472–483. http://dx.doi.org/10.1007/s12640-010-9202-2.

Yan, M. H., Wang, X., & Zhu, X. (2013). Mitochondrial defects and oxidative stress in Alzheimer disease and Parkinson disease. Free Radical Biology & Medicine, 62, 90–101. http://dx.doi.org/10.1016/j.freeradbiomed.2012.11.014.

CHAPTER 4

Lysosomal and network alterations in human mucopolysaccharidosis type VII iPSC-derived neurons

This chapter was adapted from:

Bayó-Puxan N*, Terrasso AP*, Creyssels S, Simão D, Begon-Pescia C, Lavigne M, Salinas S, Bernex F, Bosch A, Kalatzis V, Levade T, Cuervo AM, Lory P, Consiglio A[#], Brito C[#], Kremer EJ[#]. 2018. Lysosomal and network alterations in human mucopolysaccharidosis type VII iPSC-derived neurons. Journal of Cell Science. *Under Revision.*

* Equal contribution (APT performed the 3D neurospheroid culture for iPSC-NPC neural differentiation and all the characterization of the neurospheroids)
[#] Co-senior authors

Table of Contents

Abstract

Mucopolysaccharidosis type VII (MPS VII) is an ultra-rare lysosomal storage disease caused by deficient β-glucuronidase (β-gluc) activity, which leads to accumulation of glycosaminoglycans (GAGs) in many tissues, including the brain. Numerous combinations of mutations in the GUSB gene (which codes for β-gluc) cause a range of neurological features that make disease prognosis and treatment challenging. Currently, there is little understanding of why the MPS VII brain is affected. To identify a neuronal phenotype that could be used to complement genetic analyses, we generated two iPSC clones derived from skin fibroblasts of a MPS VII patient. MPS VII neurons exhibited reduced β-gluc activity and showed disease-associated phenotypes, including GAGs accumulation, expanded endocytic compartments, accumulation of lipofuscin granules, more autophagosomes, and altered lysosome function. Addition of recombinant β-gluc to MPS VII neurons to mimic enzyme replacement therapy restored disease-associated phenotypes to levels similar to the healthy control. MPS VII neurospheroids showed upregulated GFAP gene expression, which was associated with astrocyte reactivity, and downregulation of GABAergic neuron markers. Spontaneous calcium imaging analysis showed reduced neuronal activity and altered network connectivity in patient-derived neurospheroids compared to a healthy control. These results demonstrate the interplay between reduced β-gluc activity, GAG accumulation and alterations in neuronal activity, and provide a human experimental model for elucidating the bases of MPS VII-associated cognitive defects.

1. Introduction

Lysosomal storage disorders (LSD) are caused by intra- and extracellular accumulation of undigested macromolecules that induce dysfunction of the greater lysosomal system. Among LSD, mucopolysaccharidoses (MPS) are caused by deficiency in enzymatic activities that degrade glycosaminoglycans (GAGs). GAGs are the most abundant polysaccharides of the extracellular matrix (ECM) and, with the exception of hyaluronic acid, are covalently attached to protein moieties to form proteoglycans (Batzios et al., 2013). β-glucuronidase (β-gluc, EC 3.2.1.31), is found in lysosomes of all nucleated mammalian cell and is involved in the step-wise degradation of GAGs by removing glucuronic acid residues. Impaired β-gluc activity results in partial degradation and accumulation of chondroitin sulfate, dermatan sulfate and heparan sulfate GAGs.

MPS type VII (MPS VII), a neuronopathic form of MPS is an ultra-rare disease with an estimated frequency of ~1:2 000 000 (Montaño et al., 2016). It has an autosomal recessive inheritance pattern caused by mutations in GUSB (Tomatsu et al., 1990). There are at least 49 disease-associated mutations that contribute to hepatosplenomegaly, cardiac valvular abnormalities, recurrent pulmonary infections, growth retardation, mobility problems, dysostosis multiplex, facial dysmorphia, visual and hearing defects, cognitive defects and/or early death (Tomatsu et al., 2009). Most of the ~100 identified MPS VII patients present limited vocabulary and mental retardation (Montaño et al., 2016). The most severe phenotype is hydrops *fetalis*, while a mild phenotype displays a late onset and near normal intelligence (Tomatsu et al., 2009). Notably, MPS VII patients with similar mutations can have variable levels of cognitive impairment, which suggests that other factors influence disease severity and confound reliable prediction of disease progression. While most mutations underlying MPS VII are known, the mechanistic links between reduced β-gluc activity, GAG accumulation and neurological anomalies are just beginning to be addressed (Montaño et al., 2016). Human MPS brain cell models would contribute to understand how defects in the greater

lysosomal system cause progressive (instead of immediate) brain impairment/dysfunction and may also inspire novel therapies.

Using induced pluripotent stem cell (iPSC) technology (Lee and Studer, 2010; Takahashi et al., 2007), a handful of LSD cell models have been established (reviewed in (Borger et al., 2017)), including Gaucher (Tiscornia et al., 2013), Hurler (Tolar et al., 2011), Pompe (Higuchi et al., 2014), Sanfilippo B and C (Canals et al., 2015; Lemonnier et al., 2011) and Niemann-Pick type C1 (Maetzel et al., 2014). These patient-derived iPSC were differentiated in 2D cultures into several cell types, including brain cells, and recapitulated morphological, biochemical and/or functional hallmarks of the disease. LSD patient iPSC engineered to overexpress functional enzymes have been also reported (Doerr et al., 2015; Griffin et al., 2015; Meneghini et al., 2017). While clearly informative, these cell models lack the dynamic events linked to interactions with proteoglycans and hyaluronic acid, the main components of brain ECM. This may impact the interactions between neural cells and ECM that regulate neural cell fate and functionality (Srikanth and Young-Pearse, 2014). Thus, there is a need for MPS brain cell models in which the ECM and its dynamic remodeling can be taken into account.

We recently developed a 3D culture strategy, using stirred-tank bioreactors, to differentiate iPSC-derived neural precursor cells (iPSC-NPC) into neurons, astrocytes and oligodendrocytes. This strategy allows cells to produce an ECM, fostering cell-cell and cell-ECM interactions that recapitulate many facet of brain cell architecture (Simão et al., 2016, 2014). Using the classic 2D and novel 3D culture systems we set out to test whether MPS VII iPSC-NPC and mature neurons could be used to understand disease-associated cognitive deficits. We show that MPS VII neurons have elevated GAG content, expanded endocytic compartment, impaired membrane receptor lysosome-mediated degradation and altered functional connectivity. MPS VII neurospheroids were the key to identify disease-associated phenotypes and cellular defects associated with neurological deficits.

2. Materials and Methods

2.1. iPSC generation

The Vall d'Hebron Hospital ethical committee of clinical investigation approved procedures. The donor's parents gave written consent. A skin punch biopsy (2 mm^3) under local anesthesia was taken from MPS VII donor, biological samples were free of pathogens. Skin biopsies were cultured in AmnioMax™ basal medium containing AmnioMax™ C-100 Supplement (Invitrogen), 10% fetal bovine serum (FBS) (Gibco) and a mixture of penicillin-streptomycin-Amphotericin B (Lonza). Dermal fibroblasts that emerged from skin biopsies were expanded 12 days later. Then medium was switched to fibroblasts medium (DMEM-GlutaMAX, 10% FBS, sodium pyruvate, MEM non-essential amino acids and antibiotics (Gibco®). For reprogramming, fibroblasts were treated with FGF at 10 ng/mL and ascorbic acid 2-phosphate at 1 mM (Sigma) for 12 days prior to infection. Ecotropic retroviral vectors expressing 4 transcription factors (Oct4, cMyc, Sox2 and Klf4) described by Yamanaka (Takahashi et al., 2007). Vectors were produced in Plat-E cells (Morita et al., 2000) and used to infect fibroblasts pre-treated with VSV-G vesicles containing mCAT1 receptor to improve human cell infection with murine virus (Mangeot et al., 2011). One week later, infected-fibroblasts were expanded and fibroblast medium was switched to human embryonic stem (ES) cells medium (HES; KnockOut™ DMEM, 20% KnockOut™ Serum Replacement, MEM non-essential amino acids, GlutaMAX™, 2-mercaptoethanol, Gibco). HES medium was supplemented with 500 µm valproic acid sodium salt (Sigma) and 10 ng/ml FGF2 (Peprotech) for 3 weeks to increase reprogramming efficiency and maintain cells undifferentiated (Huangfu et al., 2008). A total of 20 ES-like colonies were picked for each specimen 20-35 days later. BJ1-FGF2 (provided by I-Stem) and HFF1 (ATCC) cells were used as feeders. iPSC were mechanically passaged weekly, and medium was changed daily. Rock inhibitor Y-27632 at 10 µm (Calbiochem) was added to the medium at the first passages to improve single cell survival and cell attachment to feeder cells. Three iPSC lines were generated from the MPS VII patient and seven iPSC lines from a

control were used. Two MPS VII clones (cl. 8 and cl. 13) were further characterized. Mycoplasma test (MycoAlert® Detection Kit, Lonza) was routinely performed.

2.2. Characterization of iPSC lines

Alkaline phosphatase (AP) activity was detected by a colorimetric assay following manufacture indications (SIGMA FAST™ BCIP/NBT tablets). Expression of pluripotent cell surface markers (SSEA-3, TRA-2-49 and NANOG) were assayed in iPSCs grown on HFF1 feeders layer by immunohistochemical assays (see below). RT-qPCR was done as previously described (Cereso et al., 2014). Gene expression was normalized to that of glyceraldehyde 3-phosphate dehydrogenase (GAPDH).

In vitro differentiation towards the three germ layers was performed by embryonic body formation. Briefly, iPSCs were detached from feeder cells with collagenase type IV at 1 mg/mL (Invitrogen) and cells were grown in suspension for 7 days in HES media. For further differentiation, cells were plated into 0.1% gelatin-coated plates (Sigma). Then, 14 days later, cells were fixed with 4% paraformaldehyde (PFA) (EM grade, PKS) in PBS for 15 min and expression of tissue specific markers for endoderm (α-fetoprotein), mesoderm (smooth muscle actin), and ectoderm (βIII-tub) were assayed by immunofluorescence (see below).

For teratoma formation, CB17/Icr-Prkdcscid/IcrIcoCrl Fox Chase SCID Congenic mice (Charles River Laboratories) were used. Eight-week old mice were anesthetized with xylazine (5-10 mg/kg): ketamine (100 mg/kg) mix. Cell injections were intra-testicular and under the kidney capsule (Peterson et al., 2011; Prokhorova et al., 2009; Zhu et al., 2014) with 106 cells resuspended into 10 µl of DMEM/F12 (Gibco) and 10 µl of Matrigel (BD) (Prokhorova et al., 2009). Eight weeks after injection, tumors were removed and fixed in 4% neutral buffered formalin (Diapath) at room temperature (RT) for 24 to 48 h. Samples were processed, included in paraffin and stained with hematoxylin/eosin at the RHEM histology platform (IRCM, Montpellier). Histological analysis was performed by a pathologist. The protocol followed for teratoma formation takes into account standardization rules (Müller et al., 2010). All animal experiments were conducted

following protocols previously approved by the Comité National de Réflexion Ethique sur l'Expérimentation Animale and by the Ministère de l'Enseignement Supérieur et de la Recherche (France).

For karyotyping, iPSC clones were grown on Matrigel (BD Biosciences) and treated during their exponential phase of cellular growth with 0.1 µg/ml colcemid (Karyomax Invitrogen Gibco). Karyotyping was done by CHROMOSTEM (CHRU, Montpellier).

2.3. iPSC cells differentiation into neural precursor cells

NPCs were generated and subsequently differentiated into neural cells from the iPSC lines as described previously (Chambers et al., 2009). Briefly, iPSC were mechanically dissociated from feeder-layer and small groups of iPSC were grown in suspension for 48 h in N2B27 pro-neural medium (1:2 DMEM:F12, 1:2 Neurobasal, N2, B27 without vitamin A, 2-mercaptoethanol and gentamicin, Gibco). To further differentiate cells into neuroepithelial (NEP)-rosettes, cells were seeded into 16 µg/ml poly-L-ornithine at (Sigma) and 2 µg/mm laminin (Sigma) (POLAM)-coated glass plates and medium was supplemented with 200 ng/ml Noggin (R&D Systems) and 10 µM SB431542 (Tocris) to induce neuroectoderm cell differentiation as previously described (Chambers et al., 2015, 2009). NEP-rosettes appeared between days 8-12, then were mechanically selected and expanded twice each 8-12 days obtaining a neural rosette-enriched culture. Noggin and SB431542 were removed from the medium once NEP-rosettes were formed and during the last round of expansion. When cells reached to confluence NEP-rosettes were differentiated into NPCs. Briefly NEP-rosettes were enzymatically dissociated with 0.05% trypsin/EDTA (Gibco), expanded into POLAM-coated plates in pro-neural medium supplemented with FGF2 at 10 ng/ml and EGF at 10 ng/ mL (PeproTech) prompting NPC self-renewal. NPCs were expanded for 5 passages obtaining a homogeneous and phenotypically stable cell population. NPCs were cryopreserved in cryomedium based on 95% CryoStorCS5 (Biolife Solutions) and 5% DMSO

(Sigma). NPC self-renewal and ability to generate neurons were retained after thawing.

2.4. iPSC-derived NPC differentiation in 2D cultures

For neuronal differentiation, NPCs were plated into POLAM-coated glass plates and cultured in neural induction medium (pro-neural medium supplemented with 10 ng/mL BDNF, 10 ng/mL GDNF, 10 ng/mL NT-3 (all from PeproTech) and 100 µM cAMP (Sigma-Aldrich)). Half of the medium was weekly replaced with fresh media. For immunofluorescence studies cells were plated into POLAM-HCl treated glass coverslips as previously described (Gaspard et al., 2009)).

2.5. iPSC-derived NPC differentiation in 3D cultures

NPCs were expanded as monolayers and 3D neural differentiation was performed in software-controlled stirred-tank bioreactors (DASGIP, Eppendorf), accordingly to Simão et al. (2016). Briefly, NPCs were inoculated as single cells at 4 x 10^5 cell/mL in pro-neural medium supplemented with 5 ng/mL FGF2, 5 ng/mL EGF and 5 µM Y-27632 ROCK-inhibitor (Merck-Millipore). Cell culture parameters were: pH 7.4, 15% DO and temperature 37ºC. An initial stirring of 70 rpm was used. Perfusion was initiated at day 2 after inoculation, when the cells have aggregated into compact neurospheres. A dilution rate of 0.33 day^{-1} was used. The retention of cells in the perfusion was performed using a 20 µm pore stainless steel sparger. Neural differentiation was initiated 1 week after inoculation by changing the medium to neural induction medium and induced for 3 weeks.

2.6. Lysosomal enzymes activities in cell extracts

Enzymatic activities were measured as previously described (Vitner et al., 2010). Briefly, cells were lysed using 1% Triton X-100, 10 % glycerol, 20 mM Tris-HCl pH 7.5 and 150 mM NaCl supplemented with a protease inhibitor cocktail (Roche). Cellular lysates were subjected to three cycles of freeze and thaw and centrifuged for 15 min at 15,000 g at 4ºC. Protein content of cell lysate was quantified using the Micro BCA™ Protein Assay Kit (Thermo Scientific). Enzymatic reactions were

performed in 48-well plates with 20 µl of protein extracts and 100 µl of reaction buffer (100 mM sodium acetate, pH 4.8 containing 10 mM of enzyme substrate) for 1 h at 37ºC. Substrates for β-gluc and for β-hexosaminidase (β-hex) were 4-methylumbelliferyl-β-d-glucuronide and 4-methylumbelliferyl-N-acetyl-β-d-glucosaminide (both from Sigma-Aldrich), respectively. Enzymatic reactions were stopped by adding 500 µl of 200 mM sodium carbonate pH 10, and fluorescence intensity was measured at 450 nm using Tecan Infinite® M200 Microplate Reader. Standard curves were performed using serial dilutions of 4-methylumbelliferyl (4-MU; Sigma-Aldrich). Enzyme activity is expressed in nmol 4-MU/ µg protein/h.

2.7. Immunofluorescence

For indirect immunofluorescence, NPCs and neurons were fixed with 4% PFA (EM grade, PKS) in PBS for 15 min at RT and permeabilized with 0.1% Triton X-100 in PBS at RT for 5 min. Cells were then blocked in blocking solution (BS): 2% bovine serum albumin (Sigma) and 10% horse serum in PBS for 1 h at RT. Primary antibodies were diluted in BS and incubated overnight at 4ºC, followed by incubation with secondary antibodies (Alexa Fluor series from Invitrogen) all diluted 1:500 in BS for 1 h at RT. Samples were then mounted with fluorescent mounting medium (Dako) containing DAPI at 10 ng/µl (Sigma). Primary antibodies used are: SSEA-3, TRA-2-49, Nanog, α-fetoprotein, smooth muscle actin, βIII-tub, Nestin, Sox2, OTX1-2, GFAP, LAMP1, CAR, NeuN, Tbr1, Brn2, vGLUT, and PSD95. Phalloidin Red (Sigma) to probe for F-actin was used at 1:500 in BS, 1 hour at RT.
Images were taken using Leica LSM780 and Zeiss SP5 confocal microscopes, with 20X/0.8 Plan-Apo, 40X/1.3 oil-DIC Plan-Apo or 63X/1.4 oil-DIC Plan-Apo objectives. Image analysis was performed using Fiji Software.

2.8. Glycosaminoglycans quantification

Neurospheroids were collected at days 7 and 28 of culture and lysed in papain extraction reagent (0.2 M sodium phosphate buffer, pH 6.4, containing 100 mM sodium acetate, 5 mM cysteine, 5mM EDTA, 0.1 mg/ml papain (Sigma-Aldrich)) for

3 h at 65ºC. After centrifugation at 10,000 g for 5 min., sulfated GAG content was determined in the supernatants using the Blyscan Sulfated Glycosaminoglycan Assay (Biocolor) according to manufacturer's instructions.

2.9. Protein extraction and Western blot

For protein extraction, cells were washed once with PBS and incubated with lysis buffer (1% Triton X-100, 10 % glycerol, 20 mM Tris-HCl pH 7.5 and 150 mM NaCl) supplemented with protease inhibitor cocktail (Roche) for 10 min at 4ºC. Cellular lysates were centrifuged for 15 min at 14,000 rpm at 4ºC. Supernatants of total protein extracts were quantified using BCA (Pierce) or Bradford reagent (BioRad). Proteins were denatured in SDS-containing loading buffer for 10 min at 95ºC. Proteins were separated in SDS-PAGE and transferred to PVDF membrane. The membrane was probed with anti-p62, anti-LC3-I/II, anti-β-tubulin, anti-EGFR, anti-CAR and anti-actin antibodies.

2.10. RNA extraction and qRT-PCR

Real-time quantitative PCR analysis (RT-qPCR) was performed as described in Brito et al. (2012). Briefly, total RNA was extracted with High Pure RNA Isolation kit (Roche) and quantified using a NanoDrop 2000c (Thermo Scientific). Reverse transcription was performed with Transcriptor High Fidelity cDNA Synthesis kit (Roche), using anchored-oligo (dT)18 primer. qRT-PCR analysis was performed in a LightCycler 480 (Roche) according to Light-Cycler 480 SYBR Green I Master Kit (Roche) instructions. Primers were used at 5 µM, in 20 µL reactions; each sample was performed in triplicates. See Table 1 for list of primers. Cycles threshold (Ct's) and melting curves were determined using LightCycler 480 software, version 1.5 (Roche), and results were processed using the $2^{-\Delta\Delta Ct}$ method for relative gene expression analysis (Brito et al., 2012; Livak and Schmittgen, 2001). Changes in gene expression were normalized using the housekeeping gene RPL22 (coding for ribosomal protein L22) as internal control.

Table 4.1: List of primers used in MPS VII cells qRT-PCR analysis

Target	Forward (5' →3')	Reverse (5' →3')
SOX2	GGGAAATGGGAGGGGTGCAAAAGAGG	TTGCGTGAGTGTGGATGGGATTGGTG
OCT4	GACAGGGGGAGGGGAGGAGCTAGG	CTTCCCTCCAACCAGTTGCCCCAAAC
NANOG	CAGCCCCGATTCTTCCACCAGTCCC	CGGAAGATTCCCAGTCGGGTTCACC
LIN28	AGAGTAAGCTGCACATGGAAGGGT	TATGGCTGATGCTCTGGCAGAAGT
trSOX2	TAAAGCAGCGTATCCACATAGC	GCCATTAACGGCACACTGC
trOCT4	TAAAGCAGCGTATCCACATAGC	TCACCACTCTGGGCTCTC
cMYC	TAAAGCAGCGTATCCACATAGC	CGGAAACGACGAGAACAGTTG
trKLF4	TAAAGCAGCGTATCCACATAGC	ACCACCTCGCCTTACACATG
hMYC	GCGTCCTGGGAAGGGAGATCCGGAGC	TTGAGGGGCATCGTCGCGGGAGGCTG
PCNA	CGGAGTGAAATTTTCTGCAAG	TTCAGGTACCTCAGTGCAAAAG
nestin	TAAGGTGAAAAGGGGTGTGG	GCAAGAGATTCCCTTTGCAG
βIII-tubulin	GGGCCTTTGGACATCTCTTC	CCTCCGTGTAGTGACCCTTG
Synaptophysin (SYP)	TTTGTGAAGGTGCTGCAATG	GCTGAGGTCACTCTCGGTCT
VGluT-1	GTTCTGCTGCTCGTCTCCT	ATGAGTTTCGCGCTCTCTCC
TH	AGCCCTACCAAGACCAGACG	GCGTGTACGGGTCGAACTT
GAD67	ACCAGAAAACTGGGGCTCAA	GCAGGTTCTTGGAGGATTGC
GFAP	AGAGAGGTCAAGCCAGGAG	GGTCACCCACAACCCCTACT
GLT-1	CCAGGAAAAACCCCTTCTCC	TCTTCCAGGCAACGAAAGGT
GUSB	GGCTACCTCCCCTTCGAG	GTTGAAGAACTGCGGCAGC
RPL22	CACGAAGGAGGAGTGACTGG	TGTGGCACACCACTGACATT
GAPDH	AGAACATCATCCCTGCCTCT	ACCCTGTTGCTGTAGCCAAA

2.11. Cell treatment for protein degradation assays

NPCs at 80% of confluence were incubated with 200 ng/mL EGF (PeproTech) or 200 ng/mL FK^{CAV} for 15 min at 4ºC allowing ligand-receptor binding. To synchronize ligand-receptor internalization, ligand-containing medium was replaced by fresh pre-warmed medium. Then cells were incubated at 37ºC allowing ligand-receptor internalization. At indicated times proteins were extracted and subjected to western blotting.

2.12. Calcium fluorescence imaging

For calcium fluorescence imaging experiments in 2D cultures, neuronal cultures were grown on glass coverslips coated with POLAM to prevent cells detaching or moving during imaging experiments. Prior to imaging, cells were loaded with 5 µM acetoxy-methyl-ester Fura-2 (Fura-2 AM, Invitrogen) for 45 min in Tyrode solution (physiological saline) containing 0.5% Pluronic acid at 37°C. Imaging experiments were performed at 22°C using an IX70 Nikon microscope equipped with a 20X objective. The cultures were excited alternatively at 340 and 380 nm and light emission at 510 nm was used to determine the fluorescence ratio (F340/F380) that reflect the intracellular calcium concentration. Images were acquired every 3 seconds for 10 to 15 min. Calcium signals attributable to neuronal cells were measured by switching the standard Tyrode solution to a 60 mM KCl/Tyrode solution to depolarize the cells and to activate voltage-dependent calcium channels. 1,4-dihydropyridine-derivative (5 µM) (Nimopidine (Alomone Labs) was used to specifically block L-type calcium channels, a marker of neuronal activity. All the imaged cultures were ultimately treated with 10 µM ionomycin (Sigma) to validate cell viability. Image analysis was performed using MetaFluor Imaging software (Molecular Devices) using the region of interest (ROI) analysis method. Three neuronal cultures/neuron sources were analyzed.

For calcium imaging experiments in 3D cultures, neurospheroids were collected after 3 weeks of differentiation and incubated with 1x Fluo-4 Direct™ calcium

reagent (Invitrogen) for 30 min at 37 ºC, 5% CO_2, and 3% O_2, followed by 15 min at RT. Samples were then imaged live using a spinning-disk confocal microscope (Nikon Eclipse Ti-E, confocal scanner: Yokogawa CSU-x1). Image analysis was performed using FluoroSNNAP – Fluorescence Single Neuron and Network Analysis Package, an open-source software developed in MatLab for automated quantification of calcium dynamics of single cells and network activity patterns (Patel et al., 2015).

2.13. Synaptic vesicle trafficking assay

Synaptic vesicles trafficking assays were based on (Gaffield and Betz, 2006). Neurospheroids were plated in POLAM-coated glass coverslips and incubated with 5 mM HEPES-NaOH, pH 7.4; 10 mM glucose; 2.5 mM $CaCl_2$; 1 mM $MgCl_2$; 100 mM KCl; 37 mM NaCl (referred to as 100 mM KCl buffer) for 5 min. Afterwards, 100 mM KCl buffer was removed and neurospheroids incubated with 10 M FM-1-43 dye (Invitrogen) in 5 mM HEPES-NaOH, pH 7.4; 10 mM glucose; 2.5 mM $CaCl_2$; 1 mM $MgCl_2$; 5 mM KCl; 37 mM NaCl (referred to as 5 mM KCl buffer) for 15 min. Neurospheroids were washed for 1 min with 5 mM KCl buffer with ADVASEP-7 (Sigma), followed by three washes with 5 mM KCl buffer. Exocytosis was stimulated with 100 mM KCl buffer and samples were visualized live using a fluorescence microscope (Leica DMI6000) in order to monitor the decreasing of fluorescence intensity overtime. Fluorescence intensity was measured using ImageJ software version 1.47q (http://rsbweb.nih.gov/ij/).

2.14. TEM on ultrathin sections and toluidine blue stained thin sections

Neurons were differentiated from NPCs and grown for 6 and 9 weeks in 60 mm POLAM-coated glass dishes as described above. Cells were fixed with 2.5% glutaraldehyde in cacodylate buffer (0.1 M pH 7.1-7.4) for 2 h at 4ºC and washed three times with cacodylate buffer (0.1 M pH 7.1-7.4). Then cells were collected and treated with 1% osmium tetroxide in cacodylate buffer (0.1 M pH 7.1-7.4) for 2

h at room temperature, dehydrated with ethanol and embedded in EPON. Thin (250-1000 nm) and ultrathin (80 nm) sections were obtained with ultra-microtome Leica EM UC6. 500-1000 nm-thick sections were stained with toluidine blue and images were acquired with Leica DM6000B upright microscope. Ultrathin sections were then contrasted with uranyl acetate. Images were acquired with JEOL-JEM-1011. Images were analyzed using ImageJ software.

2.15. Experimental design and statistical analysis

Data are mean ± SD of, at least, 3 independent experiments and were analyzed with GraphPad Prism 6 software. One-way ANOVA followed by Tukey's post-hoc multiple comparison analysis was used (* $p < 0.05$, *** $p < 0.001$).

For 3D cultures, analysis of neurospheroids from different stirred-tank bioreactor cultures are considered biological replicates, while analysis of different neurospheroids sampled from the same bioreactor culture are considered technical replicates.

3. Results

3.1. Generation and characterization of human MPS VII iPSC

We generated iPSC from dermal fibroblasts of an MPS VII patient who was diagnosed at 3 years old based on decreased β-gluc activity and increased GAG storage (Chabas et al., 1991). At the time of skin biopsy, the MPS VII patient was 27 years old and had severe mental retardation. The homozygous point mutation that induced a Leu to Phe change at amino acid 176 in β-gluc was consistent with a severe MPS VII phenotype (Chabas et al., 1991; Tomatsu et al., 2009). Primary cultures of dermal fibroblasts were established. MPS VII patient fibroblasts had approximately 2% of β-gluc activity compared to the fibroblasts from the healthy individual (Fig. 4.1a).

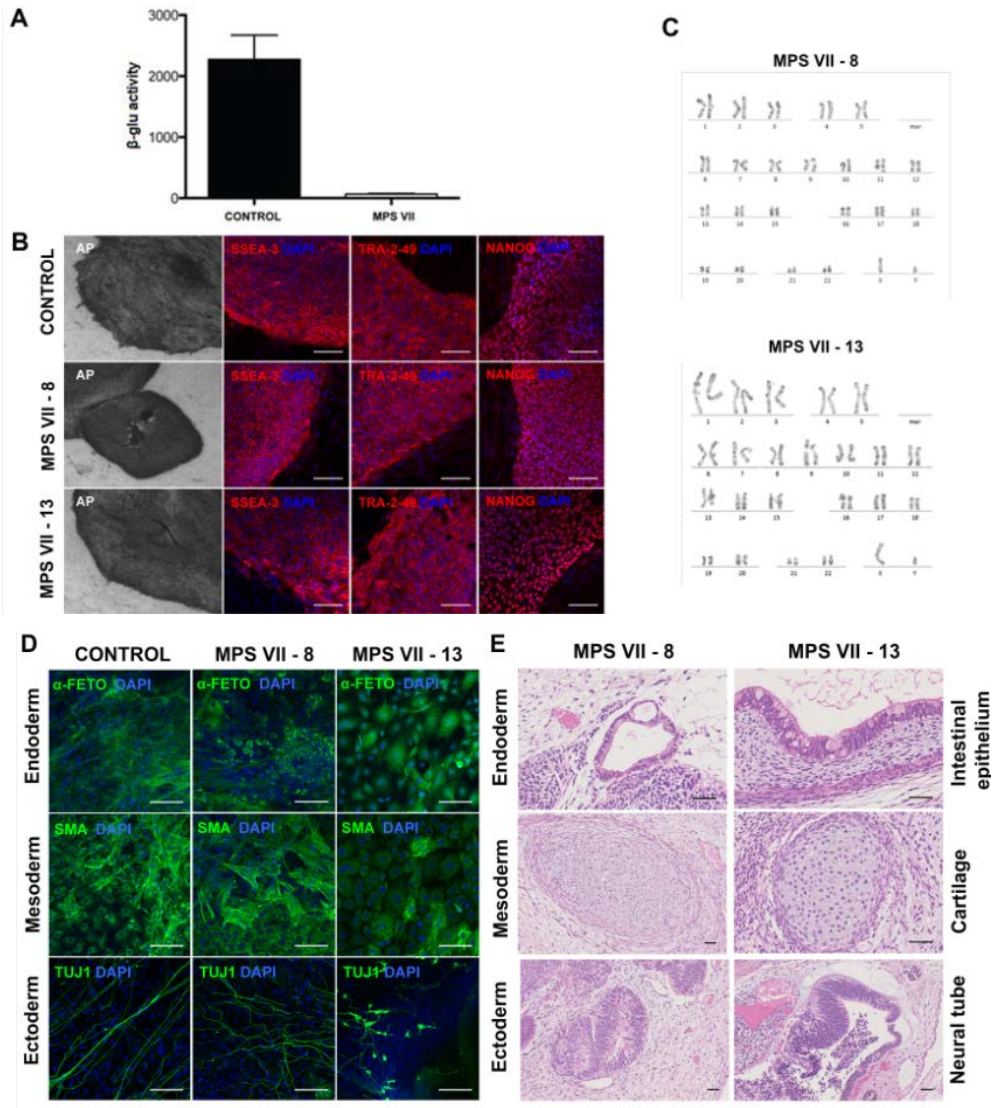

Figure 4.1: Generation and characterization of human MPS VII iPSC. (a) β-gluc enzymatic activity (expressed in nmol 4-MU/µg of protein/h) in control and MPS VII patient's fibroblasts. (b) Gene expression analysis of control (white) and MPS VII (grey and black) IPSC-like colonies; gene expression relative units of the retroviral-derived reprogramming vectors (exogenous) and endogenous expression levels (endogenous). (c) Representative colonies of control and MPS VII iPSC stained for alkaline phosphatase (AP) and the pluripotency-associated markers SSEA-3, Tra-2-49 and Nanog (all in red) and DAPI (blue); scale bars 200 µm (AP) and 100 µm (SSEA-3, Tra-2-49 and Nanog). (d) Karyotype of MPS VII iPSC. (e) Immunofluorescence microscopy of control and MPS VII iPSC differentiated *in vitro* and stained for the endoderm, mesoderm and ectoderm markers α-fetoprotein (green), smooth muscle actin (SMA, green) and βIII-tubulin (Tuj1, green), respectively; scale bars 100 µm. (f) Control and MPS VII iPSC differentiated *in vivo* by teratoma formation, stained with hematoxylin and eosin, showing potential to differentiate into endoderm (intestinal epithelium), mesoderm (cartilage) and ectoderm (neural tube); scale bars 100 µm.

Fibroblasts were reprogrammed at passages 2-4 with retroviral vector-mediated production of OCT4, cMYC, SOX2 and KLF4 (Takahashi et al., 2007). Following 3-4 weeks of culture, 20 compact PSC-like colonies emerged. These colonies were mechanically selected, expanded for at least 10 passages and tested for the expression of pluripotency markers.

Due to the scarcity of MPS VII patients, consequence of the MPS ultra-rare subtype, we characterized 2 MPS VII iPSC clones (#8 and #13) independently. iPSC clones from healthy individuals (a gift from the Institute for Stem Cell Therapy and Exploration of Monogenic diseases, France) were used as controls. Alkaline phosphatase activity (Fig. 4.1b) and expression of the transcription factor NANOG, the tumor-related antigen TRA-2-49 and the stage-specific embryonic antigen SSEA-3 (Fig. 4.1b) are consistent with pluripotency. The MPS VII iPSC clones had a normal karyotype after more than 20 passages (Fig. 4.1c). The ability of iPSC to differentiate into the three different germ layers was assessed by *in vitro* embryonic body (EB) formation and *in vivo* teratoma formation. After EB formation, expression of tissue-specific markers for mesoderm (α-smooth muscle actin), endoderm (α-fetoprotein) and ectoderm (βIII-tubulin) was demonstrated by immunofluorescence analyses (Fig. 4.1d). The presence of germ layers derivatives was also confirmed in teratomas by hematoxylin and eosin staining and histological analyses (Fig. 4.1e). Together these data demonstrate that these clones harbored characteristics indicative of bona fide iPSC.

3.2. Generation and characterization of human MPS VII iPSC-NPC

NPC were differentiated from control and MPS VII (cl. 8 and cl. 13) iPSC by the dual SMAD inhibition protocol (Chambers et al., 2009). This involves induction of neuroepithelial cell (NE)-rosettes from iPSC and NPC generation. NE-rosettes appeared 8-12 days after induction and a homogeneous, expandable and phenotypically stable NPC population, as judged by the uniform co-expression of

the neural progenitor markers Nestin and Sox2, was obtained after few passages (Fig. 4.2a).

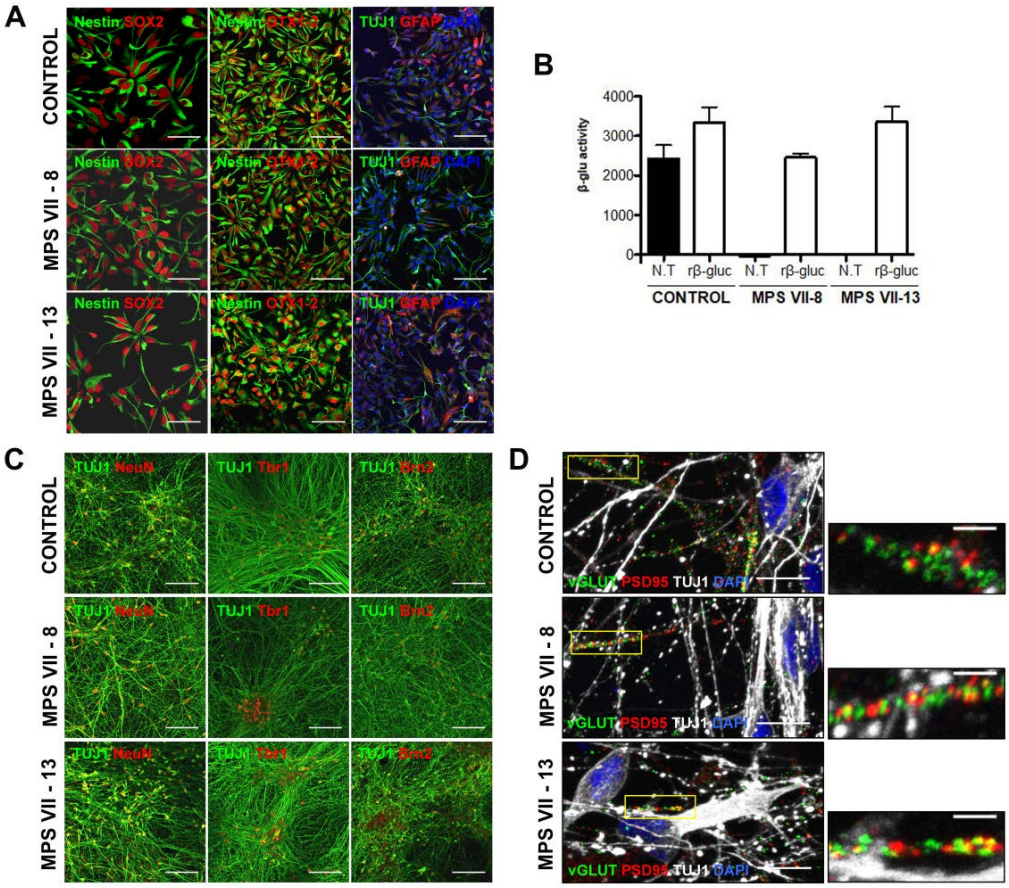

Figure 4.2: Characterization of human MPS VII iPSC-NPC and neurons in 2D cultures. (a) Immunofluorescence microscopy of control and MPS VII iPSC-NPC stained for NPC markers nestin (green) and Sox2 (red; first panel), scale bars 50 µm; nestin (green) and forebrain and midbrain progenitor marker Otx1/2 (red; second panel; and neuronal and astrocytic βIII-tubulin (Tuj1, green) and GFAP (red), respectively, DAPI (blue; third panel), scale bars 100 µm. (b) β-gluc enzymatic activity (expressed in nmol 4-MU/µg of protein/h) in control (black) and MPS VII (white) iPSC-NPC, non-treated (N.T.) and treated with recombinant β-gluc (rβ-gluc). (c) Representative images of control and MPS VII neurons stained for βIII-tubulin (Tuj1, green) and NeuN or cortical markers Tbr1 or Brn2 (red), respectively in first, second and third panels, scale bars 100 µm; (d) pre-synaptic protein vGLUT1 (green), post-synaptic protein PSD95 (red), βIII-tubulin (Tuj1, grey) and DAPI (blue), scale bars 100 µm; inserts (right) show synapsis formation at higher magnification, scale bars 5 µm.

Expression of the transcription factor OTX-1/2 was also consistent with forebrain and midbrain NPC (Fig. 4.2a). Early neuronal and astrocytic lineage

markers (βIII-tubulin and GFAP), suggestive of the potential of NPCs to differentiate into neurons and astrocytes, were also detected (Fig. 4.2a).

NPC generated from control and MPS VII iPSC showed self-renewal capability and ability to generate cells with neuron-like morphology for at least 18 passages, indicating they were bona fide NPC. No differences in self-renewal capability or viability were observed between NPC derived from healthy and MPS VII iPSC (not shown). Of note, a stromal feeder-free system was used to differentiate iPSC into NEP-rosettes and NPC. Therefore, there was no exogenous β-gluc in the media, demonstrating that β-gluc deficiency did not interfere in the first stages of neuroectodermal differentiation. β-gluc activity in MPS VII NPC was 50-fold lower than that in control NPC, confirming deficient β-gluc activity, and in line with that observed for MPS VII fibroblasts (Fig. 4.2b). To mimic enzyme replacement therapy (ERT), recombinant β-gluc (rβ-gluc) was added to NPC cultures and led to a >500-fold increase in β-gluc activity in MPS VII NPC, which was then similar to that of control NPCs (Fig. 4.2b). Together these data demonstrate that NPC with decreased β-gluc activity were generated from MPS VII iPSC.

3.3. Neural cells differentiated from MPS VII iPSC-NSC recapitulate disease features

To identify possible cellular defects in MPS VII brain cells, control and MPS VII (cl. 8 and cl. 13) NPC were further differentiated using 2D and 3D culture strategies (Fig. 4.3), as these approaches could impact neural differentiation and cellular functions.

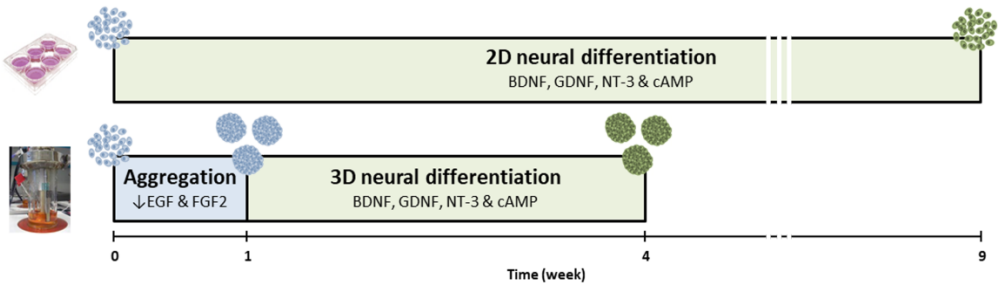

Figure 4.3: Schematic experimental workflow for differentiation of neural cells from control and MPS VII iPSC-NPC in 2D (top) and 3D (bottom) culture systems. For 2D differentiation, iPSC-NPC were

plated and neural differentiation was induced by exposure to BDNF, GDNF, NT-3 and cAMP for 9 weeks. For 3D differentiation iPSC-NPC were inoculated in a stirred suspension culture system, with reduced concentrations of growth factors EGF and FGF, and aggregated for 1 week, followed by induction of neural differentiation with BDNF, GDNF, NT-3 and cAMP for 3 weeks.

For 2D differentiation, NPC were cultured in neuronal induction medium (NIM) and differentiated into neurons within 3 weeks as determined by the expression of the neuronal markers βIII-tubulin and NeuN (Fig. 4.2c). Moreover, $Tbr1^+$ and $Brn2^+$ neurons were observed, indicating the capability of MPS VII NPC to give rise to neurons with cortical characteristics (Fig. 4.2c). Pre-synaptic (vGLUT1) and post-synaptic (PSD95) protein co-localization, suggestive of synapse formation and neuronal maturation, was achieved 7 weeks post-differentiation (Fig. 4.2d). iPSC-derived neurons presented membrane potentials of -50 mV and had voltage-dependent K^+ channels consistent with synapse functionality (not shown).

For 3D differentiation, NPC were inoculated as single cells in stirred-tank bioreactors, allowed to aggregate for 1 week, and then cultured in NIM for 3 weeks. With this strategy, obtained neurospheroids contain a mix of neural cells and allow accumulation of endogenous ECM components (Simão et al., 2016, 2014). Control and MPS VII neurospheroids maintained high cell viability along culture time (Fig. 4.4a) and spheroid size was stable after the aggregation period (Fig. 4.4b).

NPC proliferation, evaluated by the percentage of EdU^+ cells, decreased along culture time suggesting differentiation towards a post-mitotic neuronal lineage (Fig. 4.4c). Concomitantly, downregulation of proliferation (PCNA) and NPC (nestin) markers was observed along culture time (Fig. 4.4d), with no differences between control and MPS VII cells. These data are in line with 2D differentiation, indicating that MPS VII NPC have no apparent alterations in the potential to undergo neural differentiation.

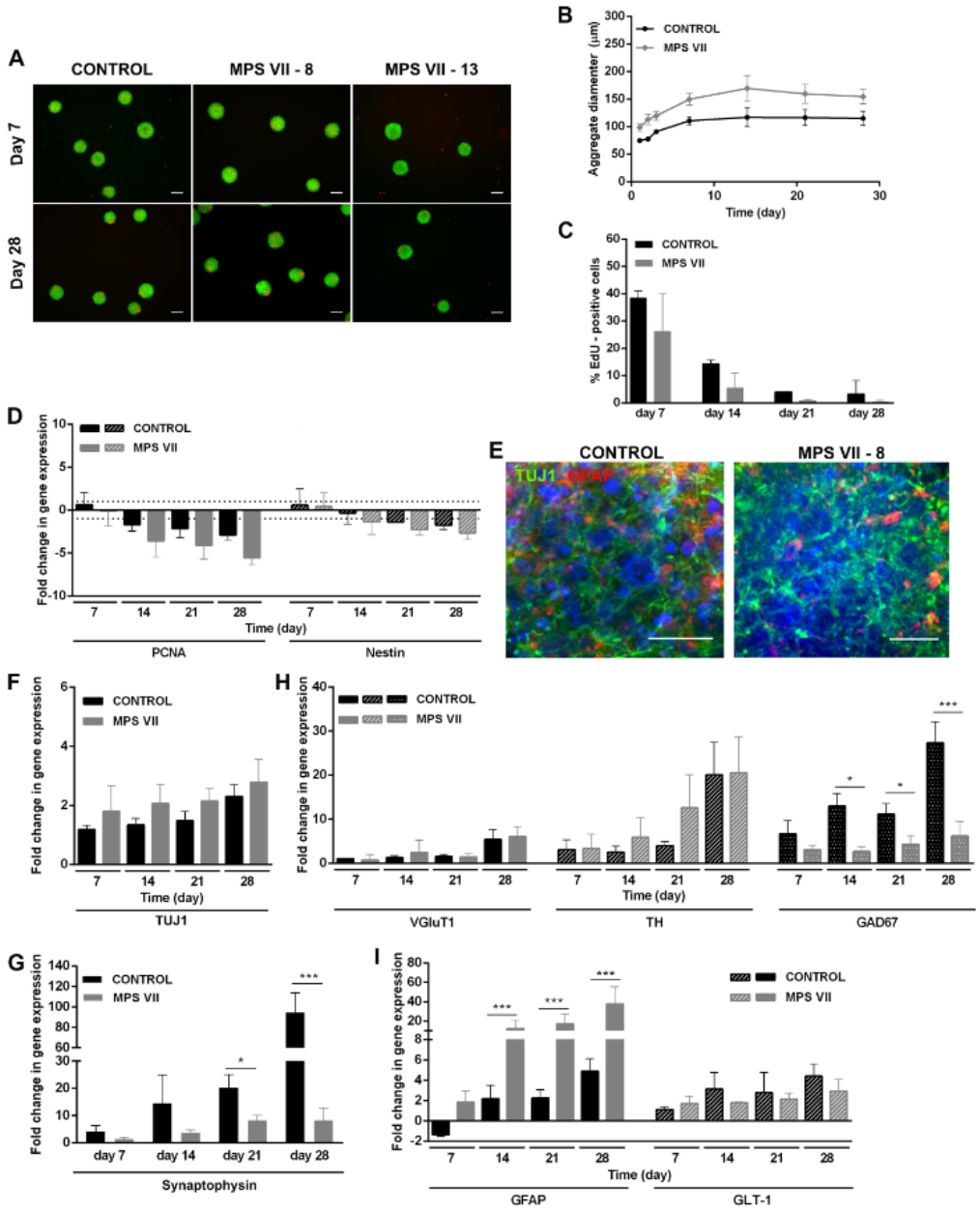

Figure 4.4: Characterization of MPS VII neurospheroids. (a) Representative images of control and MPS VII neurospheroids cell viability at day 7 and 28 by live/ dead assay using fluorescein diacetate (FDA) for stainig of live cells (green) and propidium iodide (PI) for dead cells (red). (b) Control (black) and MPS VII (grey) neurospheroid diameter profile along culture time. (c) Percentage of EdU+ cells in control (black) and MPS VII (grey) neurospheroids along culture time. (d) Gene expression analyses of control (black) and MPS VII (grey) neurospheroids; fold-changes (normalized to undifferentiated cells) of proliferation (PCNA) and NPC (nestin) markers. Data are mean ± SD of 3 (control) and 4 (MPS VII; 2 with MPS VII-cl.8 and 2 with MPS VII-cl.13) independent cultures. (e) Immunofluorescence confocal microscopy of control and MPS VII neurospheroids stained for astrocytic GFAP (red), neuronal βIII-

tubulin (green) and DAPI (blue); scale bars 20 µm. Gene expression analyses of control (black) and MPS VII (grey) neurospheroids; fold-change (normalized to undifferentiated cells) of: (f) βIII-tubulin, (g) the synaptic vesicle marker synaptophysin, (h) glutamatergic (VGluT1), dopaminergic (TH) and GABAergic (GAD67) neuronal subtypes markers, (i) astrocytic markers GFAP and GLT1. Data are mean ± SD of 3 (control) and 4 (MPS VII; 2 with MPS VII-cl.8 and 2 with MPS VII-cl.13) independent cultures. Asterisks indicate significant difference: * $P < 0.05$, *** $P < 0.001$.

Neuronal differentiation in 3D was confirmed by gene expression and detection of βIII-tubulin+ cells within neurospheroids by day 28 of culture (Fig. 4.4e and 4.4f). Importantly, gene expression of the pre-synaptic vesicle marker synaptophysin (syn) was significantly lower in MPS VII neurons (Fig. 4.4g), suggesting that synaptic dysfunction occurs. The presence of glutamatergic, dopaminergic and GABAergic neuronal subtypes was suggested by the upregulation of vGluT1, TH and GAD67 mRNAs, respectively (Fig. 4.4h). Moreover, a significantly ($p < 0.05$) lower (4-fold) level of GAD67 gene expression was detected in MPS VII neurospheroids by day 28 (Fig. 4.4h), suggesting decreased numbers of GABAergic inhibitory neurons. An increase in astrocytic differentiation within 2D and MPS VII neurospheroids was consistent with the time-dependent increase in gene expression of GFAP and GLT-1, which codes for a glutamate transporter. Notably, significant higher GFAP gene expression was observed in MPS VII neurospheroids (Fig. 4.4i), while no differences in GLT-1 were observed, suggesting that the number of potential astrocytes was not affected. Together, these results indicate that GFAP mRNA enrichment was not directly related to astrocyte differentiation or numbers, but rather a characteristic of MPS VII.

β-gluc activity in extracts of MPS VII neurons (2D) and neurospheroids (3D), showed up to 50-fold lower levels compared to control neurons (Fig. 4.5a and 4.5b). After treatment with rβ-gluc, the activity was restored to levels similar to the control (Fig. 4.5a) suggesting that rβ-gluc reached the lysosomes in MPS VII neurons, as previously observed for NPC (Fig. 4.2b). These results are in line with the low enzymatic activities found in MPS VII patient fibroblasts (Fig. 4.1a) and iPSC-NPC (Fig. 4.2b). Nevertheless, *GUSB* mRNA levels were stable along culture time in control and MPS VII neurospheroids (Fig. 4.5c).

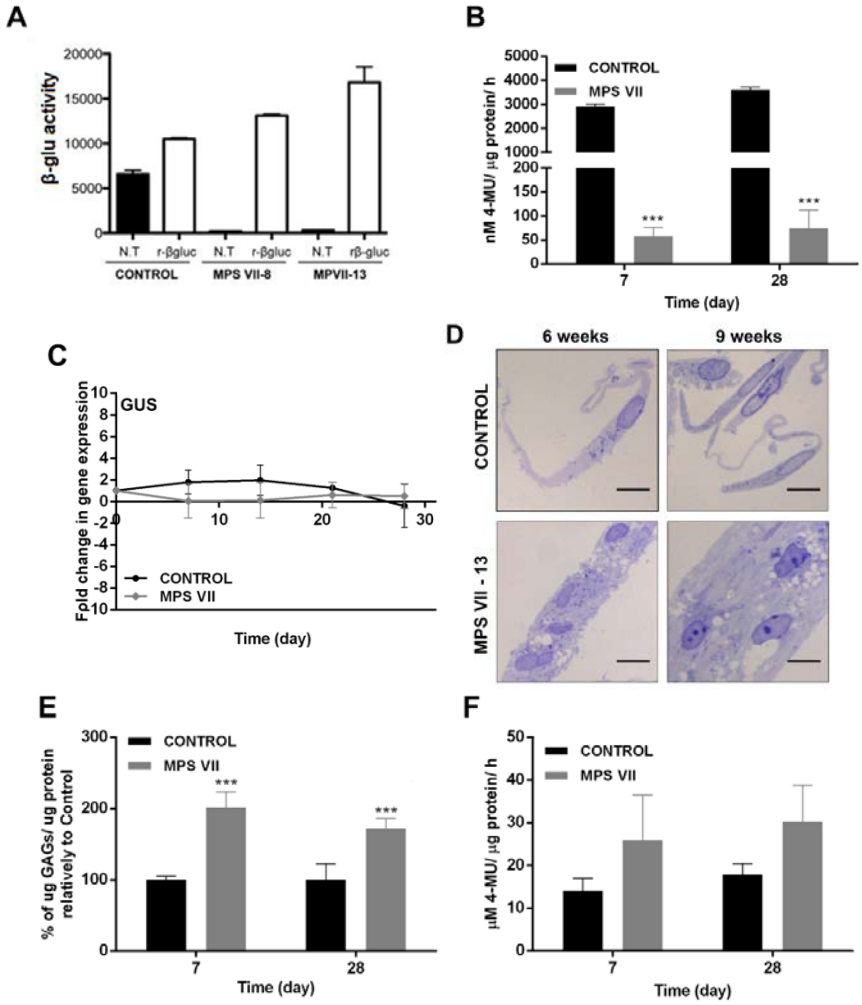

Figure 4.5: MPS VII neural cells recapitulate known disease features. (a) β-gluc enzymatic activity (expressed in nmol 4-MU/µg of protein/h) in control (black) and MPS VII (white) neurons, non-treated (N.T.) and treated with rβ-gluc. (b) β-gluc enzymatic activity in control (black) and MPS VII (grey) neurospheroids at day 7 and 28. (c) Gene expression analysis of control (black) and MPS VII (grey) neurospheroids; fold-change (normalized to undifferentiated cells) of GUSB. (d) GAGs storage in control and MPS VII neurons by toluidine blue staining at 6 and 9 weeks; scale bars 5 µm. (e) GAGs quantification in control (black) and MPS VII (grey) neurospheroids by Blyscan Sulphated Glycosaminoglycan assay. (f) β-hex enzymatic activity (expressed in nmol 4-MU/µg of protein/h) in control (black) and MPS VII (grey) neurospheroids at day 7 and 28. Data are mean ± SD of 3 (control) and 4 (MPS VII; 2 with MPS VII-cl.8 and 2 with MPS VII-cl.13) independent cultures. *** $P < 0.001$.

GAG accumulation, secretion and presence of enlarged intracellular vesicles are the main histological hallmarks and biomarkers for MPS VII (Montaño et al., 2016). We first investigated whether MPS VII neurons accumulate GAGs and harbor extended vesicles. By toluidine blue staining, we found more and bigger non-

staining vesicles in MPS VII neurons versus control neurons (Fig. 4.5d). In MPS VII neurospheroids, total GAG content almost doubled that of controls and this increase was already observed by day 7 of culture and maintained up to day 28 (Fig. 4.5e). This phenotype in human MPS VII neurons resembles that observed in mice (Ariza et al., 2014; Karolewski and Wolfe, 2006) and canine (Cubizolle et al., 2013) MPS VII brain. Additionally, in several MPS one can detect increased expression of other genes coding for lysosomal enzymes via the transcription factor EB (Sardiello et al., 2009). β-hexosaminidase (β-hex) is one lysosomal enzyme whose production and activity are elevated when the greater lysosomal system is perturbed. Notably, we observed a 1.7-fold increase in β-hex activity in the MPS VII neurospheroids, both at days 7 and 28 (Fig. 4.5f). Similarly, increased β-hex activity had been reported in MPS VII mouse and dog brains (Ariza et al., 2014; Cubizolle et al., 2013). Together, these data demonstrate that we generated human iPSC-derived MPS VII neurons that harbored the histological hallmarks of MPS VII pathology.

3.4. TEM reveals anomalies in the endocytic compartment of MPS VIII neurons

Transmission electron microscopy (TEM) was used to examine differences in the endocytic compartment between control and MPS VII neurons at 6 and 9 weeks of culture. In culture conditions that mimic the suboptimal conditions in the MPS VII brain, control neurons had a slightly high autophagy activity as indicated by the presence of double membrane structures (Fig. 4.6).

Consistent with the immunofluorescence studies, control neurons contained a well-defined endocytic compartment with amphisomes and multivesicular bodies (Fig. 4.6a and 4.6c), while MPS VII neurons harbored expanded endocytic compartments that were heterogeneous and formed clusters (Fig. 4.6b and 4.6d). TEM confirmed the presence of lipofuscin granules and micro-vacuolation of neuronal cell cytoplasm with fusion between homotypic vesicles, indicating defects in membrane fusion and compromised neuronal lysosomal function (Fig. 4.6a to

4.6d). These data identify pathological changes in human MPS VII neurons, which may impact learning and memory disabilities observed in MPS VII mice and some MPS VII patients.

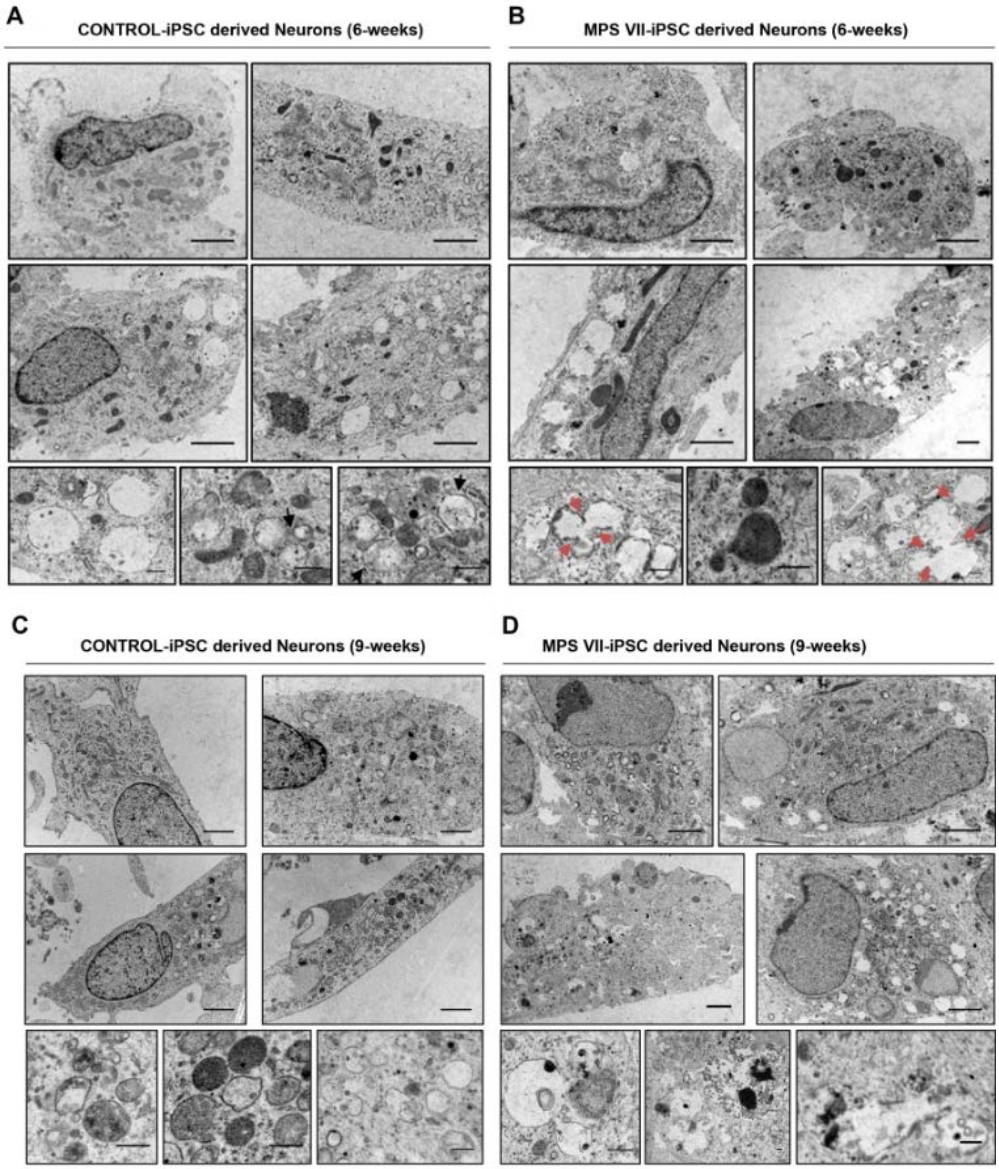

Figure 4.6: Transmission electron microscopy (TEM) of MPS VII neurons. Ultrastructure of control (a, c) and MPS VII (b, d) neurons at 6 (a, b) and 9 (c, d) weeks of culture. Black arrows in (a) show well-defined endocytic compartment with amphisomes and multivesicular bodies in control neurons, while MPS VII neurons harbor expanded and heterogeneous endocytic compartments that formed clusters. Red arrows in (b) indicate fusion between homotypic vesicles in MPS VII neurons. Scale bars 2 µm (top panels) and 0.5 µm (bottom panels).

3.5. Functional alterations in the greater lysosomal system of MPS VII neurons

We next asked if other aspects of the greater lysosomal system were altered in MPS VII NPC and neurons. Lysosomes fuse with autophagosomes to degrade long-lived proteins, organelles and pathogens. The autophagosome marker, LC3-I/II and the adaptor molecule p62/SQSTM1, which label molecules to be delivered to autophagosomes, were used to probe steady-state autophagy levels. The amount of LC3-I/II and p62/SQSTM1 were similar in control and MPS VII NPC ± rβ-gluc, suggesting that autophagy was not unbalanced in MPS VII NPC (Fig. 4.7a).

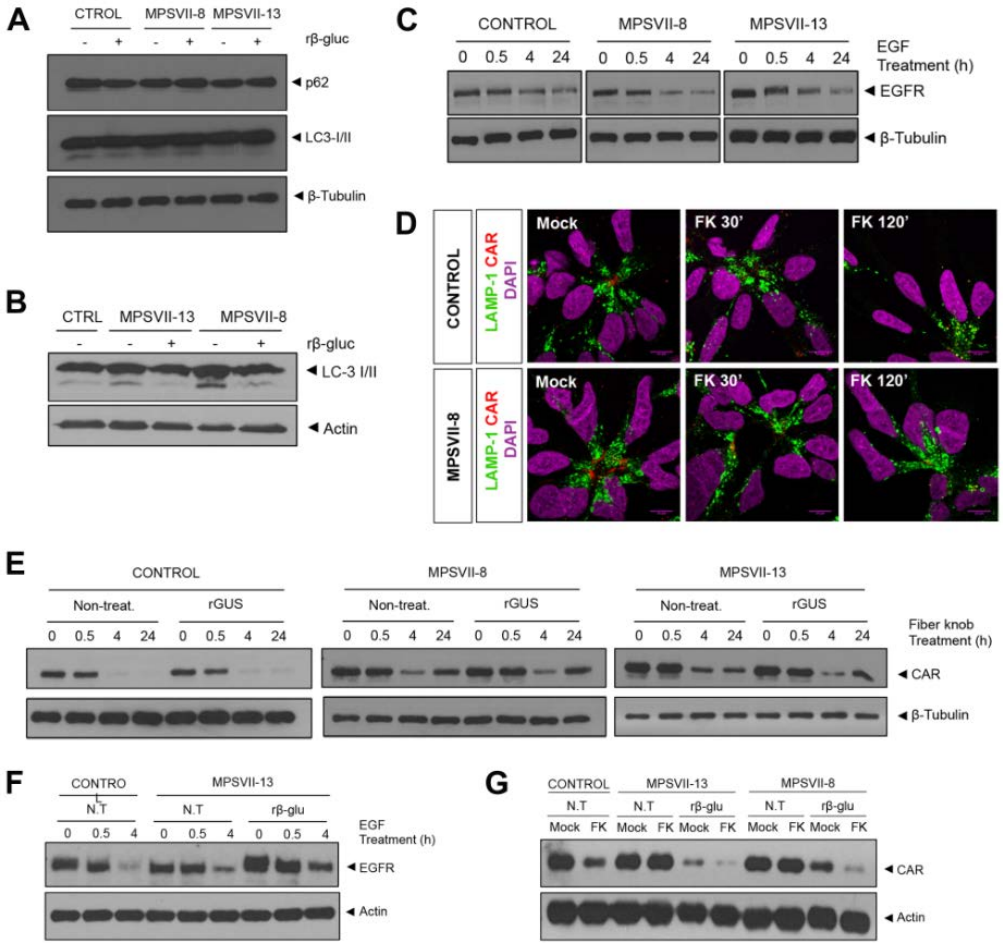

Figure 4.7: Lysosome function alteration in MPS VII NPC and neurons. Autophagy basal levels in control and MPS VII NPC (a) and neurons (b). P62 and LC3-I/ II were analyzed by western blot of control and MPS VII NPC protein extracts, non-treated (-) and treated (+) with rβ-gluc. Data from one

representative experiment of 4 independent experiments. (c) Control and MPS VII NPC lysosome ability to degrade membrane proteins internalized by endosomes assayed by an EGFR degradation assay. EGFR content analyzed by Western blot. Data from one representative experiment of 2 independent experiments. (d) Immunofluorescence confocal microscopy of control and MPS VII NPC, after induction of CAR degradation, stained for Lamp1 (green), CAR (extra- and intracellular domains, red) and DAPI (blue). CAR localized at the membrane, internalized into lysosomes (LAMP1 and CAR co-localization, 30') and degraded (120'). (e) Lysosome ability to degrade CAR assayed in control and MPS VII NPC, non-treated (non-treat.) and treated with rβ-gluc. CAR content analyzed by Western blot. Data from one representative experiment of 2 independent experiments. (f) Lysosome ability to degrade membrane proteins internalized by endosomes assayed by an EGFR degradation assay in control and MPS VII neurons, non-treated (N.T.) and treated with rβ-gluc. EGFR content analyzed by Western blot. Data from one representative experiment of 5 independent experiments. (g) Control and MPS VII neurons lysosome ability to degrade CAR, non-treated (N.T.) and treated with rβ-gluc. CAR content was analyzed by Western blot. Data from one representative experiment of 5 independent experiments.

While cytosolic LC3-I levels were similar in MPS VII and control neurons, LC3-II basal levels were increased in MPS VII neurons compared to controls, and restored to control levels when rβ-gluc was added to the medium (Fig. 4.7b). These results suggest a defect in autophagosome-lysosome fusion (autophagosome maturation) or a dysfunction of lysosomal protein degradation in MPS VII neurons.

In addition to intracellular degradation of host proteins, lysosomes also play a role in the regulation of signaling pathways by degrading cell surface receptors. Epidermal growth factor (EGF) signal transduction requires EGF receptor (EGFR) engagement, internalization of the EGF-EGFR complex into endosomes and degradation of EGFR in lysosomes, while EGF signaling endosomes reach the nucleus. We therefore addressed the function of endo-lysosomal system determining if EGFR is degraded in MPS VII NPC and neurons. EGFR levels in cell extracts at basal levels (time 0) and after recombinant EGF treatment (0.5, 4 and 24 h) were analyzed by immunoblotting. EGFR levels decreased over time in control and MPS VII NPC, with a 60 - 75% loss at 24 h, indicating that lysosomes functioned properly for EGFR degradation (Fig. 4.7c). To address lysosomal function using another cell surface protein, receptor-mediated endocytosis and lysosomal degradation was assayed for coxsackievirus and adenovirus receptor (CAR) (Loustalot et al., 2016). We previously showed that the canine adenovirus type 2 fiber knob (FK^{CAV}) binds CAR (Seiradake et al., 2006) and induces its lysosome-

mediated degradation in neuronal cells (Salinas et al., 2014). Importantly, EGFR and CAR occupy different microdomains in the plasma membrane: EGFR is globally spread while CAR is enriched in lipid rafts (Salinas et al., 2014), and therefore different internalization routes are used. MPS VII NPC were incubated with FK^{CAV}. CAR internalization and degradation were followed by immunofluorescence of CAR and LAMP1. In resting conditions, CAR was preferentially found at the cell membrane that contacts other NPC. Thirty minutes post-incubation with FKCAV, CAR was internalized and co-localized with LAMP1. At 2 h, CAR levels decreased compared with resting conditions, indicating its degradation both in control and MPS VII NPC (Fig. 4.7d). CAR levels were also quantified by immunoblotting (Fig. 4.7e). Control and MPS VII NPC ± rβ -gluc degraded CAR to a comparable extent (Fig. 4.7e). These data suggest that MPS VII NPC lysosome-mediated degradation is not notably altered and that lysosomes function properly in terms of autophagy and receptor degradation.

Because neurons use specific signaling pathways related to membrane remodeling, axonal growth and synapses plasticity, these pathways could be more susceptible to metabolite accumulation and perturbations of the endo-lysosomal system. Thus, levels and processing of EGFR and CAR were also evaluated in MPS VII neurons. We found that the levels of EGFR after EGF treatment were reduced in control, MPS VII and rβ-gluc treated MPS VII neurons (Fig. 4.7f). Moreover, ERT had no effect in EGFR levels, further indicating that there were no alterations in EGFR degradation due to MPS VII pathology. CAR levels diminished after FK^{CAV} treatment in control neurons (Fig. 4.7g), while in MPS VII neurons were unchanged, indicating an alteration in the endo-lysosomal pathway. Of note, CAR levels were diminished in rβ-gluc-treated MPS VII neurons similar to control neurons (Fig. 4.7g). These data are consistent with specific defects in the greater lysosome system of MPS VII neurons.

3.6. Network alterations in MPS VII neurons

MPS VII neuron functionality was assessed by imaging cytosolic calcium (Ca^{++}) concentration using the ratiometric fluorescent dye, Fura-2, which monitors Ca++ entry through voltage-gated Ca^{++} channels in neurons. Upon KCl-induced depolarization, approximately 50% of the cells exhibited signals in both control and MPS VII cultures (Fig. 4.8a).

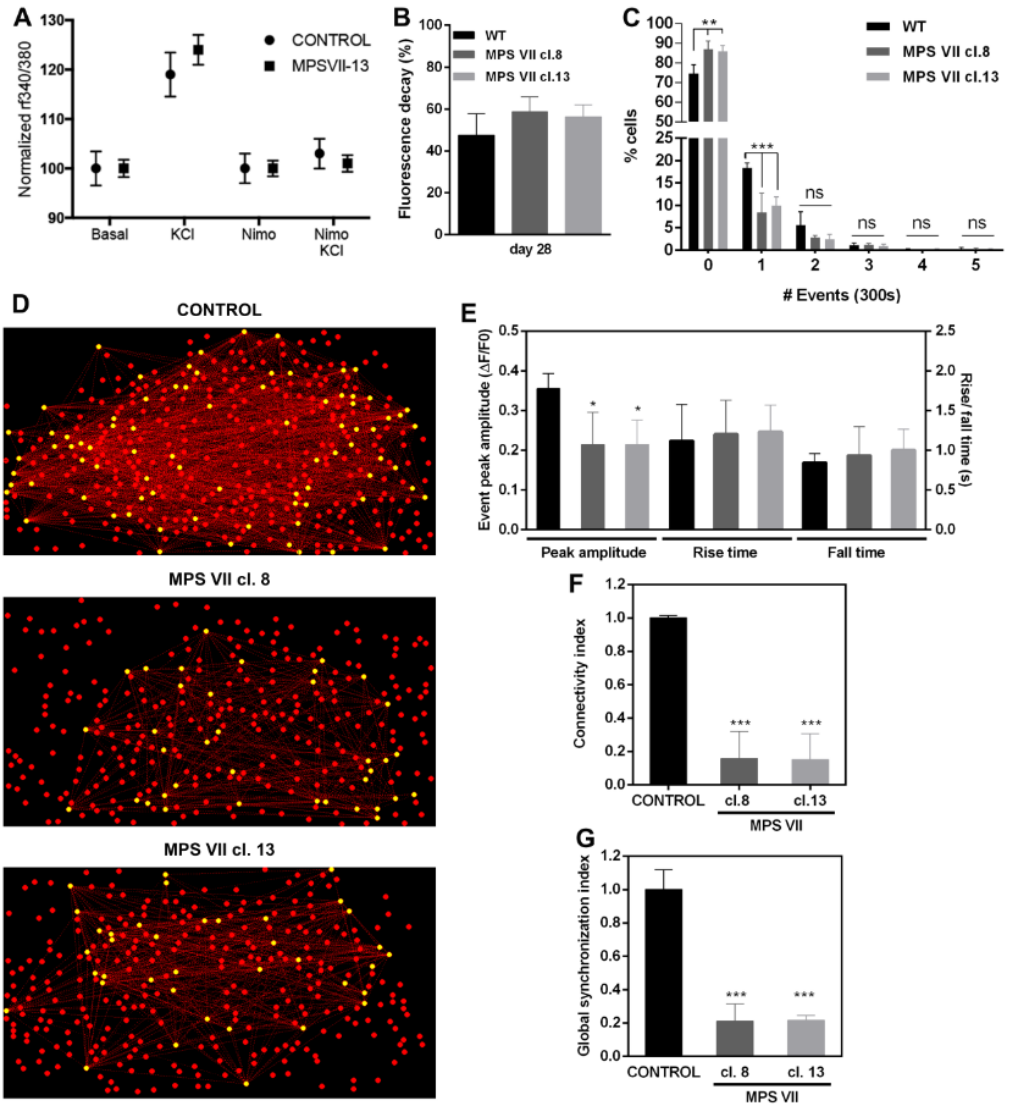

Figure 4.8: MPS VII neuronal activity and MPS VII neurospheroids calcium (Ca^{++}) imaging analysis. (a) Ca^{++} release in control and MPS VII neurons, upon KCl induction and reduction of Ca^{++} signaling upon inhibition with nimodipine. (b) FM-1-43 fluorescence decay in control (black) and MPS VII (grey)

neurospheroids at day 28. Data are mean ± SD of 3 independent cultures. (c) Percentage of cells per number of spontaneous Ca^{++} events in 300 seconds for control (black) and MPS VII (cl. 8 grey; cl. 13 light grey) neurospheroids. (d) Visual representations of neural networks from control and MPS VII neurospheroids reconstructed using FluoroSNNAP; circles show the position of cells in culture, yellow circles represent functionally connected nodes and red lines represent the functional connectivity of pair-wise neurons. (e) Ca^{++} events peak amplitude, rise time and fall time in control (black) and MPS VII (cl. 8 grey; cl. 13 light grey) neurospheroids. Network properties: Connectivity index (f) and Global synchronization index (g) in control (black) and MPS VII (cl. 8 grey; cl. 13 light grey) neurospheroids. Data are mean ± SD of 3 (control) and 4 (MPS VII; 2 with MPS VII-cl.8 and 2 with MPS VII-cl.13) independent cultures. Asterisks indicate significant difference: * $P < 0.05$, *** $P < 0.01$, *** $P < 0.001$.

The effectiveness of nimodipine, a L-type Ca^{++} channel blocker, to inhibit Ca^{++} signals in depolarizing conditions further demonstrated the presence of differentiated neurons in both conditions (Fig. 4.8a). These data indicated that after 7 weeks in culture MPS VII neurons were functionally similar to control neurons. In MPS VII neurospheroids synaptic functionality was initially assessed by imaging KCl-induced synaptic vesicle exocytosis. Control and MPS VII neurospheroids responded similarly to the depolarizing stimuli, indicating no differences in total synaptic vesicle trafficking (Fig. 4.8b). Next, Ca^{++} fluorescence imaging was used to evaluate the differences in spontaneous neuronal activity between control and MPS VII neurons and alterations in neuronal network functional connectivity within MPS VII neurospheroids. MPS VII neurospheroids had significantly lower neuronal activity than control, with 8.5% (MPS VII cl.8) and 10.0% (MPS VII cl.13) of cells presenting one spontaneous Ca^{++} event, compared to 18.4 % in control neurospheroids, and with a higher percentage of cells that did not present spontaneous Ca^{++} events during the monitoring time (Fig. 4.8c).

To characterize MPS VII neuronal networks, connectivity was evaluated using FluoroSNNAP software, which allows one to infer functional connectivity between neurons using the temporal correspondence of Ca^{++} events. These analyses generate maps of neuronal interactions where one can quantify the connectivity indexes for each active cell (Patel et al., 2015). Representative connectivity maps of control and MPS VII neurospheroids are provided in Fig. 4.8d. The average peak amplitude of the spontaneous Ca^{++} events of MPS VII neurospheroids was

significantly ($p < 0.05$) smaller than in control neurospheroids, while no significant differences were found in rise and fall times (Fig. 4.8e).

In control network structures, most of the cells established several connections with other cells (Fig. 4.8d). By contrast, connections were formed only between some of the cells in MPS VII network, leaving the remaining cells weakly connected or disconnected (Fig. 4.8d). Concomitantly, the average connectivity index for active cells was significantly ($p < 0.001$) lower in MPS VII neurospheroids (Fig. 4.8f). A similar pattern was observed for the global synchronization index, which was also significantly ($p < 0.001$) lower in MPS VII networks (Fig. 4.8g), further indicating alterations in MPS VII neuronal networks. Together, these results demonstrate that MPS VII neurospheroids have less active cells with smaller Ca^{++} peak amplitudes, the cells are weakly connected and poorly synchronized, which may impact the MPS VII brain network topology and functionality.

4. Discussion

One of our primary, long-term, goals at the core of our studies is to identify quantifiable neuronal phenotype that could complement genetic analyses to help us predict the severity of MPS VII-associated cognitive anomalies. This is because GUSB heterogeneity, in combination with other genetic or environmental factors, causes a range of pathological features that make prognosis, and in turn recommending treatment options, challenging. We reasoned that the current pace of technological improvements in cellular reprograming and directed differentiation will allow one to rapidly and inexpensively generate neural cells from many cell types. The unique functions of neural cells could then be probed for MPS VII-associated defects.

Here, we used human MPS VII iPSC-derived neural cells, cultured in 2D and 3D culture systems, to try to identify neuronal defects. We found that ERT, in this case supraphysiological levels of β-gluc activity, was not necessary for fibroblast reprogramming, iPSC generation or expansion. The requirement for ERT is similar

to that described for MPS IIIC iPSC (Canals et al., 2015), but in contrast to that reported for MPS IIIB and Pompe disease iPSC (Higuchi et al., 2014; Lemonnier et al., 2011). Generating NPC is primordial during normal brain development. Despite limited β -gluc activity, a homogeneous, expandable and phenotypically stable population of NSCs was obtained. These *in vitro* data are consistent with the clinical manifestation of MPS VII, and with early brain development of MPS VII mouse and dogs, which appears histologically normal (Ariza et al., 2014; Cubizolle et al., 2013; Karolewski and Wolfe, 2006). These data suggest that deficiency in β-gluc activity may not have a discernable impact on initial stages of neural development. A caveat is that during fetal development maternal β-gluc would be present for uptake in brain cells until the fetal blood brain barrier is formed.

We then asked whether some aspects of neural cell homeostasis could be perturbed by decreased β-gluc activity. We show that MPS VII neurons differentiated in 2D cultures formed functional synapses. Similar differentiation patterns were observed during 2D differentiation of control and MPS VII neurons indicating that reduced β-gluc activity did not affect the onset of the neuronal differentiation of MPS VII NPC in this culture system. Differentiation of MPS VII NPC in a 3D culture system revealed downregulation of proliferating cells, prototypic NPC gene expression, and upregulation of neuronal βIII-tubulin, consistent with the ability of MPS VII NPC to undergo neuronal differentiation. Neuronal differentiation was consistent with the expression of synaptophysin and markers of glutamatergic, dopaminergic and GABAergic neurons. Notably, GAD67 gene expression was lower in MPS VII neurospheroids, suggesting that there was a reduction in GABAergic neuronal differentiation. GABA is the main inhibitory neurotransmitter within the brain and GABAergic neurons are involved in several physiological functions, including stabilization of neuronal activity. A balance between excitation and inhibition ensures the normal functioning of the neuronal networks (Błaszczyk, 2016), so decreased GABAergic neurons could potentially lead to neuronal networks alterations. Indeed, GABAergic neurons exhibit neuroaxonal dystrophy

more than other cells types in a MPS VII mouse model and in other LSD, such as MPS I, and GM1 and GM2 gangliosidosis (Parente et al., 2012; Walkley, 1998; Walkley et al., 1991). Concomitantly, a 8-fold down-regulation in OTX1-2, a transcription factor that controls neuron subtype identity and the fate of GABAergic neurons, was found in the brain of a MPS VII mouse model (Parente et al., 2012) and in human MPS IIB brain the density of GABAergic neurons in the cerebral cortex was markedly reduced when compared with age-matched controls (Hamano et al., 2008).

Despite decreased synaptophysin gene expression in MPS VII neurospheroids, functional synapses were equivalent to controls. However, it is possible that this approach, and/or our culture conditions were not optimized to detect subtle differences in neuronal functionality during the depolarization assays. More specifically, overall fluorescence of the neurospheroids was quantified in medium optimized for culturing and maintaining healthy neuronal cells, and therefore this environment poorly recapitulate the environment in the MPS VII brain. Detecting alterations in GABAergic neurons synaptic activity may require a "stressed/challenging" environment. For example, astrocytes provide neurotrophic support, help synchronize neurotransmitter metabolism and release and regulate the extracellular milieu. Thus, alterations in astrocyte function can be a major contributor to neurodegeneration and/or cognitive defects (Phatnani and Maniatis, 2015; Sofroniew and Vinters, 2010). Notably, higher GFAP mRNA levels were found in MPS VII neurospheroids. Similarly, in recent studies performing transcriptome analyses of the MPS VII mouse brain, thirteen astrocyte-specific mRNAs (including GFAP) were upregulated (Parente et al., 2016, 2012). Upregulation of GFAP is the hallmark of astrocyte reactivity in response to an insult or injury in the CNS (Ben Haim et al., 2015; Phatnani and Maniatis, 2015). An increase in the number of GFAP+ astrocytes was also found in the cerebral cortex of MPS II and IIIB patients (Hamano et al., 2008). Mediators of innate immunity, such as lipopolysaccharide (LPS) and other toll-like receptor (TLR) ligands, as well as neurodegenerative

diseases, are able to trigger reactive astrogliosis to different extents (Phatnani and Maniatis, 2015; Sofroniew and Vinters, 2010). Of note, GAG breakdown products are structurally similar to LPS, the canonical ligand of TLR4 (Ballabio and Gieselmann, 2009; Xing et al., 2015). Therefore, GAGs accumulation could activate TLR4 signaling pathway inducing a pro-inflammatory response. Priming of microglia via the TLR4 pathway has been demonstrated in the mouse MPS IIIC brain (Ausseil et al., 2008) and MPS VII mice presented elevated levels of p-STAT1-Ser727 and p-STAT3-Tyr705, consistent with TLR4 activation (Metcalf et al., 2009). Further exploring the astrocytes in 3D MPS VII neurospheroids could help us determine if they are activated through a TLR pathway.

In addition to intracellular degradation of host proteins, lysosomes also play a role in the regulation of signaling pathways by degrading cell surface protein receptors. Our data suggested that lysosomes function properly in terms of EGFR degradation both in MPS VII NPC and neurons and CAR degradation in MPS VII NPC, but not in MPS VII neurons. As neurons use specific signaling pathways related to membrane remodeling, axonal growth and synapse plasticity, these could be more susceptible to metabolite accumulation and perturbations of the endo-lysosomal system. These data suggest that signaling pathways following similar internalization routes like CAR, which is lipid microdomain-, actin-, and dynamin-dependent (Salinas et al., 2014), may be affected in MPS VII neurons. Importantly, these alterations in MPS VII neurons were restored by ERT.

The functional and networking alterations in MPS VII neurons are ideal starting points to understand MPS VII cognitive defects. A consequence of lower connectivity and poor synchronization could be related with the decrease in GABAergic neurons. There is a strong interplay between Ca^{++} levels and GABA, as a GABAergic neuron decline is initiated by abnormal increased intracellular Ca^{++} levels (Błaszczyk, 2016). Moreover, as the balance between excitation and inhibition ensures the normal functioning of the networks, a decrease in GABAergic neurons could negatively impact the networks (Błaszczyk, 2016). This disturbance

in MPS VII neuronal activity and network functional connectivity is, to the best of our knowledge, the first report of *in vitro* functional impairment that may recapitulate the mechanisms underlying brain dysfunction and cognitive impairment in MPS VII patients. The deregulation of Ca^{++} levels and GABA levels further link LSD and Parkinson's disease, which shared genetic, clinical and neuropathological features (Beck, 2016). Furthermore, these observations are important to provide new insights in the relation between alterations in the network in MPS VII disease and GAG's accumulation and its impact in impaired cognition. Now that quantifiable readouts have been identified, future studies are needed to include iPSC-derived neurons from a cohort of MPS VII patients to identify inter-individual differences to be correlated with patient's mutations and to provide mechanistic insights on whether disease phenotype is affecting neural differentiation and neuronal network functionality. This could represent a step towards improved post-natal diagnosis and therapeutic strategies to prevent/ reverse MPS VII -associated cognitive defects. Given the similarities between MPS VII and other MPS and LSD, our study has broad implications.

In summary, we identified MPS VII-associated perturbations through differentiation of iPSC into NPC and neurons. Our study provides an iPSC-based model that reproduces the major biochemical and histological features of the MPS VII, especially neuronal phenotypes. This provides a platform upon which the cellular processes responsible for brain dysfunction in MPS VII can be further elucidated and used for testing and optimizing therapies. 3D neurospheroid culture systems combined with neuronal connectivity assays have the potential to assess neurological defects in other LSD and neurodegenerative diseases with variable phenotypes.

5. Acknowledgments

We thank Eric Kremer laboratory members, specially to Eric Kremer for the fruitful discussions and to Neus Bayó-Puxan and Sophie Creyssels who

reprogrammed the iPSC, differentiated the iPSC into NPC, and performed the differentiation of NPC in the 2D culture system and all the 2D neuronal culture characterization. Thanks to EKL former members, Jordi Barquinero (VHIR Vall d'Hebron Research Insitute, Barcelona, Spain), Jordi Cruz Villalba (MPS Spain), Tristan Bouschet and Christian Barrère (Institute of Functional Genomics, Montpellier, France), Manel Bosch and Elena Rebollo Arredondo (University of Barcelona), Mercè Martí and Cristina Pardo (Center of Regenerative Medicine in Barcelona) for constructive comments during the course of this study. We are grateful to Emil Kakkis and Michael Vellard from Ultragenyx for the gift of rβ-gluc. We thank the technological platforms in Montpellier (MRI, RHEM, RAM, & CHROMOSTEM), and Barcelona (Advanced Optical Microscopy facility, Bioimaging and Histology platform), and Evry (I-Stem).

This study was funded in part by the European commission (FP7 BrainCAV 222992 (EJK), Government of Catalonia (With the support of the Secretary for Universities and Research of the Ministry of Economy and Knowledge of the Government of Catalonia and the COFUND program of the Marie Curie Actions of the 7th R&D Framework Program of the European Union) (NBP), IGMM (EJK), LabEx EpiGenMed, an "Investissements d'avenir" program, ANR-10-LABX-12-01 (SC, EJK), La Fondation pour la Recherche Médicale (EJK), E-Rare (AB, EJK), Vaincre les Maladies Lysosomales (NBP, EJK), iNOVA4Health - UID/Multi/04462/2013, a program financially supported by Fundação para a Ciência e Tecnologia (FCT)/Ministério da Educação e Ciência, Portugal, through national funds and co-funded by FEDER under the PT2020 Partnership Agreement (APT, DS, CB); FCT, Portugal, by the PhD fellowship to APT (PD/BD/52473/2014), European Research Council (2012-StG-311736-PD-HUMMODEL (AC)), the Spanish Ministry of Economy and Competitiveness-MINECO (BFU2016-80870-P (AC)), Instituto de Salud Carlos III-ISCIII/FEDER (Red de Terapia Celular - TerCel RD16/0011/0024), AGAUR (2014-SGR-1460 (AC)).

6. References

Ariza, L., Giménez-Llort, L., Cubizolle, A., Pagès, G., García-Lareu, B., Serratrice, N., Cots, D., Thwaite, R., Chillón, M., Kremer, E.J., Bosch, A., 2014. Central Nervous System Delivery of Helper-Dependent Canine Adenovirus Corrects Neuropathology and Behavior in Mucopolysaccharidosis Type VII Mice. Hum. Gene Ther. 25, 199–201. doi:10.1089/hum.2013.152

Ausseil, J., Desmaris, N., Bigou, S., Attali, R., Corbineau, S., Vitry, S., Parent, M., Cheillan, D., Fuller, M., Maire, I., Vanier, M.-T., Heard, J.-M., 2008. Early neurodegeneration progresses independently of microglial activation by heparan sulfate in the brain of mucopolysaccharidosis IIIB mice. PLoS One 3, e2296.

Ballabio, A., Gieselmann, V., 2009. Lysosomal disorders: from storage to cellular damage. Biochim. Biophys. Acta 1793, 684–696.

Batzios, S., Zafeiriou, D., Papakonstantinou, E., 2013. Extracellular matrix components: An intricate network of possible biomarkers for lysosomal storage disorders? FEBS Lett. 587, 1258–1267.

Beck, M., 2016. The Link Between Lysosomal Storage Disorders and More Common Diseases. J. Inborn Errors Metab. Screen. 4, 232640981668276. doi:10.1177/2326409816682767

Ben Haim, L., Carrillo-de Sauvage, M.-A., Ceyzériat, K., Escartin, C., 2015. Elusive roles for reactive astrocytes in neurodegenerative diseases. Front. Cell. Neurosci. 9, 278. doi:10.3389/fncel.2015.00278

Błaszczyk, J.W., 2016. Parkinson's disease and neurodegeneration: GABA-collapse hypothesis. Front. Neurosci. 10. doi:10.3389/fnins.2016.00269

Borger, D.K., McMahon, B., Roshan Lal, T., Serra-Vinardell, J., Aflaki, E., Sidransky, E., 2017. Induced pluripotent stem cell models of lysosomal storage disorders. Dis. Model. Mech. 10, 691–704. doi:10.1242/dmm.029009

Canals, I., Soriano, J., Orlandi, J.G., Torrent, R., Richaud-Patin, Y., Jiménez-Delgado, S., Merlin, S., Follenzi, A., Consiglio, A., Vilageliu, L., Grinberg, D., Raya, A., 2015. Activity and high-order effective connectivity alterations in sanfilippo C patient-specific neuronal networks. Stem Cell Reports 5, 546–557. doi:10.1016/j.stemcr.2015.08.016

Cereso, N., Pequignot, M.O., Robert, L., Becker, F., De Luca, V., Nabholz, N., Rigau, V., De Vos, J., Hamel, C.P., Kalatzis, V., 2014. Proof of concept for AAV2/5-mediated gene therapy in iPSC-derived retinal pigment epithelium of a choroideremia patient. Mol. Ther. - Methods Clin. Dev. 1, 14011. doi:10.1038/mtm.2014.11

Chabas, A., Giros, M., Guardiola, A., 1991. Low beta-glucuronidase activity in a healthy member of a family with mucopolysaccharidosis VII. J Inherit Metab Dis 14, 908–914.

Chambers, S.M., Craft, C.A., Papapetrou, E.P., Tomishima, M., Sadelain, M., Studer, L., 2009. Highly efficient neural conversion of human ES and iPS cells by dual inhibition of SMAD signaling. Nat Biotechnol 27, 275–280.

Chambers, S.M., Mica, Y., Lee, G., Studer, L., Tomishima, M.J., 2015. Dual-SMAD Inhibition/WNT Activation-Based Methods to Induce Neural Crest and Derivatives from Human Pluripotent Stem Cells. Methods Mol. Biol. 1307, 329–343. doi:10.1007/7651_2013_59

Cubizolle, A., Serratrice, N., Skander, N., Colle, M.-A., Ibanes, S., Gennetier, A., Bayo-Puxan, N., Mazouni, K., Mennechet, F., Joussemet, B., Cherel, Y., Lajat, Y., Vite, C., Bernex, F., Kalatzis, V., Haskins, M.E., Kremer, E.J., 2013. Corrective GUSB transfer to the canine mucopolysaccharidosis VII brain. Mol. Ther. 181, 22–31. doi:10.1038/mt.2013.283

Doerr, J., Böckenhoff, A., Ewald, B., Ladewig, J., Eckhardt, M., Gieselmann, V., Matzner, U., Brüstle, O., Koch, P., 2015. A overexpressing human iPSC-derived neural cells reduce CNS sulfatide storage in a mouse model of metachromatic leukodystrophy. Mol. Ther. 23, 1519–1531. doi:10.1038/mt.2015.106

Gaffield, M. a, Betz, W.J., 2006. Imaging synaptic vesicle exocytosis and endocytosis with FM dyes. Nat. Protoc. 1, 2916–21. doi:10.1038/nprot.2006.476

Gaspard, N., Bouschet, T., Herpoel, A., Naeije, G., van den Ameele, J., Vanderhaeghen, P., 2009. Generation of cortical neurons from mouse embryonic stem cells. Nat. Protoc. 4, 1454–1463. doi:10.1038/nprot.2009.157

Griffin, T.A., Anderson, H.C., Wolfe, J.H., 2015. Ex vivo gene therapy using patient iPSC-derived NSCs reverses pathology in the brain of a homologous mouse model. Stem Cell Reports 4, 835–846. doi:10.1016/j.stemcr.2015.02.022

Hamano, K., Hayashi, M., Shioda, K., Fukatsu, R., Mizutani, S., 2008. Mechanisms of neurodegeneration in mucopolysaccharidoses II and IIIB: Analysis of human brain tissue. Acta Neuropathol. 115, 547–559. doi:10.1007/s00401-007-0325-3

Higuchi, T., Kawagoe, S., Otsu, M., Shimada, Y., Kobayashi, H., 2014. The generation of induced pluripotent stem cells (iPSCs) from patients with infantile and late-onset types of Pompe disease and the effects of treatment with acid- α -glucosidase in Pompe iPSCs Phase control TRA-1-60 TRA-1-81. Mol. Genet. Metab. 112, 44–48. doi:10.1016/j.ymgme.2014.02.012

Huangfu, D., Maehr, R., Guo, W., Eijkelenboom, A., Snitow, M., Chen, A.E., Melton, D.A., 2008. Induction of pluripotent stem cells by defined factors is greatly improved by small-molecule compounds. Nat. Biotechnol. 26, 795–797. doi:10.1038/nbt1418

Karolewski, B.A., Wolfe, J.H., 2006. Genetic correction of the fetal brain increases the lifespan of mice with the severe multisystemic disease mucopolysaccharidosis type VII. Mol. Ther. 14, 14–24. doi:10.1016/j.ymthe.2006.02.012

Lee, G., Studer, L., 2010. Induced pluripotent stem cell technology for the study of human disease. Nat Methods 7, 25–27. doi:10.1038/nmeth.f.283

Lemonnier, T., Blanchard, S., Toli, D., Roy, E., Bigou, S., Froissart, R., Rouvet, I., Vitry, S., Heard, J.M., Bohl, D., 2011. Modeling neuronal defects associated with a lysosomal disorder using patient-derived induced pluripotent stem cells. Hum. Mol. Genet. 20, 3653–3666. doi:10.1093/hmg/ddr285

Loustalot, F., Kremer, E.J., Salinas, S., 2016. Chapter Six – Membrane Dynamics and Signaling of the Coxsackievirus and Adenovirus Receptor, in: International Review of Cell and Molecular Biology. pp. 331–362. doi:https://doi.org/10.1016/bs.ircmb.2015.10.006

Maetzel, D., Sarkar, S., Wang, H., Abi-Mosleh, L., Xu, P., Cheng, A., Gao, Q., Mitalipova, M., Jaenisch, R., 2014. Genetic and chemical correction of cholesterol accumulation and impaired autophagy in hepatic and neural cells derived from Niemann-Pick Type C patient-specific iPS cells. Stem Cell Reports 2, 866–880. doi:10.1016/j.stemcr.2014.03.014

Mangeot, P.E., Dollet, S., Girard, M., Ciancia, C., Joly, S., Peschanski, M., Lotteau, V., 2011. Protein transfer into human cells by VSV-G-induced nanovesicles. Mol. Ther. 19, 1656–1666. doi:10.1038/mt.2011.138

Meneghini, V., Frati, G., Sala, D., De Cicco, S., Luciani, M., Cavazzin, C., Paulis, M., Mentzen, W., Morena, F., Giannelli, S., Sanvito, F., Villa, A., Bulfone, A., Broccoli, V., Martino, S., Gritti, A., 2017. Generation of Human Induced Pluripotent Stem Cell-Derived Bona Fide Neural Stem Cells for Ex Vivo Gene Therapy of Metachromatic Leukodystrophy. Stem Cells Transl. Med. 6, 352–368. doi:10.5966/sctm.2015-0414

Metcalf, J., Zhang, Y., Hilton, M., Long, F., Ponder, K., 2009. Mechanism of shortened bones in mucopolysaccharidosis VII. Mol Genet Metab 97, 202–211.

Montaño, A.M., Lock-Hock, N., Steiner, R.D., Graham, B.H., Szlago, M., Greenstein, R., Pineda, M., Gonzalez-Meneses, A., Çoker, M., Bartholomew, D., Sands, M.S., Wang, R., Giugliani, R., Macaya, A., Pastores, G., Ketko, A.K., Ezgü, F., Tanaka, A., Arash, L., Beck, M., Falk, R.E., Bhattacharya, K., Franco, J., White, K.K., Mitchell, G.A., Cimbalistiene, L., Holtz, M., Sly, W.S., 2016. Clinical course of sly syndrome (mucopolysaccharidosis type VII). J. Med. Genet. jmedgenet-2015-103322-. doi:10.1136/jmedgenet-2015-103322

Morita, S., Kojima, T., Kitamura, T., 2000. Plat-E: an efficient and stable system for transient packaging of retroviruses. Gene Ther. 7, 1063–1066. doi:10.1038/sj.gt.3301206

Müller, F.J., Goldmann, J., Löser, P., Loring, J.F., 2010. A call to standardize teratoma assays used to define human pluripotent cell lines. Cell Stem Cell 6, 412–414. doi:10.1016/j.stem.2010.04.009

Parente, M.K., Rozen, R., Cearley, C.N., Wolfe, J.H., 2012. Dysregulation of gene expression in a lysosomal storage disease varies between brain regions implicating unexpected mechanisms of neuropathology. PLoS One 7. doi:10.1371/journal.pone.0032419

Parente, M.K., Rozen, R., Seeholzer, S.H., Wolfe, J.H., 2016. Integrated analysis of proteome and transcriptome changes in the mucopolysaccharidosis type VII mouse hippocampus. Mol. Genet. Metab. 118, 41–54. doi:10.1016/j.ymgme.2016.03.003

Patel, T., Man, K., Firestein, B., Meaney, D., 2015. Automated quantification of neuronal networks and single-cell calcium dynamics using calcium imaging. J. Neurosci. 243, 26–38.

Peterson, S.E., Tran, H.T., Garitaonandia, I., Han, S., Nickey, K.S., Leonardo, T., Laurent, L.C., Loring, J.F., 2011. Teratoma Generation in the Testis Capsule. J. Vis. Exp. 9, 9–11. doi:10.3791/3177

Phatnani, H., Maniatis, T., 2015. Astrocytes in Neurodegenerative Disease. Cold Spring Harb. Perspect. Biol. 7, a020628. doi:10.1101/cshperspect.a020628

Prokhorova, T.A., Harkness, L.M., Frandsen, U., Ditzel, N., Schrøder, H.D., Burns, J.S., Kassem, M., 2009. Teratoma formation by human embryonic stem cells is site dependent and enhanced by the presence of Matrigel. Stem Cells Dev. 18, 47–54. doi:10.1089/scd.2007.0266

Salinas, S., Zussy, C., Loustalot, F., Henaff, D., Menendez, G., Morton, P., Parsons, M., Schiavo, G., Kremer, E., 2014. Disruption of the coxsackievirus and adenovirus receptor-homodimeric interaction triggers lipid microdomain- and dynamin-dependent endocytosis and lysosomal targeting. J Biol Chem 289, 680–695. doi:10.1074/jbc.M113.518365

Sardiello, M., Palmieri, M., di Ronza, A., Medina, D., Valenza, M., Gennarino, V. et al., 2009. A gene network regulating lysosomal biogenesis and function. Science (80-.). 325, 473–477.

Schindelin, J., Arganda-Carreras, I., Frise, E., Kaynig, V., Longair, M., Pietzsch, T., Preibisch, S., Rueden, C., Saalfeld, S., Schmid, B., Tinevez, J.-Y., White, D.J., Hartenstein, V., Eliceiri, K., Tomancak, P., Cardona, A., 2012. Fiji: an open-source platform for biological-image analysis. Nat. Methods 9, 676–682. doi:10.1038/nmeth.2019

Seiradake, E., Lortat-Jacob, H., Billet, O., Kremer, E., Cusack, S., 2006. Structural and mutational analysis of human Ad37 and canine adenovirus 2 fiber heads in complex with the D1 domain of coxsackie and adenovirus receptor. J Biol Chem 281. doi:10.1074/jbc.M605316200

Simão, D., Arez, F., Terasso, A.P., Pinto, C., Sousa, M.F.Q., Brito, C., Alves, P.M., 2016. Perfusion Stirred-Tank Bioreactors for 3D Differentiation of Human Neural Stem Cells. Methods Mol. Biol. doi:10.1007/7651_2016_333

Simão, D., Pinto, C., Piersanti, S., Weston, A., Peddie, C.J., Bastos, A.E.P., Licursi, V., Schwarz, S.C., Collinson, L.M., Salinas, S., Serra, M., Teixeira, A.P., Saggio, I., Lima, P.A., Kremer, E.J., Schiavo, G., Brito, C., Alves, P.M., 2014. Modeling human neural functionality *in vitro*: 3D culture for dopaminergic differentiation. Tissue enginnering, Part A.

Sofroniew, M. V, Vinters, H. V, 2010. Astrocytes : biology and pathology 7–35. doi:10.1007/s00401-009-0619-8

Srikanth, P., Young-Pearse, T.L., 2014. Stem cells on the brain: modeling neurodevelopmental and neurodegenerative diseases using human induced pluripotent stem cells. J. Neurogenet. 28, 5–29. doi:10.3109/01677063.2014.881358

Takahashi, K., Tanabe, K., Ohnuki, M., Narita, M., Ichisaka, T., Tomoda, K., Yamanaka, S., 2007. Induction of pluripotent stem cells from adult human fibroblasts by defined factors. Cell 131, 861–72. doi:10.1016/j.cell.2007.11.019

Tiscornia, G., Vivas, E., Matalonga, L., Berniakovich, I., Barragán Monasterio, M., Eguizábal, C., Gort, L., González, F., Ortiz Mellet, C., García Fernández, J., Ribes, A., Veiga, A., Izpisua Belmonte, J., 2013. Neuronopathic Gaucher's disease: induced pluripotent stem cells for disease modelling and testing chaperone activity of small compounds. Hum Mol Genet 22, 633–645. doi:10.1093/hmg/dds471

Tolar, J., Park, I.-H., Xia, L., Lees, C.J., Peacock, B., Webber, B., McElmurry, R.T., Eide, C.R., Orchard, P.J., Kyba, M., Osborn, M.J., Lund, T.C., Wagner, J.E., Daley, G.Q., Blazar, B.R., 2011. Hematopoietic differentiation of induced pluripotent stem cells from patients with mucopolysaccharidosis type I (Hurler syndrome). Blood 117, 839–847.

Tomatsu, S., Montaño, A.M., Dung, V.C., Grubb, J.H., Sly, W.S., 2009. Mutations and Polymorphisms in GUSB Gene in Mucopolysaccharidosis VII (Sly Syndrome). Hum Mutat. 30, 511–519. doi:10.1002/humu.20828

Tomatsu, S., Sukegawa, K., Ikedo, Y., Fukuda, S., Yamada, Y., Sasaki, T., Okamoto, H., Kuwabara, T., Orii, T., 1990. Molecular basis of mucopolysaccharidosis type VII: replacement of Ala619 in ??-glucuronidase with Val. Gene 89, 283–287. doi:10.1016/0378-1119(90)90019-N

Vitner, E.B., Platt, F.M., Futerman, A.H., 2010. Common and uncommon pathogenic cascades in lysosomal storage diseases. J Biol Chem 285, 20423–20427. doi:10.1074/jbc.R110.134452

Walkley, S.U., 1998. Cellular pathology of lysosomal storage disorders. Brain Pathol. 8, 175–193. doi:10.1111/j.1750-3639.1998.tb00144.x

Walkley, S.U., Baker, H.J., Rattazzi, M.C., Haskins, M.E., Wu, J.Y., 1991. Neuroaxonal dystrophy in neuronal storage disorders: Evidence for major GABAergic neuron involvement. J. Neurol. Sci. 104, 1–8. doi:10.1016/0022-510X(91)90208-O

Wang, P., Sorenson, J., Strickland, S., Mingus, C., Haskins, M., Giger, U., 2015. Mucopolysaccharidosis VII in a Cat Caused by 2 Adjacent Missense Mutations in the GUSB Gene. J Vet Intern Med 29, 1022–1028. doi:10.1111/jvim.13569

Xing, E.M., Wu, S., Ponder, K.P., 2015. The effect of Tlr4 and/or C3 deficiency and of neonatal gene therapy on skeletal disease in mucopolysaccharidosis VII mice. Mol. Genet. Metab. 114, 209–216. doi:10.1016/j.ymgme.2014.12.305

Zack, G.W., Rogers, E., 1977. Automatic Measurement of Sister Chromatid Exchange Frequency. J. Histochem. Cytochem. 25, 741–753. doi:10.1177/25.7.70454

Zhu, F., Sun, B., Wen, Y., Wang, Z., Reijo Pera, R., Chen, B., 2014. A modified method for implantation of pluripotent stem cells under the rodent kidney capsule. Stem Cells Dev. 23, 2119–25. doi:10.1089/scd.2014.0099

CHAPTER 5

Discussion

Table of Contents

1. Discussion

Brain diseases represent a major social and economic burden worldwide and are expected to rise dramatically with the increase in life expectancy (DiLuca et al., 2014; Harper, 2014; Rosemann, 2015). Most neurological disorders have no effective treatments that target the pathological mechanisms and halt disease progression. Human models that recapitulate phenotypic and functional features of the human brain and brain-related pathologies, not only provide new tools to accurately identify and validate potential therapeutic targets and drug candidates, but can also give insights into the mechanisms of disease onset and progression.

The work developed herein aimed at exploiting 3D differentiation of human stem cells to develop, characterize and interrogate 3D neural cell models for disease modeling and drug discovery. The focus was on the recapitulation of phenotypic and functional features of human brain tissue, namely the establishment of functional neuron-astrocyte interactions. These models would have applications in drug screening and disease modelling fields. The overview of the work developed in this thesis is summarized in Fig. 5.1, where the aims and achievements for chapters 2-4 are described.

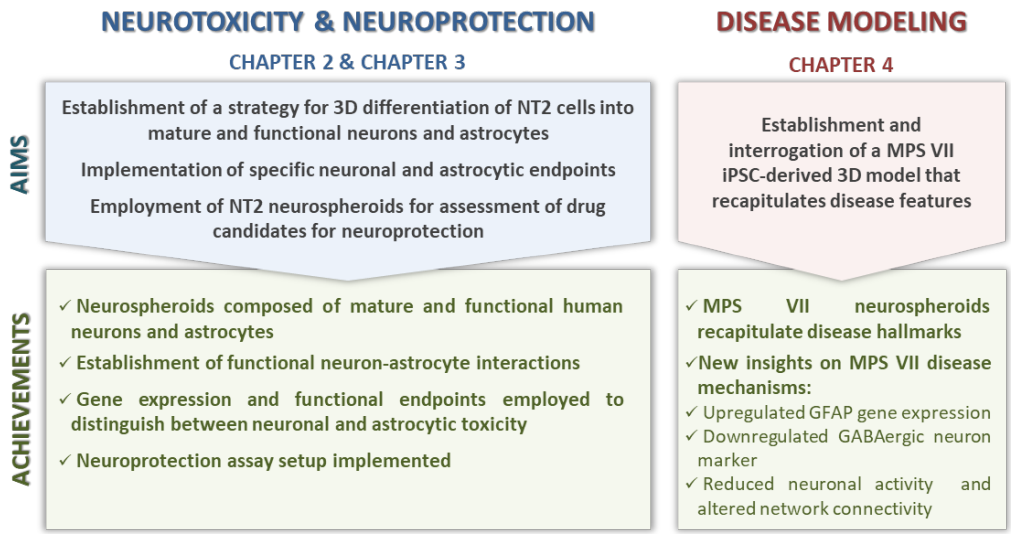

Figure 5.1: Schematic representation of the major aims of the thesis and the achievements of each chapter (2-4). NT2 – Ntera2/ clone D1 cell line; MPS VII – Mucopolysaccharidosis type VII; iPSC-NPC – induced pluripotent stem cells-derived neural progenitor cells.

When developing new models aiming at recapitulating specific features of the tissue of origin, the balance between complexity and heterogeneity and the desired application should be taken into account. Simple and robust models, with less expensive protocols and that fit into high-throughput test setups are better suited for drug testing applications. In turn, more complex models may be required for mechanistic research, as well as target discovery and validation. These should aim to mimic specific physiological and pathophysiological brain features, such as the interactions between several cell types and the microenvironment, and disease-related molecular pathways. Several 3D culture strategies have been employed to recapitulate important features of the brain tissue, including tissue-specific cellular organization (Birey et al., 2017; Lancaster et al., 2013; Ranga et al., 2016), neuron-astrocyte interactions (Simão et al., 2016a; Terrasso et al., 2015) and cell-ECM interactions (Simão et al., 2018). We employed agitation-based culture systems to develop scaffold-free culture strategies for PSC aggregation and neural differentiation. The stirring increases the frequency of cell-cell interactions, allowing cells to self-assemble and form aggregates, and enhances mass and gases transfer coefficients, which are function of the agitation speed (Kinney et al., 2011; Sargent et al., 2010). After the initial aggregation period, neural differentiation was induced by addition of morphogens or neurotrophic factors. This general culture strategy was implemented for NT2 cell line (Chapters 2 and 3) and adapted for iPSC-NPC neural differentiation, using health and diseased cells (Chapter 4).

1.1. 3D human brain cell model for drug screening

In Chapters 2 and 3 the main focus was (1) the establishment of a robust and reproducible strategy for 3D neural differentiation of human NT2 cell line into neurons and astrocytes (neurospheroids), allowing the establishment of functional neuron-astrocyte interactions; (2) the establishment of endpoints to distinguish between neuronal and astrocytic toxicity within neurospheroids; and (3) proof-of-concept of neurospheroid applicability in drug screening applications. Spinner vessels were used for NT2 cell line differentiation as these are simple agitation-

based culture systems, easy to implement in any laboratory, without major investment or engineering expertise. Our starting point was the bioprocess already implemented in our laboratory for NT2 neuronal differentiation in stirred-tank bioreactors (Serra et al., 2009, 2007), using RA as neurotrophic factor. Nevertheless, this bioprocess resulted in immature neuronal cells and did not include glial cells. Indeed, few works have been able to demonstrate the capacity of NT2 cell line to differentiate into the astrocytic lineage, in 2D culture systems (Bani-Yaghoub et al., 1999; Goodfellow et al., 2011). *In vivo*, during prenatal brain development, neurogenesis precedes gliogenesis (Molofsky and Deneen, 2015). Also, during ESC neural differentiation *in vitro*, neurons appear in culture during the first month, while astrocytes take 2-3 months to differentiate (Gupta et al., 2012; Hu et al., 2010). Following this rational, the culture time was extended, in order to allow astrocytic differentiation, as well as neuronal and astrocytic maturation. As described in Chapter 2, after 3 weeks of RA treatment and 2 additional weeks in culture, we obtained neurospheroids enriched into mature and functional human neurons and astrocytes. The major neuronal phenotypes in the human brain, excitatory glutamatergic and inhibitory GABAergic neurons, were detected in neurospheroids. Neuronal synaptic maturation and functionality were suggested by the presence of synaptophysin-positive vesicles and confirmed by the ability of neurospheroids to perform stimuli-induced vesicle exocytosis and neurotransmitter release. Astrocytic maturation was suggested by the presence of GLT-1, the predominant glutamate transporter in astrocytes. This transporter is responsible for 90% of glutamate uptake by excitatory aminoacid transporters in human brain (Kim et al., 2011). The ability of neurospheroids to perform glutamate uptake from the extracellular media and glutamine production, upon glutamate challenge, indicated the presence of functional astrocytes. This suggests that astrocytes in culture present: (1) functional glutamate transporters, the main mediators of glutamate clearance by astrocytes, (2) active glutamine synthase, the astrocyte-specific enzyme responsible for conversion of glutamate into glutamine (Zou et al.,

2010) and (3) glutamine efflux to the extracellular space via functional glutamine transporters. These are the main steps of the well-described glutamine-glutamate cycle, involved into the supply of glutamine to neurons (Amaral et al., 2011; Zou et al., 2010). Concomitantly, in the continuation of this work, we later demonstrated by nuclear magnetic resonance (NMR) spectroscopy using ^{13}C-labeled substrates, the establishment of neuronal and astrocytic metabolic signatures and of the glutamine-glutamate-GABA shuttle within NT2 neurospheroids (Simão et al., 2016a). These results highlight the relevance of this model for better understanding the metabolic crosstalk between human neurons and astrocytes. Furthermore, the presence of functional neurons and astrocytes enables modelling of neuron-astrocyte interactions and increases the model's reliability in drug screening. Functional human astrocytes provided an extra layer of complexity to the model, since these were described to be implicated in many neurodegenerative disease processes and impact neuronal response to neurotoxic and neuroprotective chemicals (Gupta et al., 2012; Sofroniew and Vinters, 2010). Astrocyte impairment has been found to contribute to neuronal dysfunction in several neurodegenerative diseases, such as ALS, AD, PD and Huntington's disease (Fraldi et al., 2016; Liu et al., 2017; Oksanen et al., 2017). Astrocytes produce and secrete neurotrophic factors, cytokines and chemokines that play both neurotoxic (inflammatory) and neuroprotective (immunoregulatory) roles (Choi et al., 2014; Phatnani and Maniatis, 2015). *In vivo*, astrocytes can facilitate the delivery of toxic or neuroprotective compounds to neurons. Indeed, several studies demonstrated that screens focusing on the direct effect of compounds on neurons overlook potentially important activities that act via astrocytes. Generally, astrocyte-containing *in vitro* models show increased tolerance to toxicant insult and impairment of astrocytic functions, such as maintenance of antioxidant defense and cellular energy levels, which can critically influence neuronal survival (Gupta et al., 2012; Woehrling et al., 2010).

For a cell platform to be used for *in vitro* drug screening, it is essential that models can be available in large amounts and in consistent quality. Indeed, the advantages of the NT2-derived model include the scalability and robustness of the culture system, allowing to reproducibly produce high number of differentiated neurospheroids, with low batch-to-batch variation. From one 125 mL spinner culture, one can feed more than one hundred 96-well plates using the assay setup implemented in chapters 2 and 3. The process developed for NT2 neural differentiation is also 50% less time-consuming and 10-fold more efficient than the 2D culture system. Moreover, NT2 3D differentiation is within the same duration than PSC neuronal and astrocytic differentiation protocols. Besides, it provides a more amenable and cost-effective process, as it only requires RA for neural differentiation instead of neurotrophic factors, such as BDNF, GDNF or CTNF, which are considerably more expensive.

The applicability of the NT2 neurospheroid model for drug testing was explored, including neurotoxicity (Chapter 2) and neuroprotection (Chapter 3) assessment. Neuronal and astrocytic specific gene expression and functionality endpoints were applied to distinguish between neuronal and astrocytic toxicity within neurospheroids. These were implemented using two prototypical neurotoxicants, acrylamide and chloramphenicol. Acrylamide decreased synaptophysin gene expression, even at subtoxic concentrations, while chloramphenicol decreased gene expression of neuronal (βIII-tubulin) and, at a major extent, astrocytic (GFAP) cytoskeletal proteins. The response of acrylamide-treated neurospheroids to depolarizing stimuli decreased, indicating loss of ability of synaptic vesicles to fuse with the plasma membrane and perform exocytosis.

Our data suggested that acrylamide neurotoxicity mechanism involves impairment of presynaptic function, interference with synaptic vesicle trafficking and changes in the ability of synaptic vesicles to fuse with the plasma membrane and perform exocytosis. Supporting this hypothesis, we later showed that acrylamide leads to intracellular accumulation of glutamate and decreases GABA

synthesis (Simão et al., 2016a), indicating an imbalanced glutamine-glutamate-GABA cycle. This can be due to impairment in synaptic vesicle trafficking, leading to loss of cell-cell contacts at synaptic sites. Indeed, nowadays there are 3 hypothesis for acrylamide neurotoxicity mechanisms: inhibition of kinesin-based fast axonal transport, alteration of neurotransmitter levels, and direct inhibition of neurotransmission by interference with membrane fusion processes at the nerve terminals (Erkekoglu and Baydar, 2014; Lopachin and Gavin, 2012). The consequence of the last is a failure of synaptic vesicles to fuse with their target membranes, which results in reduced release of neurotransmitters and eventually nerve terminal degeneration (Erkekoglu and Baydar, 2014).

There are few reports of chloramphenicol neurotoxicity mechanisms, but our results are in line with a previous report (Woehrling et al., 2011), and suggest that chloramphenicol induces cytoskeletal injury, being more toxic to astrocytes than to neurons. Still, in lung and liver cancer cells, chloramphenicol is described to cause senescence-associated morphological changes, including changes in the expression pattern of cytoskeleton genes (Li et al., 2010, 2005). Similar mechanisms can potentially be occurring in neurospheroids.

Importantly, the gene expression and neuronal functionality endpoints employed allowed early detection of changes in neuronal and astrocytic gene expression and disturbed neuronal functions and their correlation with mechanisms of toxicity. This suggests that these are sensitive endpoints that can be used to distinguish between neuronal and astrocytic toxicity in complex 3D models.

For the proof-of-concept of the applicability of the NT2 neurospheroids for testing the neuroprotective effect of drug candidates an *in vitro* assay setup, in a 96-well plate format, was implemented. This combined neurospheroids with a tBHP-induced oxidative insult and a fluorescence-based cell viability endpoint. 36 potential neuroprotective compounds from different origins, ranging from chemically-synthetized compounds to natural extracts, were tested.

Robustness and simplicity of the neurospheroids production process and of the neuroprotection assay, combined with the evaluation of cell viability using a fluorescence-based endpoint, makes this a versatile assay setup suitable for early-stage drug screening. Neurospheroids can be easily collected from an agitation-based culture system, be distributed in multi-well plates with a robotic system and employed to test drug candidates. Moreover, the general assay setup developed herein for drug testing can be applied to other 3D cell models, using different cell sources and different insults.

Human neurospheroids can also be applied to feed microfluidic devices, such as multi-organ chip platforms, allowing long-term cultures of various cell types from different tissues, in a miniaturized controlled environment. The application of NT2 neurospheroids developed in this work to feed multi-organ chip microfluidic devices was evaluated by co-culturing the neurospheroids with human liver microtissues (Materne et al., 2015). Also, a 2-week toxicity assay, with repeated substance exposure, showed that neurospheroids can be useful for repeated dose applications in these platforms (Materne et al., 2015). Nevertheless, as multi-organ-chips are technically demanding and present a lower throughput than multi-well plates, this approach should be more useful in later stages of drug discovery pipeline, when few drugs are being better characterized. Besides, multi-well plates, by allowing a higher throughput, can be useful in primary screenings, to test a high number of drugs. Still, multi-organ chips provide additional *in vitro* tools that can more closely recapitulate systemic application of drugs and be employed to predict more accurately drug safety and efficacy in preclinical studies using 3D cell models.

1.2. 3D human brain cell model for MPS VII disease modeling

Typically when trying to recapitulate neurological defects the focus is on neuronal cells. However, astrocytes have important roles on neuronal cell function and on the secretion of ECM components and regulation of the extracellular milieu, potentially impacting the development and progression of neurological diseases. Besides, we showed that neurospheroids differentiation in scaffold-free agitation-

based culture systems allows the establishment of functional neuron-astrocyte interactions (Simão et al., 2016b; Terrasso et al., 2015) and accumulation of endogenous ECM and secreted components (Simão et al., 2018). We hypothesized that through recapitulation of neuron-astrocyte and cell-ECM interactions within neurospheroids, it would be possible to recapitulate pathological features, in which impairment of neuron-astrocyte and cell-ECM interactions can be relevant.

MPS VII is an orphan neuronopathic LSD, caused by a deficiency in β-gluc enzymatic activity (Tollersrud and Berg, 2005; Tomatsu et al., 2009), which results in an abnormal accumulation of GAGs partially degraded in the lysosomes of many tissues, including in the brain (Montaño et al., 2016). Whereas the primary effects of the disorder are described, the mechanistic events downstream to GAGs accumulation that can lead to more deleterious neuronal effects are still unknown. Proteoglycans are one of the major components of brain ECM, thus alterations in GAGs can potentially impact neural cell interactions and cell ECM interactions, which in turn regulate neural cell functionality (Srikanth and Young-Pearse, 2014). Moreover, it was reported that the aberrant behavior of neural cells derived from a canine MPS VII model was lost after standard culture *in vitro*, suggesting that the neural microenvironment is critical for disease phenotype (Walton and Wolfe, 2007). Thus, MPS VII patient-derived iPSC cells were employed to generate neurospheroids and test our hypothesis.

In Chapter 4, the main focus was on (1) the establishment of a neurospheroid model differentiated from MPS VII patient-derived iPSC, with the presence of several brain cell types and allowing for the recapitulation of neuron-astrocyte interactions and (2) to test whether MPS VII neurospheroids could recapitulate MPS VII disease hallmarks, which would enable them to be used to understand the disease-associated cognitive deficits and try to identify disease-related neuronal defects.

MPS VII iPSC were generated by reprogramming of MPS VII patient skin fibroblasts, followed further differentiation into neural precursor cells (iPSC-NPC)

by dual SMAD inhibition protocol (Chambers et al., 2009). Reduced β-gluc activity had no significant impact on iPSC-NPC and these did not show major lysosome structural alterations. MPS VII neurons, differentiated in 2D, showed several MPS VII-associated phenotypes, including GAGs accumulation, expanded endocytic compartments, accumulation of lipofuscin granules, more autophagosomes, and altered lysosome function. While clearly very informative, this 2D cellular model lacked the interactions between neurons and astrocytes and between these and the proteoglycans.

The strategies developed by our group for NT2 neural differentiation, allowing establishment of neuron-astrocyte interactions (Terrasso et al., 2015) and for iPSC-NPC neural differentiation, allowing the accumulation of endogenous ECM and secreted components (Simão et al., 2016b; Simão et al., 2018), were used as starting point for MPS VII neurospheroids culture. MPS VII iPSC-NPC differentiation was induced by mitogen (FGF and EGF) removal and exposure to a membrane-permeable analogue of cAMP and to the neurotrophic factors BDNF, GDNF and NT-3. Downregulation of prototypic NPC genes and upregulation of glutamatergic, dopaminergic and GABAergic neuronal markers in MPS VII neurospheroids were observed. MPS VII neurospheroid cultures recapitulated disease-associated molecular hallmarks, mainly GAGs accumulation. Interestingly, MPS VII neurospheroids revealed an upregulation in GFAP, and a downregulation in GABAergic inhibitory neuron markers. This upregulation in GFAP in MPS VII neurospheroids can be related with an increase in GFAP-positive astrocytic cells or associated with astrocytic reactivity. Since astrocyte-specific glutamate transporter GLT-1 gene expression is similar between control and MPS VII neurospheroids we hypothesized that the GFAP upregulation is associated with astrocytic reactivity. Supporting this hypothesis, in recent studies performing transcriptomic analysis of the MPS VII mouse brain GFAP was highly upregulated (Parente et al., 2016). GFAP upregulation is the hallmark of astrocyte reactivity (Ben Haim et al., 2015; Phatnani and Maniatis, 2015; Sofroniew and Vinters, 2010). Reactive astrocytes were found

in brains of AD and ALS patients before clinical symptoms (Carter et al., 2012; Philips and Robberecht, 2011) and in animal models of the same neurological disorders (Maragakis and Rothstein, 2006; Olabarria et al., 2010). Mediators of innate immunity such as lipopolysaccharides (LPS) and other Toll-like receptor (TLR) ligands are able to trigger reactive astrogliosis to different extents. GAGs breakdown products are structurally similar to LPS, the canonical ligand of TLR4 (Ballabio and Gieselmann, 2009; Xing et al., 2015). Therefore, GAGs accumulation in MPS can activate TLR4 signaling pathway, eliciting pro-inflammatory cytokine production (e.g. TNF-α and IL-1β) and inducing a pro-inflammatory response (Ballabio and Gieselmann, 2009; Simonaro et al., 2010; Xing et al., 2015). Indeed, priming of microglia via TLR4 was demonstrated in MPS IIIC (Ausseil et al., 2008) and MPS VII mouse brains (Metcalf et al., 2009). Further studies are required to confirm that astrocytes within MPS VII neurospheroids are reactive and if this occurs through activation of TLR4 pathway by accumulation of GAG breakdown products. Increasing one layer of complexity to the MPS VII neurospheroid disease model, adding MPS VII iPSC-derived microglial cells to the culture could contribute to give insights on astrocyte and microglia reactivity in MPS diseases, as usually both cell types become reactive. Probably, this model would also better recapitulate the disease phenotype.

The evaluation of neuronal connectivity by spontaneous calcium imaging revealed disturbances in the functional connectivity of the MPS VII neurospheroid neuronal network. These alterations can possibly be related with the decrease in GABAergic neurons, as these are involved in the stabilization of neuronal activity, through the maintenance of the balance between excitation and inhibition (Błaszczyk, 2016). The maintenance of this balance, together with the calcium homeostasis, ensures the correct functioning of neuron-astrocyte networks. Calcium-GABA interactions were used to adjust the fast electrical neuronal activity to the slower cell biochemical and metabolic processes (Błaszczyk, 2016). To control excessive neuronal activity and protect neurons, GABA system controls

calcium influx. This can be done directly, by increased GABA inhibition and reduction of GABA receptors and calcium channels or indirectly, via astrocytes (Allaman et al., 2011). These are activated by the neurotransmitters released within neuronal networks and inhibit the influx of calcium ions into the presynaptic neurons via GABA. Thus, if GABA concentration decreases, neurons become more excitable (Allaman et al., 2011) and this excitability of the neuronal network is adjusted through the elimination of neurons with excessive activity, initiating neurodegeneration (Błaszczyk, 2016). Our data is the ideal starting point to understand MPS VII-associated cognitive defects, providing insights into the interplay between reduced β-gluc activity, GAG accumulation and alterations in the neural network. The iPSC-derived MPS VII 3D neurospheroids provide a platform to further elucidate the molecular and cellular processes responsible of MPS VII-associated brain dysfunction. These can also be used for testing and optimizing new therapies. Moreover, the 3D neurospheroid culture combined with the 3D neuronal connectivity assay are new tools with potential to assess other LSD and neurodegenerative diseases with variable phenotypes, contributing to better understand the cellular changes induced by the disease itself or by novel therapeutics. Lysosomes are nowadays viewed not only as degradative and recycling centers, but also as important organelles to maintain brain homeostasis. Additionally, lysosomal dysfunction has been increasingly associated with age-related pathologies, like AD and PD neurological disorders (Carmona-Gutierrez et al., 2016; Fraldi et al., 2016). Thus, insights from the mechanisms of neuronal degeneration in LSD, such as MPS VII, can contribute to unveil new knowledge related with these mechanisms in other neurological disorders.

2. Challenges and future opportunities

The work developed in this thesis describes the development and application of 3D human neural cell models for disease modeling and drug discovery. This work contributed to the brain cell modelling field, providing new methodologies for

human neural cell differentiation and neural cell model development and ultimately providing model systems for the disease modeling and drug discovery fields.

In recent years, the rise of 3D models derived from PSC, and the implementation of characterization tools adapted to 3D cultures, triggered an exponential evolution in the neural cell models toolbox. Despite the significant improvements, the lack of efficient neural differentiation protocols that provide mature cells able to form the functional neuronal networks present in the adult tissue *in vivo*, remains one bottleneck. Still, there is no evidence indicating whether the neural maturation stage attained *in vitro* is enough to reflect disease pathogenesis and/ or to mimic the drug response of neural cells.

In the last years, the cerebral organoids methodology emerged (Lancaster et al., 2013) and, nowadays, there are several groups working on this and making efforts to improve the differentiation protocols and further characterize them (Camp et al., 2015; Qian et al., 2017; Quadrato et al., 2017). Cerebral organoids have proven their utility to study human brain development and developmental diseases, as various brain regions are present in those models (Kelava and Lancaster, 2017). However, for drug screening applications the differentiation protocols need to be further improved in order to generate more homogeneous cultures, with low intra-batch and batch-to-batch variations. Furthermore, the validity of cerebral organoids to address microenvironment-related questions remains uncertain, due to the use of a heterologous matrix (Matrigel) that poorly resemble the brain ECM, and that may introduce confounding effects. Taking this into consideration, for drug discovery or to study diseases where ECM is involved, or has important roles in disease progression, neurospheroids appear as a better option. Another alternative are the defined synthetic 3D matrices that are under investigation (Ranga et al., 2016) and can be further explored to recapitulate the roles of ECM in human brain.

Importantly, 3D models should not be viewed as platforms to replace animal models, but instead as complementary *in vitro* tools to find more effective drugs before going to animal models or to address specific aspects that cannot be addressed in animals due to the differences between species. This will reduce the number of animals used and the attrition rates observed in drug discovery pipelines. It must also be recognized that the utility of 3D cell models need to be further explored and thoroughly validated to attain definitive conclusions on their physiological relevance and correlation with the *in vivo* situation. Furthermore, the establishment of novel models in drug discovery and drug testing pipelines requires extensive validation studies, including evaluation of robustness, specificity and reproducibility of the assays. Additional data demonstrating robust *in vivo* and *in vitro* correlations are needed to enhance confidence and ensure widespread use of the 3D models for drug testing in the future.

In the future, models would be complex in its morphology while still maintaining reproducibility, thus coming closer to the *in vivo* features. Further optimization of the existing models is still required, to recapitulate in the models the functional interactions of the three neural cell lineages (neurons, astrocytes and oligodendrocytes). Additionally, immune microglia cells should also be incorporated in the models, since these contribute directly to brain physiology and microenvironment, both in health and pathological conditions. Moreover, mimicking the brain vascular networks, and ultimately, the blood brain barrier, will not only overcome the oxygen and nutrients/ chemicals supply to the 3D tissue-like structures, but also influence the drug response. In this context, 3D models still have a lot to evolve until fully replicating the complex *in vivo* environment, with multiple and functional cells types surrounded by the ECM and the vascular network, while reproducing organ function, which up to now has been impossible to fully mimic.

3. References

Allaman, I., Bélanger, M., Magistretti, P.J., 2011. Astrocyte-neuron metabolic relationships: For better and for worse. Trends Neurosci. 34, 76–87. doi:10.1016/j.tins.2010.12.001

Amaral, A.I., Teixeira, A.P., Håkonsen, B.I., Sonnewald, U., Alves, P.M., 2011. A comprehensive metabolic profile of cultured astrocytes using isotopic transient metabolic flux analysis and C-labeled glucose. Front. Neuroenergetics 3, 5. doi:10.3389/fnene.2011.00005

Bani-Yaghoub, M., Felker, J.M., Naus, C.C.G., 1999. Human NT2/D1 cells differentiate into functional astrocytes. Neuroreport 10, 3843–3846. doi:10.1097/00001756-199912160-00022

Ben Haim, L., Carrillo-de Sauvage, M.-A., Ceyzériat, K., Escartin, C., 2015. Elusive roles for reactive astrocytes in neurodegenerative diseases. Front. Cell. Neurosci. 9, 278. doi:10.3389/fncel.2015.00278

Birey, F., Andersen, J., Makinson, C., Islam, S., Wei, W., Huber, N., Fan, H., Metzler, K., Panagiotakos, G., Thom, N., O'Rourke, N., Steinmetz, L., Bernstein, J., J, H., JR, H., Paşca, S., 2017. Assembly of functionally integrated human forebrain spheroids. Nature. doi:10.1038/nature22330

Błaszczyk, J.W., 2016. Parkinson's disease and neurodegeneration: GABA-collapse hypothesis. Front. Neurosci. 10. doi:10.3389/fnins.2016.00269

Camp, J.G., Badsha, F., Florio, M., Kanton, S., Gerber, T., Wilsch-Bräuninger, M., Lewitus, E., Sykes, A., Hevers, W., Lancaster, M., Knoblich, J., Lachmann, R., Pääbo, S., Huttner, W., Treutlein, B., 2015. Human cerebral organoids recapitulate gene expression programs of fetal neocortex development. Proc. Natl Acad. Sci. USA 112, 15672–15677.

Carmona-Gutierrez, D., Hughes, A.L., Madeo, F., Ruckenstuhl, C., 2016. The crucial impact of lysosomes in aging and longevity. Ageing Res. Rev. 32, 2–12. doi:10.1016/j.arr.2016.04.009

Carter, S.F., Scholl, M., Almkvist, O., Wall, A., Engler, H., Langstrom, B., Al., T., 2012. Evidence for astrocytosis in prodromal Alzheimer disease provided by 11C-deuterium-L-deprenyl: a multitracer PET paradigm combining 11C- Pittsburgh compound B and 18F-FDG. J. Nucl. Med. 53, 37–46. doi:10.2967/jnumed.110.087031

Chambers, S.M., Craft, C.A., Papapetrou, E.P., Tomishima, M., Sadelain, M., Studer, L., 2009. Highly efficient neural conversion of human ES and iPS cells by dual inhibition of SMAD signaling. Nat Biotechnol 27, 275–280.

Choi, S.S., Lee, H.J., Lim, I., Satoh, J.I., Kim, S.U., 2014. Human astrocytes: Secretome profiles of cytokines and chemokines. PLoS One 9. doi:10.1371/journal.pone.0092325

DiLuca, M., Olesen, J., Gustavsson, A., McDaid, D., Ersek, K., Georges, J., Gulácsi, L., Karpati, K., Kenigsberg, P., Valtonen, H., Group, C., al., et, 2014. The Cost of Brain Diseases: A

Burden or a Challenge? Neuron 82, 1205–1208. doi:10.1016/j.neuron.2014.05.044

Erkekoglu, P., Baydar, T., 2014. Acrylamide neurotoxicity. Nutr. Neurosci. 17, 49–57. doi:10.1179/1476830513Y.0000000065

Fraldi, A., Klein, A.D., Medina, D.L., Settembre, C., 2016. Brain Disorders Due to Lysosomal Dysfunction. Annu. Rev. Neurosci. 39, 277–295. doi:10.1146/annurev-neuro-070815-014031

Goodfellow, C.E., Graham, S.E., Dragunow, M., Glass, M., 2011. Characterization of NTera2/D1 cells as a model system for the investigation of cannabinoid function in human neurons and astrocytes. J. Neurosci. Res. 89, 1685–97. doi:10.1002/jnr.22692

Gupta, K., Patani, R., Baxter, P., Serio, a, Story, D., Tsujita, T., Hayes, J.D., Pedersen, R. a, Hardingham, G.E., Chandran, S., 2012. Human embryonic stem cell derived astrocytes mediate non-cell-autonomous neuroprotection through endogenous and drug-induced mechanisms. Cell Death Differ. 19, 779–87. doi:10.1038/cdd.2011.154

Harper, S., 2014. Economic and social implications of aging societies. Science (80-.). 346, 587–91. doi:10.1126/science.1254405

Hu, B., Weick, J.P., Yu, J., Ma, L., Zhang, X., Thomson, J.A., 2010. Neural differentiation of human induced pluripotent stem cells follows developmental principles but with variable potency 1. doi:10.1073/pnas.0910012107

Kelava, I., Lancaster, M.A., 2017. Stem Cell Models of Human Brain Development. Cell Stem Cell 18, 736–748. doi:10.1016/j.stem.2016.05.022

Kim, K., Lee, S.-G., Kegelman, T.P., Su, Z.-Z., Das, S.K., Dash, R., Dasgupta, S., Barral, P.M., Hedvat, M., Diaz, P., Reed, J.C., Stebbins, J.L., Pellecchia, M., Sarkar, D., Fisher, P.B., 2011. Role of excitatory amino acid transporter-2 (EAAT2) and glutamate in neurodegeneration: opportunities for developing novel therapeutics. J. Cell. Physiol. 226, 2484–93. doi:10.1002/jcp.22609

Kinney, M., Sargent, C.Y., McDevitt, T.C., 2011. The multiparametric effects of hydrodynamic environments on stem cell culture. Tissue Eng. Part B Rev 37, 249–262.

Lancaster, M. a, Renner, M., Martin, C., Wenzel, D., Bicknell, S., Hurles, M.E., Homfray, T., Penninger, J.M., Andrew, P., 2013. Cerebral organoids model human brain development and microcephaly. Nature 501, 373–379. doi:10.1038/nature12517.

Li, C.H., Cheng, Y.W., Liao, P.L., Yang, Y.T., Kang, J.J., 2010. Chloramphenicol causes mitochondrial stress, decreases ATP biosynthesis, induces matrix metalloproteinase-13 expression, and solid-tumor cell invasion. Toxicol. Sci. 116, 140–150. doi:10.1093/toxsci/kfq085

Li, C.H., Tzeng, S.L., Cheng, Y.W., Kang, J.J., 2005. Chloramphenicol-induced mitochondrial stress increases p21 expression and prevents cell apoptosis through a p21-dependent

pathway. J. Biol. Chem. 280, 26193–26199. doi:10.1074/jbc.M501371200

Liu, B., Teschemacher, A.G., Kasparov, S., 2017. Astroglia as a cellular target for neuroprotection and treatment of neuro-psychiatric disorders. Glia 65, 1205–1226. doi:10.1002/glia.23136

Lopachin, R.M., Gavin, T., 2012. Review Molecular Mechanism of Acrylamide Neurotoxicity : Lessons Learned from Organic Chemistry. Env Health Perspectives. 120. 1650–1657. doi:10.1289/ehp.1205432.

Maragakis, N.J., Rothstein, J.D., 2006. Mechanisms of Disease: astrocytes in neurodegenerative disease. Nat. Clin. Pract. Neurol. 2, 679–89. doi:10.1038/ncpneuro0355

Materne, E.-M., Ramme, A.P., Terrasso, A.P., Serra, M., Alves, P.M., Brito, C., Sakharov, D.A., Tonevitsky, A.G., Lauster, R., Marx, U., 2015. A multi-organ chip co-culture of neurospheres and liver equivalents for long-term substance testing. J. Biotechnol. 205. doi:10.1016/j.jbiotec.2015.02.002

Milosevic, J., Schwarz, S.C., Krohn, K., Poppe, M., Storch, A., Schwarz, J., 2005. Low atmospheric oxygen avoids maturation, senescence and cell death of murine mesencephalic neural precursors. J. Neurochem. 92, 718–729.

Molofsky, A.V., Deneen, B., 2015. Astrocyte development: A Guide for the Perplexed. Glia 63, 1320–1329. doi:10.1002/glia.22836

Montaño, A.M., Lock-Hock, N., Steiner, R.D., Graham, B.H., Szlago, M., Greenstein, R., Pineda, M., Gonzalez-Meneses, A., Çoker, M., Bartholomew, D., Sands, M.S., Wang, R., Giugliani, R., Macaya, A., Pastores, G., Ketko, A.K., Ezgü, F., Tanaka, A., Arash, L., Beck, M., Falk, R.E., Bhattacharya, K., Franco, J., White, K.K., Mitchell, G.A., Cimbalistiene, L., Holtz, M., Sly, W.S., 2016. Clinical course of sly syndrome (mucopolysaccharidosis type VII). J. Med. Genet. jmedgenet-2015-103322-. doi:10.1136/jmedgenet-2015-103322

Oksanen, M., Petersen, A., Naumenko, N., Puttonen, S., Lehtonen, S., Olivé, M., Shakirzyanova, A., Seskelä, S., Sarajärvi, T., Viitanen, M., Rinne, J., Hiltunen, M., Haapasalo, A., Giniatullin, R., Tav, P., Koistinaho, J., 2017. PSEN1 Mutant iPSC-Derived Model Reveals Severe Astrocyte Pathology in Alzheimer's Disease. Stem Cell Reports. doi:10.1016/j.stemcr.2017.10.016

Olabarria, M., Noristani, H.N., Verkhratsky, A., Rodriguez, J.J., 2010. Concomitant astroglial atrophy and astrogliosis in a triple transgenic animal model of Alzheimer's disease. Glia 58, 831–838. doi:10.1002/glia. 20967

Phatnani, H., Maniatis, T., 2015. Astrocytes in Neurodegenerative Disease. Cold Spring Harb. Perspect. Biol. 7, a020628. doi:10.1101/cshperspect.a020628

Philips, T., Robberecht, W., 2011. Neuroinflammation in amyotrophic lateral sclerosis: role of glial activation in motor neuron disease. Lancet Neurol. 10, 253–263. doi:10.1016/S1474-4422(11)70015-1

Qian, X., Nguyen, H.N., Jacob, F., Song, H., Ming, G., 2017. Using brain organoids to understand Zika virus-induced microcephaly. Development 144, 952–957. doi:10.1242/dev.140707

Quadrato, G., Nguyen, T., Macosko, E.Z., Sherwood, J.L., Min Yang, S., Berger, D.R., Maria, N., Scholvin, J., Goldman, M., Kinney, J.P., Boyden, E.S., Lichtman, J.W., Williams, Z.M., McCarroll, S.A., Arlotta, P., 2017. Cell diversity and network dynamics in photosensitive human brain organoids. Nature. doi:10.1038/nature22047

Ranga, A., Girgin, M., Meinhardt, A., Eberle, D., Caiazzo, M., Tanaka, E., Lutolf, M., 2016. Neural tube morphogenesis in synthetic 3D microenvironments. Proc. Natl. Acad. Sci. U. S. A. E6831–E6839.

Rosemann, A., 2015. Stem cell treatments for neurodegenerative diseases: challenges from a science, business and healthcare perspective. Neurodegener. Dis. Manag. 5, 85–87. doi:10.2217/nmt.15.2

Sargent, C.Y., Berguig, G.Y., Kinney, M. a, Hiatt, L. a, Carpenedo, R.L., Berson, R.E., McDevitt, T.C., 2010. Hydrodynamic modulation of embryonic stem cell differentiation by rotary orbital suspension culture. Biotechnol. Bioeng. 105, 611–26. doi:10.1002/bit.22578

Serra, M., Brito, C., Costa, E.M., Sousa, M.F.Q., Alves, P.M., 2009. Integrating human stem cell expansion and neuronal differentiation in bioreactors 14, 1–14. doi:10.1186/1472-6750-9-82

Serra, M., Leite, S.B., Brito, C., Carrondo, M.J.T., Alves, P.M., 2007. Novel Culture Strategy for Human Stem Cell Proliferation and Neuronal Differentiation 3566, 3557–3566. doi:10.1002/jnr

Simão, D., Arez, F., Terasso, A.P., Pinto, C., Sousa, M.F.Q., Brito, C., Alves, P.M., 2016. Perfusion Stirred-Tank Bioreactors for 3D Differentiation of Human Neural Stem Cells. Methods Mol. Biol. doi:10.1007/7651_2016_333

Simão, D., Pinto, C., Piersanti, S., Weston, A., Peddie, C.J., Bastos, A.E.P., Licursi, V., Schwarz, S.C., Collinson, L.M., Salinas, S., Serra, M., Teixeira, A.P., Saggio, I., Lima, P.A., Kremer, E.J., Schiavo, G., Brito, C., Alves, P.M., 2014. Modeling human neural functionality *in vitro*: 3D culture for dopaminergic differentiation. Tissue enginnering, Part A. 21. 654-668. doi: 10.1089/ten.TEA.2014.0079

Simão, D., Silva, M.M., Terrasso, A.P., Arez, F., Sousa, M.F., Mehrjardi, N.Z., Šarić, T., Gomes-Alves, P., Raimundo, N., Alves, P.M., Brito, C., 2018. 3D differentiation of iPSC-derived NPC recapitulates human brain microenvironment. Stem Cell Reports, *under revision*

Simão, D., Terrasso, A.P., Teixeira, A.P., Brito, C., Sonnewald, U., Alves, P.M., 2016. Functional metabolic interactions of human neuron-astrocyte 3D *in vitro* networks. Sci. Rep. 6. doi:10.1038/srep33285

Sofroniew, M. V, Vinters, H. V, 2010. Astrocytes : biology and pathology 7–35.

doi:10.1007/s00401-009-0619-8

Srikanth, P., Young-Pearse, T.L., 2014. Stem cells on the brain: modeling neurodevelopmental and neurodegenerative diseases using human induced pluripotent stem cells. J. Neurogenet. 28, 5–29. doi:10.3109/01677063.2014.881358

Terrasso, A.P., Pinto, C., Serra, M., Filipe, A., Almeida, S., Ferreira, A.L., Pedroso, P., Brito, C., Alves, P.M., 2015. Novel scalable 3D cell based-model for *in vitro* neurotoxicity testing: combining human differentiated neurospheres with gene expression and functional endpoints. J. Biotechnol. 205, 82–92. doi:10.1016/j.jbiotec.2014.12.011

Terrasso, A.P., Pinto, C., Serra, M., Filipe, A., Almeida, S., Ferreira, A.L., Pedroso, P., Brito, C., Alves, P.M., 2015. Novel scalable 3D cell based model for *in vitro* neurotoxicity testing: Combining human differentiated neurospheres with gene expression and functional endpoints. J. Biotechnol. 205. doi:10.1016/j.jbiotec.2014.12.011

Tollersrud, G., Berg, T., 2005. Lysosomal storage disorders, in: Lysosomes. Wiley-Blackwell, West Susex, pp. 60–73.

Tomatsu, S., Montaño, A.M., Dung, V.C., Grubb, J.H., Sly, W.S., 2009. Mutations and Polymorphisms in GUSB Gene in Mucopolysaccharidosis VII (Sly Syndrome). Hum Mutat. 30, 511–519. doi:10.1002/humu.20828

Walton, R., Wolfe, J., 2007. Abnormalities in neural progenitor cells in a dog model of lysosomal storage disease. J Neuropathol Exp Neurol. 66, 760–769. doi:10.1097/nen.0b013e31812571c8

Woehrling, E.K., Hill, E.J., Torr, E.E., Coleman, M.D., 2011. Single-Cell ELISA and Flow Cytometry as Methods for Highlighting Potential Neuronal and Astrocytic Toxicant Specificity 472–483. doi:10.1007/s12640-010-9202-2

Zou, J., Wang, Y.-X., Dou, F.-F., Lü, H.-Z., Ma, Z.-W., Lu, P.-H., Xu, X.-M., 2010. Glutamine synthetase down-regulation reduces astrocyte protection against glutamate excitotoxicity to neurons. Neurochem. Int. 56, 577–84. doi:10.1016/j.neuint.2009.12.021